# Collective spin and heat transport through magnetic systems

ISBN: 978-90-393-6569-4
Printed by Ipskamp Drukkers

# Collective spin and heat transport through magnetic systems

## Collectief spin en warmtetransport door magnetische systemen

(met een samenvatting in het Nederlands)

Proefschrift

ter verkrijging van de graad van doctor aan de Universiteit Utrecht
op gezag van de rector magnificus, prof. dr. G.J. van der Zwaan,
ingevolge het besluit van het college voor promoties in het openbaar
te verdedigen op maandag 10 april 2017 des middags te 2.30 uur

door

Benedetta Flebus

geboren op 18 september 1989 te Cividale del Friuli, Italië

Promotoren: Prof. dr. R.A. Duine
Prof. dr. ir. H.T.C. Stoof

# Contents

# Publications

The main Chapters of this Thesis are based on the following papers:

- B. Flebus, S. A. Bender, Y. Tserkovnyak, and R. A. Duine, *Two-Fluid Theory for Spin Superfluidity in Magnetic Insulators*, Phys. Rev. Lett. **116**, 117201 (2016).
- B. Flebus, P. Upadhyaya, R. A. Duine, and Y. Tserkovnyak, *Local thermomagnonic torques in two-fluid spin dynamics*, Phys. Rev. B. **94**, 214428 (2016).
- B. Flebus, K. Shen, T. Kikkawa, K. Uchida, Z. Qiu, E. Saitoh, R. A. Duine, and G. E. W. Bauer, *Magnon-polaron transport in magnetic insulators* (submitted to PRB).
- B. Flebus, R. A. Duine, and Y. Tserkovnyak, *Landau-Lifshitz theory of the magnon-drag thermopower*, EPL **115**, 57004 (2016).

Other publications to which the author has contributed:

- B. Flebus, R. A. Duine, G.E.W. Bauer, and Y. Tserkovnyak, *Theory of magnon-mediated magneto-Seebeck effect*, in preparation.
- Y. Tserkovnyak, S. A. Bender, R. A. Duine, and B. Flebus, *Bose-Einstein Condensation of Magnons Pumped by the Bulk Spin Seebeck Effect*, Phys. Rev. B **93**, 100402 (2016).
- T. Kikkawa, K. Shen, B. Flebus, R. A. Duine, K. Uchida, Z. Qiu, G. E. W. Bauer, and E. Saitoh, *Magnon Polarons in the Spin Seebeck Effect*, Phys. Rev. Lett. **117**, 207203, (2016).
- M. T. J. van Loenhout, I. De Vlaminck, B. Flebus, J. F. den Blanken, L. Zweifel, K. M. Hooning, J. W. J. Kerssemakers, and C. Dekker, *Scanning a DNA molecule for bound proteins using hybrid magnetic and optical tweezers*, Plos One **8**, e65329 (2013).

# 1 Introduction

This Thesis is concerned with magnons, phonons, and electrons, and how their mutual interaction gives rise to novel transport phenomena. In this introduction we give a brief motivation and provide the necessary basics to understand the remaining part of this Thesis.

## 1.1 Magnons, phonons, and electrons.

A magnon, or semiclassically, a spin wave, is a collective excitation of the spin or magnetization direction in magnetically-ordered materials. Taking as an example the ground state of the simplest magnetically-ordered material, i.e., a ferromagnet, where all the spins are spontaneously aligned, one could naively think that the lowest energy excitation is created by flipping a single spin. Instead, due to the strong interactions between spins in a magnet, the most energetically favorable excitation is a collective one, which can be though as a wave of neighboring spins precessing at the same frequency but with a different phase, as shown in Fig. 1.1(a). Each magnon carries energy and linear momentum, and the total number of magnons populating a system can be interpreted as a measure for the deviation from a perfectly saturated magnetic state order.

Both in metallic and insulating materials, magnons stem from the spin degrees of freedom of electrons. As these spins are embedded in their respective lattice sites and interact with each other, one can intuitively see that a collective lattice vibration (phonon) might affect their mutual interaction as it shortens or lengthens the distance between neighbouring spins [see Fig. 1.1(b)]. Quantum mechanically, this effect can be described in terms of magnon-phonon coupling. Understanding the latter appears to be essential especially for magnetic insulating systems as magnetic and elastic excitations fully determine, due to the lack of charge degrees of freedom, their thermal and spin transport properties.

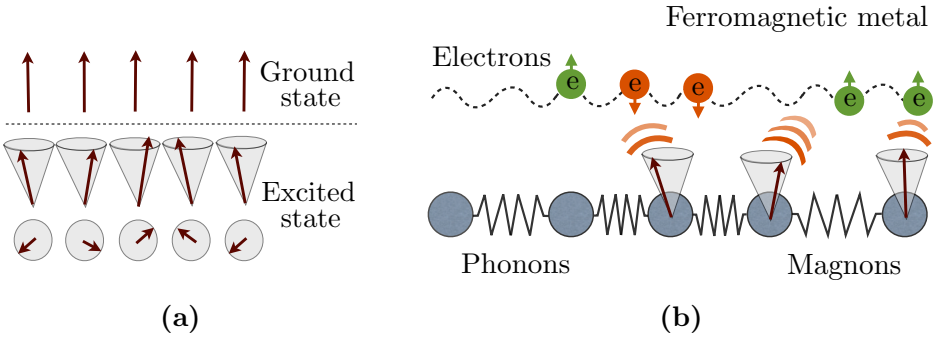


**Figure 1.1:** (a) In the ground state of a ferromagnet, all the spins point in the same direction. The lowest energy excitation is a spin wave, i.e., a collective precession of the magnetic moments around their equilibrium orientation. (b) Cartoon of magnon-phonon and magnon-electron interactions in a ferromagnetic metal.

In metals, the itinerant electrons engendering charge transport interact as well with the localized magnetic moments, as depicted in Fig. 1.1(b). The interactions between magnons and conduction electrons affect the transport of charge current, giving rise to phenomena such as magnon drag [1, 2]. As heat flows are known to induce the diffusive motion of both electrons and magnons, understanding and harnessing their interaction could open up new prospects for improving existing thermoelectric devices. While some progress has been made in this direction, a complete theoretical framework is still lacking.

In the majority of magnetic insulating materials, magnons have been observed as incoherent thermal fluctuations of the underlying magnetization. Nonetheless, the bosonic nature of magnons suggests the possibility of achieving a magnon Bose-Einstein condensate (BEC), i.e, a coherent state surviving even at room temperature. Due to the lack of charge degrees of freedom, magnetic insulating systems are an ideal testing ground for studying such phenomena. The first observation of a magnon Bose-Einstein condensate in YIG was reported by Demokritov *et al.* [3]. In this experiment, the high density of magnons needed for the condensate to form was achieved via external pumping; this is in principle a non-equilibrium phenomenon, and the resulting state is a quasi-equilibrium magnon BEC with a finite lifetime. There are, however, magnetic systems in which a magnon BEC can emerge as a true equilibrium ordered state, such as easy-plane magnets [4, 5], which will be discussed in detail in the next section.

## 1.2 Easy-plane magnetic systems

In this section we calculate the ground states of an idealized easy-plane magnetic system. Specifically, we show that a BEC of magnons can be induced by sweeping the magnetic field, and that the hydrodynamic description of the spin currents carried by the magnon BEC mimics the one of neutral superfluids, thereby introducing the state dubbed as *spin superfluid*. Finally, we derive the equilibrium phase diagram of the magnetic system.

### 1.2.1 Ground states

The free-energy functional of an ideal easy-plane magnet subject to a magnetic field $\mathbf{B} = B\hat{\mathbf{z}}$ can be written as

$$\mathcal{F}[\mathbf{s}] = \int dV \left( -\frac{A}{2s}\mathbf{s} \cdot \nabla^2 \mathbf{s} + Bs_z + \frac{K}{2s}s_z^2 \right) , \tag{1.1}$$

where $\mathbf{s} = s\mathbf{n}$ is the (three-component) spin density (in units of $\hbar$), with $s$ being the saturation spin density and $\mathbf{n}$ the spin-density orientation. The energy cost of a non-collinear arrangement of the spins, which emerges as a consequence of Pauli exclusion principle, is parametrized by the exchange stiffness $A$. When $A > 0$ ($A < 0$), the spins are aligned parallel (antiparallel) to each other and the system is ferromagnetic (antiferromagnetic). Here we consider $A > 0$. The magnetic anisotropy $K$ stems from the underlying crystal structure and spin-orbit coupling, and here is taken as well to be positive, i.e., $K > 0$. For $K > 0$, Eq. (1.1) shows that the system can gain energy by having its magnetization lying within the $xy$ plane, but that there is no preferred direction in this plane. The classical ground state of Eq. (1.1) has uniform spin density, which minimizes the free energy cost of spin density non-uniformity $\propto A$. Minimizing the energy (1.1) for a uniform spin density yields, for positive $B < K$,

$$n_z = -\frac{B}{K} . \tag{1.2}$$

Equation (1.2) shows that the $z$-component of the spin density orientation is determined by the interplay between the magnetic field and the planar anisotropy. Namely, when $B < K$, the competition between the anisotropy and the magnetic field gives rise to a tilt of the spin density orientation away from the $z$ direction, as shown in Fig. 1.2(a). Note that, for our purposes, here we consider a small tilt in the $z$-projection of the spin density, i.e., $K \simeq B$. On the other hand, when $B \geq K$, the spin density orientation is

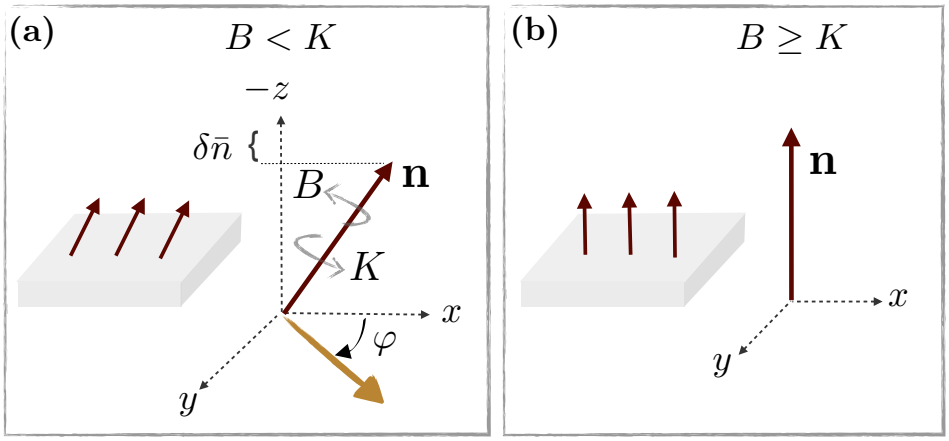


**Figure 1.2:** Ground states of an easy-plane ferromagnet. (a) For $B < K$, the interplay between the magnetic field and the anisotropy leads to a tilt of the spin density orientation $\mathbf{n}$, which can be parametrized by the reduction $\delta\bar{n}$ of its $z$-projection and the azimuthal angle $\varphi$. (b) For $B \geq K$, the unit vector $\mathbf{n}$ is aligned along $-\mathbf{z}$.

given by $n_z = -1$ [see Fig. 1.2(b)]. The small excitations above the ground states $\mathbf{n}_{g1}$ and $\mathbf{n}_{g2}$ that exist for $B \geq K$ and $B < K$, respectively, can be parametrized as

$$\mathbf{n}_{g1} = \begin{pmatrix} \delta n_x \\ \delta n_y \\ -1 \end{pmatrix}, \qquad \mathbf{n}_{g2} = \begin{pmatrix} \cos\varphi \\ \sin\varphi \\ -1 + \delta\bar{n} \end{pmatrix}, \tag{1.3}$$

where $\varphi$ and $\delta n_{x,y}$ are the azimuthal angle and transverse fluctuations of the spin density orientation, respectively, and $\delta\bar{n}$ parametrizes the reduction of $z$-projection of the spin-density orientation.

Generally, the dynamics of the spin density obeys the Landau-Lifshitz-Gilbert equation [6]

$$\frac{\partial \mathbf{n}}{\partial t} = \mathbf{n} \times \left( -\frac{1}{\hbar} \frac{\delta \mathcal{F}[\mathbf{n}]}{\delta \mathbf{n}} \right) - \alpha \mathbf{n} \times \frac{\partial \mathbf{n}}{\partial t}, \tag{1.4}$$

where the Gilbert damping parameter $\alpha$ is a dimensionless number accounting for spin relaxation [7]. Plugging Eq. (1.1) into Eq. (1.4) leads to

$$\frac{\partial \mathbf{n}}{\partial t} = \frac{A}{\hbar} \mathbf{n} \times \nabla^2 \mathbf{n} - \frac{K}{\hbar} \mathbf{n} \times n_z \hat{\mathbf{z}} - \frac{B}{\hbar} \mathbf{n} \times \mathbf{z} - \alpha \mathbf{n} \times \frac{\partial \mathbf{n}}{\partial t}. \tag{1.5}$$

Up to linear order in the transverse fluctuations, i.e., $|\delta n_x|, |\delta n_y| \ll 1$, the transverse spin dynamics of $\mathbf{n}_{g1}$ can be determined from Eq. (1.5) as

$$\hbar \frac{\partial \delta n_x}{\partial t} = +A\nabla^2 \delta n_y + (K - B)\delta n_y - \alpha\hbar \frac{\partial \delta n_y}{\partial t}\,, \tag{1.6}$$

$$\hbar \frac{\partial \delta n_y}{\partial t} = -A\nabla^2 \delta n_x - (K - B)\delta n_x + \alpha\hbar \frac{\partial \delta n_x}{\partial t}\,. \tag{1.7}$$

Taking the second order time derivative of $\delta n_x$ and making use of Eqs. (1.6) and (1.7) leads to the quadratic dispersion of the ferromagnetic ground state (for $\alpha \to 0$):

$$\hbar\omega_k = Ak^2 + \hbar\Omega\,, \tag{1.8}$$

where $\hbar\Omega = B - K$ is the magnon gap.
We proceed by computing the dynamics of the fluctuations around the tilted ground state $\mathbf{n}_{g2}$ which, up to linear order in $\delta\bar{n}$ and $\partial_x\varphi$, leads to

$$\hbar \frac{d\delta\bar{n}}{dt} = A\nabla^2\varphi\,, \tag{1.9}$$

$$\hbar \frac{d\phi}{dt} = B - K + K\delta\bar{n} - A\nabla^2\delta\bar{n}\,. \tag{1.10}$$

By plugging Eq. (1.9) into the second-order time derivative of Eq. (1.10), and Fourier transforming the resulting equation, we obtain, for the low momentum regime, the following linear spin-wave dispersion

$$\hbar\omega_k = \hbar ck\,, \tag{1.11}$$

where we have defined the spin-wave velocity $c = \sqrt{AK}/\hbar$. According to Landau's criterion [8], the observation of such linear dispersion at low momentum regime is an indication of superfluidity. This dispersion indeed shows that the ground state behaves as a superfluid, meaning that if an object is moved in the condensate at a velocity smaller than $c$, it will not be energetically favorable to produce excitations and the object will move without dissipation.

Here, the superfluidity arises from the spontaneous symmetry breaking of the global $U(1)$ symmetry of the free energy (1.1). For $B < K$, the possible ground states of the theory are given by a tilted spin with an azimuthal angle $\varphi$, which is the same at every lattice point, but may itself take any value. The phase of the ground state breaks the global $U(1)$ symmetry of the theory, giving rise to a Goldstone mode with dispersion described by Eq. (1.11).

### 1.2.2 Magnon BEC and superfluid dynamics

Superfluidity and BEC are intimately related. Indeed, the analogy between the supercurrent of electric charge in superconductors and the mass superflow in helium relies on the common origin of these phenomena, i.e., the spontaneous breaking of the $U(1)$ symmetry underlying Bose-Einstein condensation (of either atoms or Cooper pairs) and the associated macroscopic quantum coherence. This suggests that spin superfluidity arising in magnetic system might be interpreted in terms of Bose-Einstein condensation of magnons.

To view the tilted ground state $\mathbf{n}_{g2}$ of an easy-plane ferromagnet as a BEC of magnons, we need to introduce the Holstein-Primakoff transformation [9]:

$$\hat{s}_+ = \sqrt{2s - \hat{\Phi}^\dagger\hat{\Phi}}\,\hat{\Phi}\,, \tag{1.12}$$

$$\hat{s}_- = \hat{\Phi}^\dagger\sqrt{2s - \hat{\Phi}^\dagger\hat{\Phi}}\,, \tag{1.13}$$

$$\hat{s}_z = \hat{\Phi}^\dagger\hat{\Phi} - s\,, \tag{1.14}$$

with $\hat{s}_\pm = \hat{s}_x \pm i\hat{s}_y$ being the spin raising (lowering) operator. Equations (1.12), (1.13) and (1.14) map the spin density operators into the bosonic canonical operators $\hat{\Phi}^\dagger$ and $\hat{\Phi}$, which create and annihilate a magnon respectively. The expectation value of the spin operator (1.14) for the tilted ground state of Eq. (1.1) can be written as

$$\langle\hat{s}_z\rangle = n_c - s\,, \tag{1.15}$$

where $n_c = \langle\hat{\Phi}^\dagger\hat{\Phi}\rangle = s(1 - B/K)$ is the density of magnons in the ground state. The uniformity of the spin orientation $\mathbf{n}_{g2}$ implies a finite density of magnons at each point in space, which translates into a macroscopic occupation of the ground state by bosonic quasi-particles, in other words Bose-Einstein condensation.
This state can be described in the dilute approximation, $n_c/s \ll 1$, by the Gross-Pitaevskii (GP) theory at zero temperature [10]. In the dilute regime, Eqs. (1.12) and (1.13) can be expanded as

$$\hat{s}_+ \simeq \sqrt{2s}\hat{\Phi}\,, \tag{1.16}$$

$$\hat{s}_- \simeq \sqrt{2s}\hat{\Phi}^\dagger\,. \tag{1.17}$$

We now introduce the BEC macroscopic wavefunction as $\Phi \equiv \langle\hat{\Phi}\rangle$, where the expectation value $\langle..\rangle$ is taken over the coherent ground state. Consid-

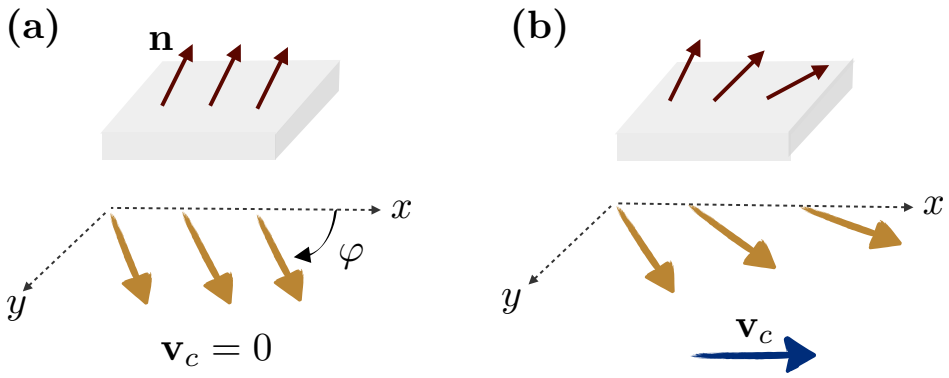


**Figure 1.3:** (a) A uniform spin density orientation $\mathbf{n}$ with azimuthal angle $\varphi$ across the entire system. This configuration corresponds to a vanishing superfluid velocity $\mathbf{v}_c$. (b) A gradient in the azimuthal angle of the spin density orientation results in a finite superfluid velocity $\mathbf{v}_c \propto -\boldsymbol{\nabla}\varphi$.

ering the Hamiltonian corresponding to Eq. (1.1), i.e.,

$$\mathcal{H} = \int dV \left( -\frac{A}{2s}\hat{\mathbf{s}} \cdot \nabla^2 \hat{\mathbf{s}} + B\hat{s}_z + \frac{K}{2s}\hat{s}_z^2 \right) . \tag{1.18}$$

and substituting Eqs. (1.14), (1.16) and (1.17) into Eq. (1.18), we derive the equation of motion for $\Phi$, taking the Gilbert damping to be zero, as

$$i\hbar \frac{\partial \Phi}{\partial t} = \left[ \hbar\Omega + \frac{K}{s}|\Phi|^2 \right] \Phi - A\nabla^2 \Phi \, . \tag{1.19}$$

which is the time-dependent GP equation. Expressing the BEC order parameter as a complex scalar function of position and time, i.e., $\Phi = \sqrt{n_c}(\mathbf{r}, t)e^{-i\varphi(\mathbf{r},t)}$, where $n_c$ and $\varphi$ are the density and (minus) the phase of the condensate respectively, the time dependent GP equation can be rewritten as coupled equations for the condensate density $n_c$ and frequency $\omega = \partial_t \varphi$ :

$$\hbar\omega = \left[ \hbar\Omega + \frac{K n_c}{s} \right] + A \left[ \frac{\nabla^2 n_c}{2n_c} - \frac{(\boldsymbol{\nabla} n_c)^2}{4n_c^2} \right] - A(\nabla\varphi)^2 \, , \tag{1.20}$$

$$\frac{\partial n_c}{\partial t} = \frac{2A}{\hbar}\boldsymbol{\nabla} n_c \cdot \boldsymbol{\nabla}\varphi + \frac{2A}{\hbar}\nabla^2\varphi \, . \tag{1.21}$$

The second equation has the form of a continuity equation if we define the superfluid current $\mathbf{j}_c$ and velocity $\mathbf{v}_c$ as

$$\mathbf{j}_c = n_c \mathbf{v}_c \, , \quad \text{with} \quad \mathbf{v}_c = -\frac{2A}{\hbar}\boldsymbol{\nabla}\varphi \, . \tag{1.22}$$

Equation (1.22) shows that the spin superfluid current arises from the gradient of the azimuthal angle of the spin density in the $xy$ plane, as schematically shown in Figs. 1.3(a) and (b). Substituting Eq. (1.22) into Eq. (1.21) yields

$$\frac{\partial n_c}{\partial t} = -\boldsymbol{\nabla} \cdot \mathbf{j}_c \,. \tag{1.23}$$

The continuity equation (1.23) is a direct consequence of the conservation of the $z$-component of the spin density in an ideal easy-plane ferromagnet[1]

The motion of the spin superfluid corresponds to that of an irrotational flow, since the velocity is proportional to the gradient of a scalar quantity. Indeed, we can immediately see from Eq. (1.22) that the motion of the condensate is irrotational:

$$\boldsymbol{\nabla} \times \mathbf{v}_c = -\frac{2A}{\hbar} \boldsymbol{\nabla} \times \boldsymbol{\nabla} \varphi = 0 \,. \tag{1.24}$$

### 1.2.3 Finite temperature

Finite temperature gives rise to quasi-particle excitations occupying higher-energy states. The coexistence of a cloud of thermal magnons with the condensate can be captured within the Gross-Pitaevskii theory by introducing the noncondensate field operator $\hat{\psi}$ as [10, 11]

$$\hat{\Phi} = \Phi + \hat{\psi} \,, \tag{1.25}$$

with $\langle \hat{\psi} \rangle = 0$. We define $f_{\mathbf{p}}(\mathbf{r}, t)$ as the Wigner transform of the field $\langle \hat{\psi}^\dagger(\mathbf{r}', t) \hat{\psi}(\mathbf{r}'', t) \rangle$ such that

$$n_x(\mathbf{r}, t) = \int d^3 p f_{\mathbf{p}}(\mathbf{r}, t) / (2\pi\hbar)^3 \,, \tag{1.26}$$

is the noncondensate density. According to the Hamiltonian (1.18), the thermal cloud experiences the Hartree-Fock mean-field potential $U = \hbar\Omega + (K/s)(2n_c + 2n_x)$. At high temperatures, $T \gg U$ (setting $k_B \equiv 1$, while still assuming that $T \ll T_c$, the Curie temperature), the thermal cloud can be described by a quantum kinetic equation for the single-particle distribution function $f_{\mathbf{p}}(\mathbf{r}, t)$

$$\partial_t f + \mathbf{p} \cdot \partial_{\mathbf{r}} f / m - \partial_{\mathbf{r}} U \cdot \partial_{\mathbf{p}} f = (f_p - f)/\tau_\alpha + (\bar{f} - f)/\tau + C_{cx} + C_{xx} \,, \tag{1.27}$$

[1] One can convince himself(herself) that the $z$-component of the spin density is conserved by noticing that the Hamiltonian (1.18) is invariant under rotations around the $z$-axis.

with $\bar{f}$ being the $\mathbf{p}$-space angular average of $f_{\mathbf{p}}(\mathbf{r},t)$ (above abbreviated as $f$) and $f_p$ is the phonon (Bose-Einstein) distribution function. The relaxation time $\tau_\alpha = \hbar/2\alpha(p^2/2m+U)$ describes the Gilbert damping (associated with the phonon bath), while the strength of spin-preserving momentum scattering of magnons is parametrized by an energy-dependent time scale $\tau$. The scattering interactions with the condensate and among the thermal magnons are respectively described by the collision integrals $C_{cx}$ and $C_{xx}$ [10]. The latter process, which is governed by the exchange interactions, is expected to be fast at high temperatures [12], forcing the cloud towards a local Bose-Einstein profile with well-defined temperature $T$ and chemical potential $\mu$. Hence, at thermal equilibrium, the thermal cloud is described then by the Bose-Einstein distribution function $f_B[(\mathbf{p}^2/2m+U-\mu)/T]$, with $f_{\rm B}(x) \equiv (e^x-1)^{-1}$, and $T$ and $\mu$ being the magnon temperature and chemical potential respectively. While the magnons in the thermal cloud are assumed to be in equilibrium among themselves, the condensate and thermal cloud components may not be in diffusive local equilibrium with each other, which leads to a generally non-vanishing condensate - thermal cloud scattering rate, i.e.,

$$\Gamma_{cx} = \int d^3p\, C_{cx}/(2\pi\hbar)^3. \tag{1.28}$$

Note that, while the scattering processes encoded by $C_{cx}$ locally change the relative number of condensate and thermal magnons, they conserve the total magnon number. From the Zaremba–Nikuni–Griffin (ZNG) approximation [10], we have

$$\Gamma_{cx} \propto \mu - \hbar\omega\,. \tag{1.29}$$

At finite temperatures, Eq. (1.20) becomes

$$\hbar\omega = \left[\hbar\Omega + K\frac{n_c+2n_x}{s}\right] + A\left[\frac{\nabla^2 n_c}{2n_c} - \frac{(\boldsymbol{\nabla} n_c)^2}{4n_c^2}\right] - A(\nabla\varphi)^2\,. \tag{1.30}$$

In a bulk equilibrium, all the quantities are spatially uniform. We can then rewrite Eq. (1.29) as

$$\Gamma_{cx} \propto \mu - \hbar\Omega - K(n_c+2n_x)/s\,. \tag{1.31}$$

In static thermal equilibrium between the thermal cloud and the condensate, Eq. (1.29) vanishes, leading to

$$\mu = \hbar\Omega + K(n_c+2n_x)/s\,. \tag{1.32}$$

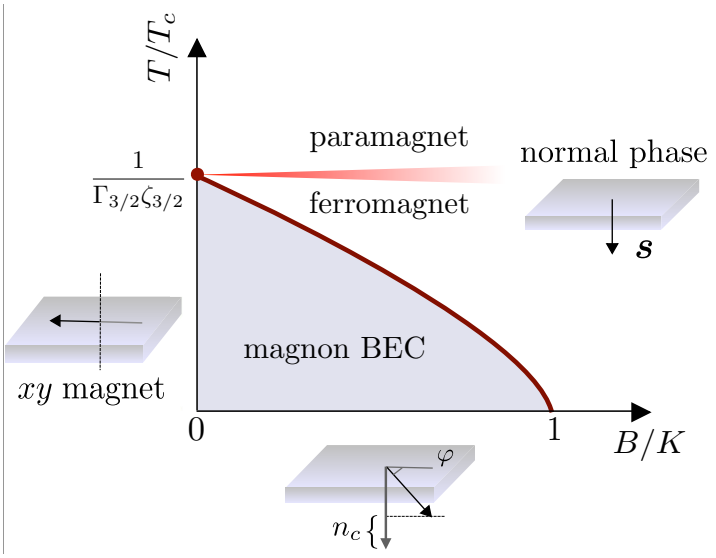


**Figure 1.4:** Equilibrium phase diagram. The condensate phase boundary is at $T/T_c = (1 - B/K)^{2/3}/\Gamma_{3/2}\zeta_{3/2}$, where $T_c \equiv As^{2/3}$. The Curie temperature $T_c/\Gamma_{3/2}\zeta_{3/2}$ is indicated by a red circle, while the fan-out line represents a sharp crossover between paramagnetic and ferromagnetic phases. In the normal phase, the net spin density $\mathbf{s}$ is oriented along the (negative) $z$ axis; the condensate spontaneously breaks $U(1)$ symmetry around the $z$ axis, as manifested by a static canting of the magnetization, whose deviation from its normal-state equilibrium value along the $z$ axis is parametrized by the condensate density $n_c$. In the absence of an applied field $B$, the ferromagnet is a planar $xy$ magnet.

Hence the thermal magnon equilibrium density reads as

$$\begin{aligned} n_x &= \int \frac{d^3p}{(2\pi\hbar)^3} \frac{1}{e^{\frac{p^2/2m + Kn_c/s}{T}} - 1} \\ &= \frac{1}{2}\left[\left(1 - \frac{B}{K}\right)s - n_c\right]. \end{aligned} \tag{1.33}$$

This provides the mean-field self-consistency relation for $n_c$ and allows to determine the transition temperature $T$ (as a function of the external field $B < K$), where $n_c \to 0$:

$$\frac{T}{T_c} \to \frac{1}{\Gamma_{3/2}\zeta_{3/2}}\left(1 - \frac{B}{K}\right)^{2/3}. \tag{1.34}$$

Here $T_c \equiv s^{2/3}A$, and $\Gamma$ and $\zeta$ are respectively gamma and Riemann zeta functions. Figure 1.4 shows the equilibrium phase diagram of the easy-plane

condensate corresponding to Eq. (1.34).

## 1.3 Electron- and phonon-magnon interactions

In this section we discuss the interactions arising between magnons and electrons, and magnons and phonons respectively. The coupling between electrons and magnons occurs in the bulk of magnetic metals and at the interface between metals and magnetic insulators. These cases are exemplified in Section 1.3.1 and 1.3.2 respectively. At finite temperatures, magnons and phonons interact in both metallic and insulating systems. We introduce the magnetoelastic coupling in Section 1.3.3 while considering for simplicity insulating systems.

### 1.3.1 Bulk electron-magnon interactions

Spin-dependent transport phenomena emerging in ferromagnetic metals can be understood within a simple model of ferromagnetism, i.e., the so-called *sd* model. The *sd* model distinguishes electrons into two different kinds according to their dynamics: itinerant $s$ electrons, which engender charge current and stem from the Fermi surface, and $d$ electrons, which are localized at the lattice sites and arise from the entire Fermi sea.

This picture is motivated by the specific band-structure of certain ferromagnets, with $d$ electrons possessing quite flat bands that constrains their mobility due to a large effective mass. Due to the strong exchange interactions within $d$ electrons, the collective dynamics of the ($d$ electrons) spins $\mathbf{S}$ is slow respect to the dynamics of the $s$ electrons spins. Hence, the local moments $\mathbf{S}$ can be described by a Zeeman-like field $\langle \mathbf{S} \rangle$ felt by the itinerant electrons, with directional unit vector $\mathbf{n}(\mathbf{r}, t)$ defined as

$$\langle \mathbf{S} \rangle = S\mathbf{n}(\mathbf{r}, t)\,, \tag{1.35}$$

where $S$ is the net spin. The interaction strength between $s$ and $d$ electrons depends on the overlap integral between the $s$ and $d$ orbitals. In the simplest case, we can approximate the overlap integral with a constant and write the *sd* Hamiltonian as

$$H_{sd} = -\frac{\Delta}{2}\boldsymbol{\sigma} \cdot S\mathbf{n}(\mathbf{r}, t)\,, \tag{1.36}$$

where $\Delta$ is the exchange field and $\boldsymbol{\sigma}$ is the vector of Pauli matrices. The interaction (1.36) is responsible for the transfer of spin angular momentum between the itinerant electron spins and the localized moments, and it

underlies the effects on which we focus in this section, namely the spin transfer torque and the spin motive force. Spin transfer torque stands for the torque exerted by a spin current on a non collinear spin texture [13,14], while the reciprocal effect, i.e., the force experienced by itinerant electrons due to a dynamical spin texture, is dubbed as spin motive force [1,2,15].

We consider a charge current $\boldsymbol{j}$ traveling in a metallic ferromagnet through a magnetization texture as the one depicted in Fig. (1.5). We assume that the spin orientation of the itinerant electrons follows the underlying magnetic landscape adiabatically while flowing through the ferromagnet. Then, the electron flow gives rise to a net spin current $\boldsymbol{j}_{s,i}$ (for the spin-$i$ component) given by

$$\boldsymbol{j}_{s,i} = \frac{\hbar P}{2e}\boldsymbol{j} n_i \,, \tag{1.37}$$

where $e$ is the carrier charge (here negative for electrons), $P = (\sigma_\uparrow - \sigma_\downarrow)/\sigma$ is the conducting spin polarization, $\sigma_\uparrow$ and $\sigma_\downarrow$ are the majority and minority electron conductivities, and $\sigma = \sigma_\uparrow + \sigma_\downarrow$ is the total electrical conductivity. When the spin current starts flowing through a sample with inhomogeneous spin density, the electrons spins orient themselves along the magnetization direction of the first domain they encounter. Then, while keeping flowing, their orientation will be altered by the spin density which exerts a torque $\propto -\Delta J$ in order to reorient them along the new local spin density direction. Assuming that the angular momentum is conserved, the conduction electrons exert an opposite torque $\propto \Delta J$ on the spin density (see Fig. 1.39). The change in the spin density dynamics resulting from this torque reads as

$$\frac{\partial \mathbf{n}}{\partial t} = -\frac{\hbar P}{2e s_0}(j_i \nabla_i)\mathbf{n} \,, \tag{1.38}$$

where $s_0$ is the equilibrium spin density. Equation (1.38) accounts for the *adiabatic* contribution to the spin-transfer torque.

However, if we include processes such as spin-flip relaxation, the electron spin density acquires a component which is transverse to the local magnetization gradient. Moreover, as the exchange field $\Delta$ in Eq. (1.36) is not infinite, there is generally a finite misalignment between the electrons spins and the magnetization. These effects give rise to a *dissipative* contribution to the spin-transfer torque, which acts perpendicular to the adiabatic torque. The change in the magnetization dynamics due to the dissipative spin-transfer torque can be written as

$$\frac{\partial \mathbf{n}}{\partial t} = \beta \mathbf{n} \times \left( -\frac{\hbar P}{2e s_0} j_i \nabla_i \right) \mathbf{n} \,, \tag{1.39}$$

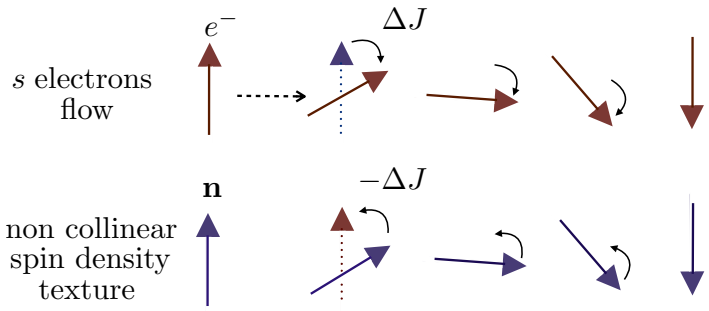


**Figure 1.5:** Schematics of the adiabatic spin transfer torque. A conduction-electron spin and the spin density orientation $\mathbf{n}$ are represented by red and blue arrows, respectively. While flowing, the electron spin follows adiabatically the spin density texture $\mathbf{n}$. When the electron spin realigns along the spin density, the electron loses spin angular momentum, which is transferred to the spin texture. This can be described in terms of a torque $\Delta J$ exerted by the electrons on the spin density, or, assuming conservation of spin angular momentum, by a torque $-\Delta J$ endeavored by the spin density on the electrons.

where we have introduced the dimensionless parameter $\beta$. The latter depends on the relaxation mechanisms of the transverse electron spin density and it is sensitive to microscopic details [1, 2].

The spin motive force is the inverse effect to the spin transfer torque. Hence, the charge current density induced by spin dynamics of the local moments can be derived from Eqs. (1.38) and (1.39) via Onsager reciprocity as [16]

$$j_i = \frac{\hbar P \sigma}{2e} \left[ \mathbf{n} \cdot (\partial_t \mathbf{n} \times \nabla_i \mathbf{n}) - \beta (\partial_t \mathbf{n} \cdot \nabla_i \mathbf{n}) \right] . \tag{1.40}$$

Equation (1.40) leads ultimately to identify the spin motive force on the conduction electrons (which is opposite for opposite spins)

$$F_i = \frac{\hbar}{2} \left[ \mathbf{n} \cdot (\partial_t \mathbf{n} \times \nabla_i \mathbf{n}) - \beta (\partial_t \mathbf{n} \cdot \nabla_i \mathbf{n}) \right] , \tag{1.41}$$

for spins up along $\mathbf{n}$. Equation (1.38), (1.39) and (1.41) show that two ingredients are essential for the spin-transfer torque and its Onsager reciprocal: the presence of a non-collinear magnetization texture and a non-equilibrium state, i.e., a charge current flow (spin transfer torque) or a dynamical magnetization (spin motive force).

### 1.3.2 Interface electron-magnon interactions

Magnon-electron interactions at the interfaces between magnetic insulator and non-magnetic metallic materials can be described in terms of interfacial spin transfer torque and spin pumping, the latter of which is the counterpart of the spin motive force near an interface. The interfacial spin transfer torque accounts for the excitation of a magnetization dynamics by spin currents generated in an adjacent nonmagnetic material. Spin pumping is the emission of spin current in a nonmagnetic material by the magnetization dynamics of an adjacent magnetic system. Essential to these processes is a coupling between the magnetic and nonmagnetic layers, which, taken to be isotropic, reads as

$$\hat{V}_{int} = \int d\mathbf{x} d\mathbf{x}' V(\mathbf{x}, \mathbf{x}') \hat{\mathbf{n}}(\mathbf{x}) \cdot \hat{\mathbf{s}}(\mathbf{x}') \,, \tag{1.42}$$

where $\hat{\mathbf{n}}(\mathbf{x})$ and $\hat{\mathbf{s}}(\mathbf{x})$ correspond to the orientation of the spin density of the localized spins in the insulator and of the electrons in the metal, respectively. The latter can be written as

$$\hat{\mathbf{s}}(\mathbf{x}) = \frac{1}{2} \sum_{\sigma,\sigma'=\uparrow,\downarrow} \hat{\psi}^\dagger_\sigma(\mathbf{x}) \boldsymbol{\sigma}_{\sigma\sigma'} \hat{\psi}_{\sigma'}(\mathbf{x}) \,, \tag{1.43}$$

where $\boldsymbol{\sigma}$ is a vector of the Pauli matrices, and $c_{\mathbf{k}\sigma}$ and

$$\hat{\psi}_\sigma(\mathbf{r}) = \frac{1}{\sqrt{\mathcal{V}}} \sum_{\mathbf{k}} \hat{c}_{\mathbf{k},\sigma} e^{i\mathbf{k}r} \,, \tag{1.44}$$

are the electron field operators (with $\mathcal{V}$ being nonmagnetic system volume, here equal to the magnetic one), which obey the following fermionic commutation relations

$$\{\hat{c}_{\mathbf{k},\sigma}, \hat{c}^\dagger_{\mathbf{k}',\sigma'}\} = \delta_{\mathbf{k}\mathbf{k}'}\delta_{\sigma\sigma'}, \quad \{\hat{\psi}_\sigma(\mathbf{r}), \hat{\psi}^\dagger_{\sigma'}(\mathbf{r}')\} = \delta(\mathbf{r}-\mathbf{r}')\delta_{\sigma\sigma'}. \tag{1.45}$$

Using Eqs. (1.12), (1.13), (1.14) and (1.43), Eq. (1.42) can be rewritten as

$$\hat{V}_{int} = \frac{1}{2\sqrt{2S}} \sum_{\mathbf{q}\mathbf{k}\mathbf{k}'} \left[ \hat{V}_{\mathbf{q}\mathbf{k}\mathbf{k}'} \hat{\Phi}_{\mathbf{q}} \hat{c}^\dagger_{\mathbf{k}',\uparrow} \hat{c}_{\mathbf{k},\downarrow} + \text{H.c.} \right] , \tag{1.46}$$

Note that we have neglected spin-preserving terms such as $\hat{c}^\dagger_{\mathbf{k},\sigma}\hat{c}_{\mathbf{k}',\sigma}\hat{\Phi}^\dagger_{\boldsymbol{\kappa}}\hat{\Phi}_{\mathbf{q}}$, since such processes do not involve transfer of the $z$-component of spin angular momentum across the interface, and therefore do not contribute to the spin pumping or spin transfer torque. The first term in Eq. (1.46) allows us to visualize spin pumping as a process involving a magnon (carrying

spin up $\hbar$) annihilating in the insulator to create a spin-down hole/spin-up electron pair in the adjacent metal. The Hermitian conjugate corresponds to a reverse electron spin-flip scattering at the interface creating a magnon in the insulator, which contributes to the interfacial spin transfer torque (see Fig. 1.6).

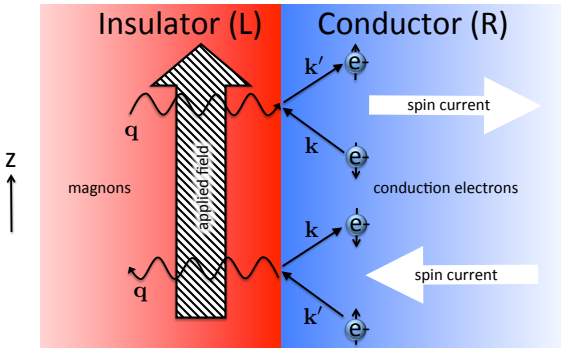


**Figure 1.6:** Cartoon depicting electron-magnon interactions at the interface between a magnetic insulator and a normal metal. Assuming negative gyromagnetic ratio, the spin density in the insulator is oriented along $-\mathbf{z}$ (antiparallel to the applied field), and, hence, a magnon carries a positive angular momentum $+\hbar$. At the metallic side of the interface, a spin-up electron scatters into a spin-down hole, emitting a magnon which tunnels into the insulator. Reversely, a magnon can be absorbed at the interface, giving rise a spin current in the metal. Taken from Ref. [12].

Let us consider a metal with spin accumulation $\boldsymbol{\mu}'$, which points in the direction of the local magnetization, here taken along $\mathbf{z}$, and whose magnitude is equal to the difference of the electrochemical potential of both electron spin species, i.e., $\mu' = \mu_\uparrow - \mu_\downarrow$. The spin accumulation is established via the Spin Hall effect, which will be discussed in detail in section 1.4.1. The temperature of the metallic system is set at $T_e$, while the magnetic insulator is equilibrated at temperature $T_m$. Moreover, we introduce the magnon chemical potential $\mu_m$, which parametrizes a long-living nonequilibrium state in the magnetic insulator that arises upon, e.g., spin injection from a normal metal. The $z$-component of the spin current flowing from the interface into the NM is given by [18, 19]

$$j_s^{int} = -\frac{g_{\uparrow\downarrow}}{4\pi}\mathbf{n} \times \left.\frac{d\mathbf{n}}{dt}\right|_z . \tag{1.47}$$

Here, we have introduced the spin-mixing conductance $g_{\uparrow\downarrow}$, which can be computed using perturbation theory in the coupling $V(\mathbf{x}, \mathbf{x}')$. However, the

value for $g_{\uparrow\downarrow}$ is usually assessed experimentally. Using the parametrization $\mathbf{n} = (\delta n_x, \delta n_y, -1)$ and Eqs. (1.12), (1.13) and (1.14), we can write

$$j_s^{int} = \frac{g_{\uparrow\downarrow}}{\pi\hbar s}\frac{1}{\mathcal{V}}\sum_{\mathbf{k}}\hbar\omega_{\mathbf{k}} n_{\mathbf{k}}\,, \tag{1.48}$$

where $\hbar\omega_{\mathbf{k}}$ is the magnon dispersion and

$$n_{\mathbf{k}} = \langle\hat{\Phi}_{\mathbf{k}}^{\dagger}\hat{\Phi}_{\mathbf{k}}\rangle = f_{BE}\left(\frac{\hbar\omega_{\mathbf{k}} - \mu_m}{k_B T_m}\right), \tag{1.49}$$

is the magnon number at wavevector $\mathbf{k}$. Note that an additional factor 2 in Eq. (1.48) stems from the constructive interference between magnons at the interface [12]. In equilibrium, the current passing across the interface is zero. The equilibrium condition can be imposed by rewriting

$$f_{BE}\left(\frac{\hbar\omega_{\mathbf{k}} - \mu_m}{k_B T_m}\right) \to f_{BE}\left(\frac{\hbar\omega_{\mathbf{k}} - \mu_m}{k_B T_m}\right) - f_{BE}\left(\frac{\hbar\omega_{\mathbf{k}} - \mu'}{k_B T_e}\right), \tag{1.50}$$

where the second contribution corresponds to the effect reciprocal to spin pumping, i.e., the spin transfer torque. Using Eq. (1.50), one can rewrite Eq. (1.47) as an integral over the energy, i.e.,

$$j_s^{int} = -\frac{g_{\uparrow\downarrow}}{\pi\hbar s}\int d\epsilon D(\epsilon)(\epsilon - \mu')\left[f_{BE}\left(\frac{\hbar\omega_{\mathbf{k}} - \mu_m}{k_B T_m}\right) - f_{BE}\left(\frac{\hbar\omega_{\mathbf{k}} - \mu'}{k_B T_e}\right)\right], \tag{1.51}$$

where $D(\epsilon)$ is the magnon density of states. Equation (1.51) has been also derived rigorously from a Fermi's Golden Rule treatment of the interface coupling in Ref. [12].

Let us now focus once more on easy-plane ferromagnets. In the normal state, Eq. (1.51) represents the only contribution to the interfacial current. In the BEC phase, the condensate magnons contribute as well. At finite temperature and up to linear order in $\partial_x\varphi$, Eq. (1.20) becomes, for a homogeneous spin density,

$$\hbar\omega = \hbar\Omega + \frac{K(n_c + 2n_x)}{s}\,. \tag{1.52}$$

Then, Eq. (4.34) can be rewritten as

$$\mu_{eq} = \hbar\omega, \tag{1.53}$$

which corresponds to the condition of static thermal equilibrium between condensate and thermal magnons. Equation (1.53) shows that $\hbar\omega$ plays the

role of a condensate chemical potential $\mu_c$. On the other side, Eq. (1.48) for the ground state, i.e., $\mathbf{k} = 0$, reads as

$$j_{s,c}^{int} = \frac{g_{\uparrow\downarrow} n_c}{2\pi\hbar s} \mu_c \,. \tag{1.54}$$

Substituting $\mu_c \to \mu_c - \mu'$ to account for the spin accumulation $\mu'$ in the metallic lead, the condensate contribution to the interfacial spin current is [17]

$$j_{s,c}^{int} = \frac{g_{\uparrow\downarrow} n_c}{2\pi\hbar s} (\mu_c - \mu') \,. \tag{1.55}$$

When imposing boundary conditions for an easy-plane magnet in the BEC phase, both Eqs. (1.51) and (1.55) have to be taken into account, as we will see in Chapter 2 of this Thesis.

### 1.3.3 Magnetoelastic coupling

It is common to assume that, within a good approximation, the lattice vibrations are unaffected by the behavior of the magnetic moments associated with the atoms or ions in a crystal. On the other hand, when focusing on magnetic excitations, the ions or atoms from which the magnetic moments stem are treated as they are frozen in their positions. For materials in which the coupling between elastic and magnetic is not negligible, this non-interacting approximation has to be abandoned. Indeed, while the lattice vibrates, the position of the spins varies, and hence the interactions among them are altered [see Fig. 4.17(a)], as well as the resulting spin transport properties. To account for the magneto-elastic coupling, the Hamitonian describing the isolated magnetic and elastic systems needs to be supplemented by an interaction Hamiltonian involving both the displacement of an atomic (or ionic) positions and the spin orientations. The eigenmodes of such Hamiltonian are magnetoelastic waves, or, in the second-quantized language, magnon-polarons, i.e., coupled magnon and phonon modes [21–24]. As shown in Fig. 4.17(b), far away from the intersection point between the uncoupled elastic and magnetic dispersion, the magnon-polaron modes behave as magnon- or phonon-like quasiparticles. In proximity of the intersection points instead, the phonon and magnon modes are strongly hybridized and the resulting dispersion of the magnon-polaron modes is neither magnon- or phonon-like.

Focusing on spin properties, it is reasonable to expect that they might be altered when magnons hybridize with phonons. The portion of momentum space over which the behavior of magnon- polaron modes differs

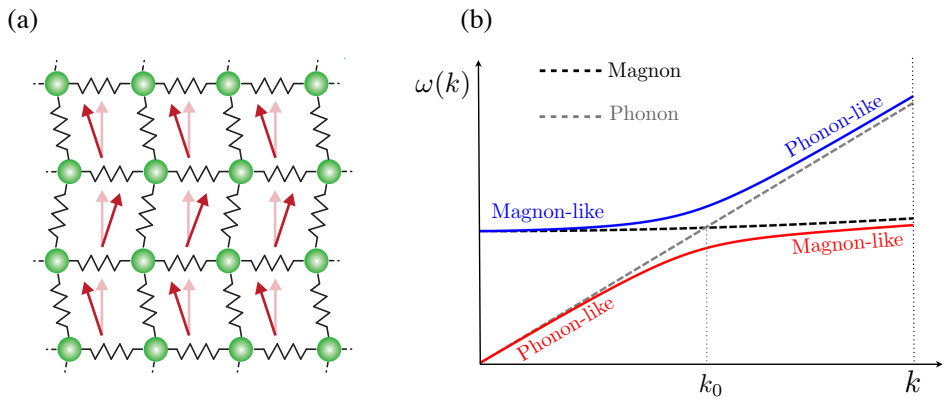


**Figure 1.7:** (a) The displacement of an atom or ion (green dot), i.e., an elastic excitation, alters the orientation of the spin (red arrow) at the corresponding lattice site. (b) Magnon, phonon, and magnon-polarons (blue and red lines) dispersions $\omega(k)$. The magnon and phonon branches intersect at $k_0$.

from the one of the uncoupled modes turns out to be maximized when the magnon dispersion is tangent to the phonon branch. This condition can be achieved by tuning the magnetic field.

Recent spin transport measurements detected anomalies at the field at which magnon and phonon branches are tangent to each other [20]. The latter suggests that the origin of these anomalies is rooted in the magneto-elastic coupling, and calls for a theoretical framework accounting for the spin transport properties of composite quasi-excitations such as magnon-polarons. This is developed in Chapter 4 of this Thesis.

## 1.4 Generation of spin currents

There are only few mechanisms which can be used to generate pure spin currents. Specifically, we focus on spin Hall effect (SHE), spin pumping, and spin Seebeck effect (SSE), where a spin current is generated as the result of, respectively, a charge current, magnetization dynamics, and thermal bias. In the following, we review the origin of these mechanisms and their experimental status.

### 1.4.1 Spin Hall and inverse Spin Hall effect

When an electrical current $\mathbf{j}_c$ flows in a nonmagnetic conductor, the electrons of opposite spins are deflected to opposite transverse directions by

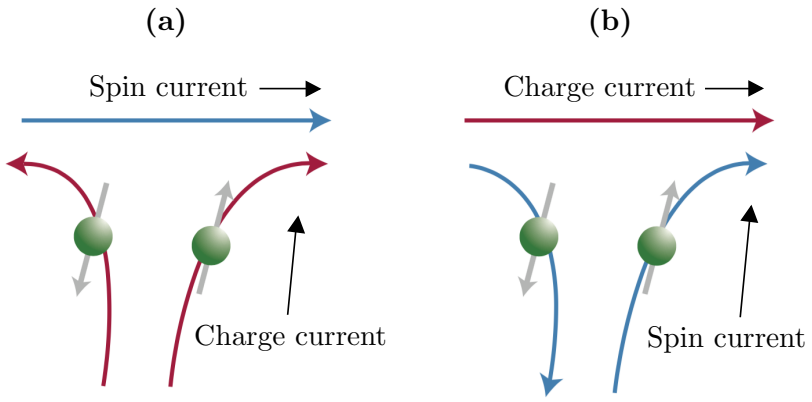


**Figure 1.8:** Schematics of SHE (a) and ISHE (b). In the SHE, a longitudinal charge current in a nonmagnetic metal with strong spin-orbit coupling is converted into a transverse pure spin current. For a pure spin current, the spin-orbit interaction gives rise to a transverse charge flow. This mechanism is known as the inverse spin Hall effect. Adapted from Ref. [27]

spin-orbit interactions, as shown in Fig. 1.8(a). The deflection gives rise to a transverse pure spin current $\mathbf{j}_s$ with a spin polarization $\boldsymbol{\sigma}$ perpendicular to the charge and spin current [25, 26]. The resulting spin current $\mathbf{j}_s$ can be written (in units of electric current) as

$$\mathbf{j}_s = \theta_{SH}\mathbf{j}_c \times \boldsymbol{\sigma}\,, \tag{1.56}$$

where $\theta_{SH}$ is the Spin Hall angle, which is of the order of $10^{-2}$ for metals with strong-orbit coupling. In the reciprocal effect, i.e., the inverse spin Hall effect, a pure spin current in a metal with strong SOC generates a charge current and charge accumulation in the transverse direction [see Fig. 1.8(b)]. The resulting charge current reads as

$$\mathbf{j}_c = \theta_{SH}\boldsymbol{\sigma} \times \mathbf{j}_s\,. \tag{1.57}$$

The spin Hall and the inverse spin Hall effect are the most widely used methods for, respectively, generating and detecting a pure spin current. In synergy with the interfacial spin transfer torque and spin pumping, these effects are deployed to manipulate and detect the magnetization dynamics.

As we saw in the previous section, the magnetization dynamics impinging on a normal metal|magnetic insulator interface triggers a pure spin current in the conductor (spin pumping). Via the inverse Spin Hall effect, the spin current is then converted into a measurable electrical voltage. These mechanisms have been experimentally verified by Kajiwara *et*

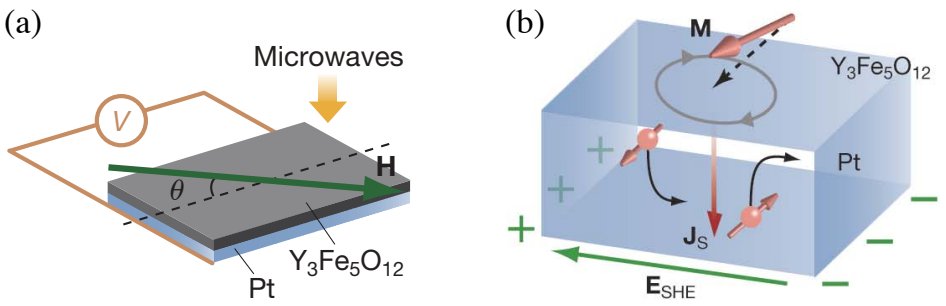


**Figure 1.9:** Cartoons depicting the deployment of a Pt|YIG ($Y_3Fe_5O_{12}$) for spin current detection via spin pumping and inverse Spin Hall effect. (a) Two voltage electrodes are connected to the Pt layer. Microwave pumping induces the precession of the magnetization **M** at cone angle $\theta$ around the in-plane magnetic field **H**. (b) The magnetization precession pumps a spin current $\mathbf{j}_s$ in the Pt layer, which is converted into the electromotive force $\mathbf{E}_{\mathrm{SHE}}$ via the inverse Spin Hall effect. Taken from Ref. [28].

*al.* [28] by deploying a magnetic insulator (YIG) / nonmagnetic metal (Pt) bilayer. In the YIG layer, microwave pumping triggers the precession of the magnetization **M** around the applied magnetic field **H** with cone angle $\theta$ [see Fig. 1.9(a)]. The precession pumps spin current into the Pt layer via spin pumping. The Pt layer is used for spin-current detection: the strong spin orbit coupling gives rise to a large spin Hall angle, and hence the spin current is converted into a measurable electromotive force, as shown in Fig. 1.9(b). Kajiwara *et al.* confirmed also the validity of the inverse mechanism, which corresponds to the conversion of a charge current in a nonmagnetic conductor into magnetization dynamics in a magnetic insulator via the SHE effect and the spin transfer torque. For this purpose, they injected a charge current into the Pt layer, which is converted into a nonequilibrium spin accumulation at the Pt|YIG interface. The latter exerts a spin-transfer torque on the YIG magnetization. In response, the magnetization oscillates emitting electromagnetic waves, whose power spectra can be measured by an antenna and ultimately related to the charge current. A natural step forward is to combine these generation and detection techniques to study the magnetization dynamics through insulating system. This can be achieved by deploying a normal metal (NM1) | ferromagnetic insulator (FI) | normal metal (NM2) heterostructure. A charge current flows into the NM1, generating a transverse spin current via SHE. The magnetization dynamics is then triggered at the NM1|M by the spin current impinging from the NM1 side, and it propagates as a spin-wave

transporting the spin angular momentum towards the second metallic layer. At the interface between the FI and NM2 layers, the magnetic precession is converted back to a spin current, which finally generates a charge current as a consequence of the inverse spin-Hall effect.

Such setup was recently deployed by the group of B. van Wees to measure the relaxation lengthscale $\lambda_m$ associated with the motion of magnons in YIG [35]. By varying the distance between the metallic injector and detector, the authors were able to identify two different regimes of magnon transport. With the separation length $d$ between the two metallic leads being smaller than $\lambda_m$, the recorded spin current signal was shown to scale as $1/d$, while for $d > \lambda_m$ the signal displayed a decay $\propto e^{-x/\lambda_m}$ (approximating the transport as one-dimensional). Hence, these regimes can be distinguished into diffusive ($d < \lambda_m$) and relaxation-limited regimes ($d > \lambda_m$), pointing out the presence of mechanisms which limit the magnon lifetime (or equivalently its propagation length) such as, e.g., the interactions with the phononic environment.

### 1.4.2 Spin Seebeck effect

The discovery of the charge Seebeck effect, i.e., the conversion of a temperature gradient into a charge voltage, dates back to 1821. It took almost two centuries to detect experimentally its spin analogue, i.e., the generation of a pure spin current via thermal bias, which is dubbed the Spin Seebeck effect (SSE) [29–32]. The discovery of the SSE in a magnetic insulating system is attributed to Uchida *et al* [30].

The experimental setup that has been deployed for this purpose is depicted in Fig. 1.10(a): a YIG slab covered by a platinum film, to which two voltage electrodes are attached. The sample is subject to a temperature gradient along the $z$ axis, induced by setting a temperature difference $\Delta T$ between the YIG substrate and the Pt film. The applied in-plane magnetic field points along the $x$ axis ($q = 90\,^\circ$, with $q$ being the angle comprised between the magnetic field and the $-y$ axis). Figure 1.10(b) shows that the measured voltage depends linearly on the temperature difference $\Delta T$, and it vanishes when $\Delta T = 0$. The Spin Seebeck voltage vanishes as well when the in-plane magnetic field is rotated along the -$y$ axis ($q = 0$). The results are consistent with the following mechanism: a linear thermal bias $\Delta T$ triggers the magnetization dynamics. The latter, at the YIG|Pt interface, pumps a spin current $j_s \propto \Delta T$ parallel to the thermal gradient into the Pt layer. The spin current is then electrically detected via ISHE in the Pt layer. According to the symmetry of the ISHE (1.57), the signal disappear for $q = 0$, and it reverses its sign when the thermal gradient is

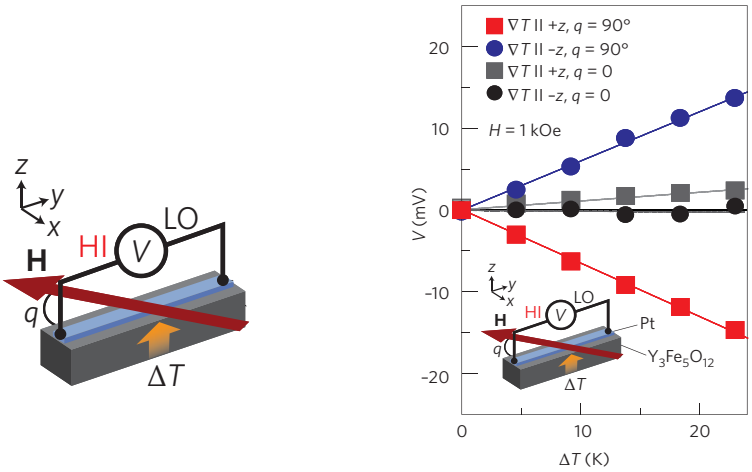


**(a)** **(b)**

**Figure 1.10:** (a) Longitudinal SSE setup. (b) Experimental data for the longitudinal SSE in a YIG|Pt bilayer. Taken from Ref. [34].

in the opposite direction.

The voltage measured in this experimental configuration corresponds to the so-called longitudinal Spin Seebeck voltage, as the spin current generated by the thermal gradient is parallel to the latter. There is a transverse Spin Seebeck effect as well; we neglect it here as the structure of the device used for the generation and detection of the spin current is more complicated, and the overall measurement is more likely to be affected by parasitic effects.

Recent investigations suggest that the observable spin Seebeck signal in magnetic insulators relies on both magnon bulk transport properties and on the interface coupling to the detection material [33]; however, there is not yet a general consensus on the SSE phenomenology. Nonetheless, SSE measurements have been already successfully deployed to unveil fundamental properties of magnon transport such as, e.g., the interactions between magnons and phonons [20]. Moreover, looking at possible technological applications, the SSE appeals as a very promising mechanism as it allows to convert otherwise-wasted heat into spin currents, opening up new prospects for a more energy-efficient generation of devices.

## 1.5 Thermopower

In metallic materials, a heat current driven by a temperature gradient $\partial_x T$ carries electronic charges with it, thereby generating a charge current $j_x$ or a thermopower electric field $E$ for open- or closed-circuit conditions. This phenomenon is dubbed as Seebeck effect. Focusing on open-circuit conditions, we can define the Seebeck coefficient $S$ (or thermopower) corresponding to the induced voltage gradient $\partial_x V = -E$ as

$$S \equiv -\left.\frac{\partial_x V}{\partial_x T}\right|_{j_x=0} . \tag{1.58}$$

The Seebeck effect finds application in thermometers, power generators and its reciprocal- the Peltier effect- in coolers. The basic constituent of these devices is a thermocouple, which consists of two conductors forming an electrical junction; most commonly an n-type and a p-type semiconductor. As shown in Fig. 1.11(a), a heat flux applied at one end of a thermocouple induces a thermal gradient through the conductors. Due to the Seebeck effect, the heat current triggers the motion of the majority carriers, i.e., electrons and holes in the n-type and p-type semiconductor, respectively. Both carriers flow in the same direction, but, as they have opposite charges, their motion ultimately results into two charge currents with opposite directionality, giving rise to an overall current flowing through the circuit. The temperature gradient applied between the two ends can be straightforwardly deduced by the resulting voltage; if the temperature of one end is known, then the thermocouple serves as thermometer. One can as well heat one end in a controlled way to build up a voltage difference (power generator) or a voltage difference can be externally applied to cool or heat one termination, serving as a temperature controller (Peltier cooler).

In reality, not only charge carriers but also magnons and phonons do contribute to the measurable thermopower (1.58). Neglecting phonon-related effects for the moment, we know from the previous section that a heat flux triggers a flow of magnons, which drift in the direction opposite to the thermal gradient. As magnons and electrons interact with each other in a bulk ferromagnetic metal, their mutual interaction gives rise to a magnon-drag contribution to the thermopower [36]. Namely, the electrons are dragged by magnons in the direction of the magnonic drift. A recent experiment of group of J. Heremans (Ohio) confirms that the magnon-drag thermopower is a nonnegligible contribution to the electron diffusive thermopower, and it even dominates the thermopower of elemental Fe and Co over a broad range of temperatures [see Fig. 1.11(b)] [37]. This result relies on modeling the electronic and magnonic band struc-

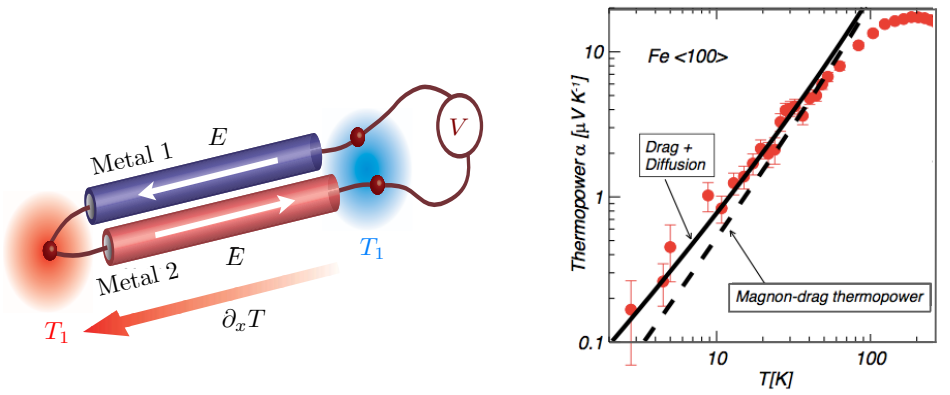


**(a)** **(b)**

**Figure 1.11:** (a) Thermocouple. A thermal gradient $\partial_x T$ triggers a thermopower electric field $E$ in a couple of conductors with opposite thermopower. A temperature-dependent voltage $V$ is established at the cold end. Taken from Ref. [29]. (b) Magnon drag is shown to dominate the thermopower of elemental Fe from 2 to 80 K. Adapted from Ref. [37].

tures with simple parabolic dispersions. Within this approximation, the diffusive thermopower scales linearly with the temperature as $T/T_F$, where $T_F$ is Fermi temperature, while the magnon-drag contribution to the thermopower scales as $(T/T_c)^{3/2}$, with $T_c$ being the Curie temperature [36]. If the Curie temperature is much lower than the Fermi one, it is reasonable to expect that the magnonic thermopower dominates over a broad range of temperatures, as experimentally observed. While deriving an analytical expression for the magnon-drag thermopower, the dissipative contribution to Eq. (1.40), i.e., the term proportional to $\beta$, was used by Lucassen *et al.* as a starting point [36]. The first term in Eq. (1.40) is proportional to $\alpha$, and, with permalloy in mind (for which $\alpha \ll \beta$), it was neglected. However, we can not assume it to be generally a valid approximation for ferromagnetic metals, and the incompleteness of the derivation calls for further theoretical investigations. In Chapter 5 of this Thesis we present a complete theory for the magnon-drag thermopower.

## 1.6 Outline

In this Thesis, the transport properties of spin superfluids, and the interplay between magnons and phonons, or electrons, play a key role. In

Chapter 2, we focus on the interactions between spin superfluid and thermally excited magnons. We derive a two-fluid model describing the coupled dynamics of condensed and thermal magnons, and we identify a possible experimental signature of spin superfluidity. In Chapter 3, we develop a general phenomenology describing the coupling between the coherent dynamics of the magnetic order parameter and the incoherent dynamics of thermal magnons in ferromagnetic insulators. Specifically, we show that the interactions between thermal and condensed magnons open up the possibility of mediating - via low dissipation spin superfluid current - nonlocal communication between an incoherent spin source and topological solitons.

In Chapter 4, we investigate how magnetoelastic coupling affects thermal spin transport. Motivated by recent spin transport measurements, we develop a transport theory for magnon-polaron modes, and we show that the experimental observations can be explained by invoking magneto-elastic coupling. Ultimately, in Chapter 5, we turn our focus onto magnon-electron interactions, and we address the magnon-drag to the thermopower arising in ferromagnetic metals subject to temperature gradient. Our findings unveil a novel contribution to the already predicted magnon-drag, opening interesting prospects for engineering new thermoelectric devices based on metallic ferromagnetic smaterials.

# 2 Two-Fluid Theory for Spin Superfluidity in Magnetic Insulators

We investigate coupled spin and heat transport in easy-plane magnetic insulators. These materials display a continuous phase transition between normal and condensate states that is controlled by an external magnetic field. Using hydrodynamic equations supplemented by Gross-Pitaevski phenomenology and magnetoelectric circuit theory, we derive a two-fluid model to describe the dynamics of thermal and condensed magnons, and the appropriate boundary conditions in a hybrid normal-metal|magnetic-insulator|normal-metal heterostructure. We discuss how the emergent spin superfluidity can be experimentally probed via a spin Seebeck effect measurement.[1]

## 2.1 Introduction

It has been many years since Kapitza first observed that helium, when cooled below a temperature of 2.17 K, displays properties attributable to a new quantum phase of matter [38], such as the ability to flow without dissipation through thin capillaries, the quantization of the vorticity and a record thermal conductivity. These properties are well understood within the framework of the two-fluid model proposed independently by Tisza [39] and Landau [40], in which He II is described as a mixture of a normal fluid, which is viscous and carries all the entropy of the system, and a superfluid that flows without friction and carries no thermal energy.

Only a few years later, the two-fluid model successfully threw light upon the apparent absence of the usual thermoelectric effects, such as the Seebeck and the Peltier effects, in the superconducting state [41]. Indeed, in

[1] This Chapter is directly based on *Two-Fluid Theory for Spin Superfluidity in Magnetic Insulators*, B. Flebus, S. A. Bender, Y. Tserkovnyak, and R. A. Duine, Phys. Rev. Lett. **116**, 117201 (2016). For this paper, B. Flebus performed all analytical calculations with the help of S. Bender. Y. Tserkovnyak and R. A. Duine conceived the project. B. Flebus drafted the paper, all other authors contributed to the text.

superconductors, all the conventional thermoelectric properties vanish due to the coexistence of the thermal quasiparticle current with a dissipationless supercurrent that counterflows with it. The analogy between the supercurrent of electric charge in superconductors and the mass superflow in helium stems from the underlying common origin of these phenomena, i.e., the spontaneous breaking of the $U(1)$ symmetry underlying Bose-Einstein condensation (BEC, of either atoms or Cooper pairs) and the associated macroscopic quantum coherence. Therefore, a superfluid phase can be described by a two-fluid model, in which the condensed and itinerant atoms are, loosely speaking, identified with the superfluid and normal components, respectively. This concept can be extended to a variety of systems exhibiting $U(1)$ symmetry breaking and thus the coexistence of a normal and a Bose-Einstein condensed fluids, such as excitons [42,43], polaritons [44,45], and magnons [46–48].

A growing interest has recently arisen in magnonic systems as promising setups for achieving room-temperature Bose-Einstein condensation, motivated in part by the experimental progress of Demokritov *et al.* [3] on parametrically pumped magnon condensates. More recently, a theoretical proposal for the realization of a BEC of magnons by means of direct spin current injection from an adjacent normal metal with strong spin-orbit coupling was put forward by Bender *et al.* [17]. Unlike BEC of real particles, BEC of quasiparticles and, in particular, quasiequilibrium magnons does not require low temperatures, since the high densities of magnons needed for the condensate to form can be produced via external pumping or by tuning the magnetic field, which is facilitated by their small effective mass (corresponding to strong exchange).

In this Chapter, we focus on a ferromagnetic insulator with easy-plane magnetic anisotropy as a simple model system that displays a transition between normal and BEC phases and exhibits superfluid behavior. The magnet is sandwiched between two metallic reservoirs that act like thermal baths, set at two different temperatures, and that may provide spin accumulation via the spin Hall effect (as illustrated in Fig. 4.1). The temperature difference applied across the ferromagnet induces a spin current into normal metals, which can be measured as an inverse spin Hall voltage and is dubbed the spin Seebeck effect [29]. By sweeping the magnetic field in the $z$ direction, the system can be tuned to a state where the $(xy)$ easy-plane rotational symmetry is spontaneously broken, and which, as a result, supports collective spin currents. We show that the spin Seebeck effect is then diminished, as a result of counterflow between condensate and thermal spin currents. As a practical utility, our results may provide novel

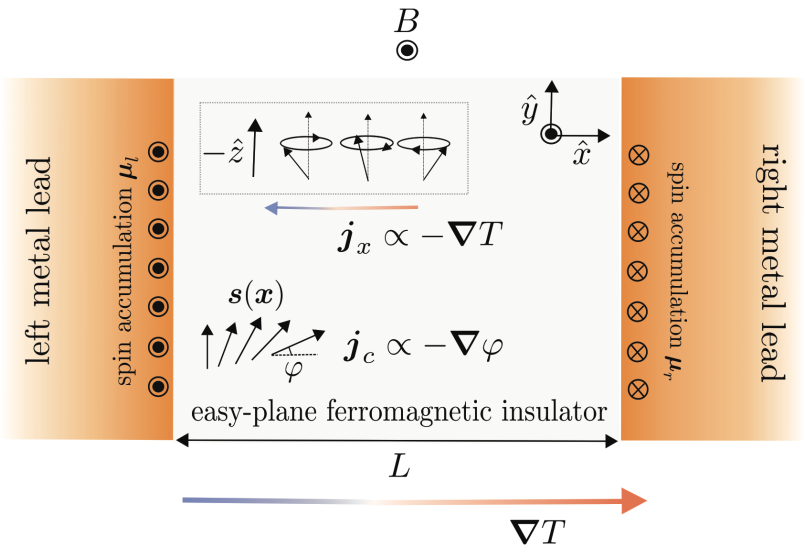


**Figure 2.1:** Normal-metal|easy-plane insulator|normal-metal hybrid heterostructure. The state of the equilibrium magnetization, which is determined by the interplay between the magnetic field $B$ and the anisotropy energy $K$, can be perturbed by magnon transport driven by temperature gradient $\boldsymbol{\nabla} T$ and spin accumulations $\boldsymbol{\mu}_{l,r} = \mu_{l,r}\hat{\mathbf{z}}$ sustained by the metal leads. At low magnetic fields, the spin Seebeck current (polarized along the $z$ axis) $\mathbf{j}_x$ induced by the temperature gradient $\boldsymbol{\nabla} T$ coexists with a superfluid spin counterflow $\mathbf{j}_c$, as discussed in the text.

routes to control thermal spin currents.

## 2.2 Model and hydrodynamic equations

We consider the following model Hamiltonian for an easy-plane magnetic insulator subjected to a field $B$ oriented along the $z$ axis:

$$\mathcal{H} = \int d^3r \left( -\frac{A}{2s}\hat{\mathbf{s}} \cdot \nabla^2 \hat{\mathbf{s}} + B\hat{s}_z + \frac{K}{2s}\hat{s}_z^2 \right) , \tag{2.1}$$

where $\hat{\mathbf{s}}$ is the spin density operator (in units of $\hbar$), $A$ the exchange stiffness, $K > 0$ the constant governing the strength of the local easy-plane anisotropy, and $s$ the saturation spin density. Performing the Holstein-Primakoff transformation [9], $\hat{s}_z = \hat{\Phi}^\dagger\hat{\Phi} - s$ and $\hat{s}_- = \sqrt{2s - \hat{\Phi}^\dagger\hat{\Phi}}\hat{\Phi}$, it is straightforward to recast the Heisenberg dynamics of $\hat{\mathbf{s}}$ as a superfluid coupled to a normal cloud (see, e.g., Ref. [12]). By, furthermore, includ-

ing phenomenologically the Gilbert damping constant $\alpha$, the corresponding Gross-Pitaevksi equation (following the Popov approximation [10]) reads as

$$(i-\alpha)\hbar\partial_t\Phi = (\hbar\Omega + Kn_c/s - iR)\,\Phi - A\nabla^2\Phi\,. \tag{2.2}$$

Here $\Phi \equiv \langle\hat{\Phi}\rangle = \sqrt{n_c}e^{-i\varphi}$ is the superfluid order parameter, with $\varphi$ being the precessional angle of the magnetization density in the $xy$ plane and $n_c$ ($n_x$) condensed (normal) magnon density. In particular, $s_z = n_c + n_x - s$. We are assuming small deviations from the ground state (in the absence of anisotropy), so that $n_c + n_x \ll s$, throughout. $\hbar\Omega \equiv B - K(1-2n_x/s)$ is the normal-phase magnon gap, and the collisional term $R$ describes the coupling to the finite-temperature normal cloud [49], which is defined by $\hat{\phi} \equiv \hat{\Phi} - \Phi$, with $\langle\hat{\phi}^\dagger\hat{\phi}\rangle$ being the normal cloud density $n_x$. At zero temperature (and thus $R \to 0$), Eq. (2.2) recasts the Landau-Lifshitz-Gilbert equation [50] for small-angle dynamics of the spin density around the $-\mathbf{z}$ direction (see Fig. 1.4). It is, furthermore, illuminating to rewrite Eq. (2.2) as the superfluid hydrodynamic equations:

$$\dot{n}_c + \boldsymbol{\nabla}\cdot\mathbf{j}_c = -\Gamma_{cx} - 2\alpha\omega n_c\,, \tag{2.3a}$$

$$\hbar(\omega-\Omega) - K\frac{n_c}{s} = A\left[(\boldsymbol{\nabla}\varphi)^2 - \frac{\nabla^2\sqrt{n_c}}{\sqrt{n_c}}\right], \tag{2.3b}$$

where $\omega = \dot{\varphi}$ is the condensate frequency and $\mathbf{j}_c = n_c\mathbf{v}_c$ the condensate spin current (polarized out of the easy plane, i.e., in the $z$ direction), where $\mathbf{v}_c = -\hbar\boldsymbol{\nabla}\varphi/m$ and $m \equiv \hbar^2/2A$ is the kinetic magnon mass. $\Gamma_{cx} = 2n_cR/\hbar$ is the collision term describing equilibration between the condensate and the thermal cloud, defined as $\Gamma_{cx} = 2\eta(\omega - \mu/\hbar)n_c$ [10], with $\mu$ and $\eta$ parametrizing the chemical potential of the thermal cloud and the rate of the thermal cloud-condensate scattering respectively [**?**]. The latter is determined according to the Fermi's golden rule as

$$\begin{aligned}\eta =& \frac{(K/s)^2}{(2\pi)^5\hbar^6 T}\int d^3p_1 d^3p_2 d^3p_3\;\delta(\mathbf{p}_1 - \mathbf{p}_2 - \mathbf{p}_3)\\ &\times\delta(\hbar\omega + \epsilon_1 - \epsilon_2 - \epsilon_3)(1+f_1)f_2 f_3\,.\end{aligned} \tag{2.4}$$

Here $\epsilon_i \equiv \mathbf{p}_i^2/2m + U$ and $f_i \equiv f_B[(\epsilon_i - \mu)/T]$, with $T$ being the equilibrium temperature.

The equilibrium phase diagram of the easy-plane condensate is shown in Fig. 2.2.. In the following, we will be interested in the linear response of magnons to a temperature gradient. Linearizing with respect to small nonequilibrium variables—$\omega$, $\mathbf{v}_c$, and $\delta n_c \equiv n_c - n_c^{(0)}$ for the condensate

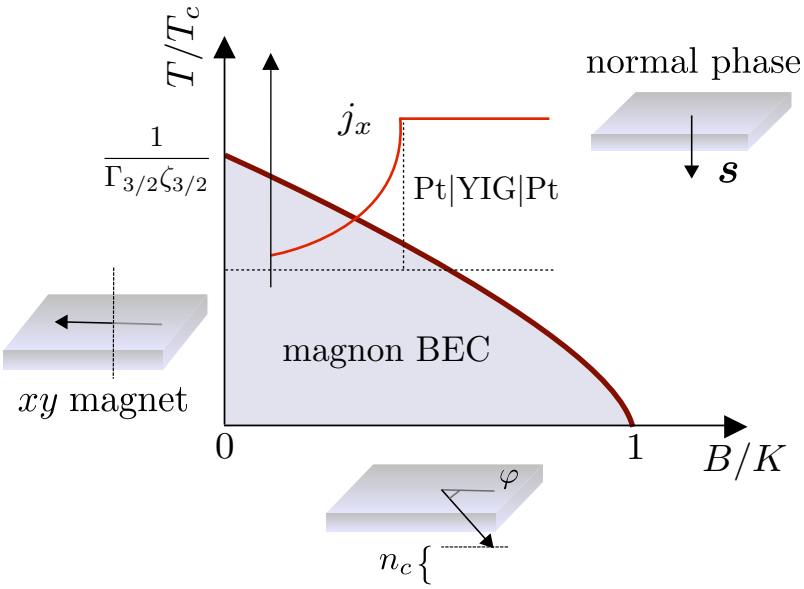


**Figure 2.2:** Equilibrium phase diagram (for more details, see Fig. 1.4). The reduction of the spin Seebeck current $j_x$ (red curve) as the magnetic field $B$ decreases below the transition point, at a fixed $T$, is a direct and observable signature of superfluidity.

and $\mu$ and $\delta T \equiv T - T^{(0)}$ for the cloud—Eqs. (2.3) become

$$\delta\dot{n}_c + n_c \boldsymbol{\nabla}\cdot\mathbf{v}_c = 2\eta(\mu/\hbar - \omega)n_c - 2\alpha\omega n_c\,, \tag{2.5a}$$

$$\hbar\omega = K\frac{\delta n_c + 2\delta n_x}{s} - A\frac{\nabla^2\delta n_c}{2n_c}\,. \tag{2.5b}$$

Here $\delta n_x \equiv n_x - n_x^{(0)}$ can be expanded in terms of $\mu$ and $\delta T$ (disregarding its subleading dependence on $\delta n_c$). The superscript (0), which was dropped in Eqs. (2.5) without danger of ambiguity, denotes the corresponding equilibrium values in the absence of the thermal flux.

The above condensate equations are complemented by hydrodynamic equations for the thermal cloud, which can be easily obtained, by integrating over the zeroth and second momentum moments of Eq. (1.27), as

$$\delta\dot{n}_x + \boldsymbol{\nabla}\cdot\mathbf{j}_x = 2\eta(\omega - \mu/\hbar)n_c - g_{n\mu}\mu - g_{nT}(T - T_p)\,, \tag{2.6a}$$

$$\delta\dot{u} + \boldsymbol{\nabla}\cdot\mathbf{j}_q = -g_{uT}(T - T_p) - g_{u\mu}\mu\,. \tag{2.6b}$$

Here $u$ is the energy density of the thermal cloud, $T_p$ is the phonon temperature, and the $g$ coefficients parametrize relaxation of magnons by the

(phononic) environment. [Note that a contribution to the energy rate equation (2.6b) from the condensate-cloud scattering is missing as it is quadratic in the nonequilibrium bias: $\delta\dot{u}|_{cx} \propto \hbar\omega(\hbar\omega - \mu)$.] The linear response spin, $\mathbf{j}_x$, and heat, $\mathbf{j}_q$, current densities, furthermore, can be expanded as

$$\mathbf{j}_x = -\sigma\boldsymbol{\nabla}\mu - \varsigma\boldsymbol{\nabla}T\,, \quad \mathbf{j}_q = -\kappa\boldsymbol{\nabla}T - \rho\boldsymbol{\nabla}\mu\,, \tag{2.7}$$

where $\sigma$, $\kappa$, $\varsigma$, and $\rho$ are respectively the bulk spin and heat conductivities and the intrinsic spin Seebeck and Peltier coefficients.

## 2.3 Boundary conditions

The spin and heat flow across the sample must be determined consistently with the boundary conditions defined at the F|N interfaces at $x = 0, L$. Accounting for interfacial static spin-transfer and spin-pumping torques, the linearized $z$-component of the condensate spin current density injected from the left reservoir with a nonequilibrium spin accumulation $\boldsymbol{\mu}_l = \mu_l\mathbf{z}$ is given by [17]

$$j_c|_{x=0} = n_c g_l^{\uparrow\downarrow}(\mu_l - \hbar\omega)/2\pi\hbar s\,, \tag{2.8}$$

where $g_l^{\uparrow\downarrow}$ is the real part of the (dimensionless) spin mixing conductance (per unit area). The thermal spin and heat currents flowing across the left interface are given by

$$j_x|_{x=0} = G(\mu_l - \mu)|_{x=0} + S(T_l - T)|_{x=0}\,, \tag{2.9a}$$
$$j_q|_{x=0} = K(T_l - T)|_{x=0} + \Pi(\mu_l - \mu)|_{x=0}\,. \tag{2.9b}$$

Here $T_l$ is the electron temperature and $G$, $K$, $S$, and $\Pi$ are the interfacial magnon spin and thermal conductances and spin Seebeck and Peltier coefficients, respectively. The boundary conditions, Eq. (2.8) and Eqs. (2.9a) and (2.9b) along with the analogous expressions for the right interface, together with the two-fluid hydrodynamic relations, Eqs. (2.5) and (2.6), constitute a complete set of linearized equations from which we can yield solutions for all the dynamical variables. We will now solve this problem in a steady state (i.e., $\delta\dot{n}_c = \delta\dot{n}_x = \delta\dot{u} = 0$ and $\omega = \text{const}$), when the normal-metal reservoirs are thermally biased: $T_l = T - \Delta T/2$ and $T_r = T + \Delta T/2$. We will suppose, for simplicity, that the phononic heat transport and thermal profile are only weakly disturbed by the magnons, so that $T_p = T + \Delta T(x/L - 1/2)$, where we, furthermore, neglected interfacial Kapitza resistances.

## 2.4 Results

Let us investigate the flow of magnonic spin and heat across a mirror-symmetric N|F|N structure driven by a small temperature bias $\Delta T$. We will consider two limiting cases: the magnet is sandwiched (1) between two heavy metals acting as good spin sinks (as may be exemplified by Pt|YIG|Pt), in which case $\mu_{l,r} = 0$, or (2) between two light metals being perfectly poor spin sinks (possibly approximated by Cu|YIG|Cu), in which case spin accumulations build in each lead to block the total spin current across the interfaces, $j_c + j_x \to 0$ at $x \to 0, L$.

Since the spin-preserving relaxation of magnon distribution towards the phonon temperature, as parametrized by $g_{uT}$ in Eq. (2.6b), does not rely on relativistic spin-orbit interactions, we may expect it to be an efficient process at high temperatures (stemming, e.g., from the modulation of exchange coupling by lattice vibrations). The corresponding lengthscale, which is governed by the inelastic magnon-phonon scattering, $\lambda_u \equiv \sqrt{\kappa/g_{uT}}$, can therefore be taken to be shorter than other relevant lengthscales, which are associated with relativistic physics (i.e., $\lambda_n$ and $\lambda_{cx}$ defined below). In this regime, we can set $T \to T_p$, which decouples the spin transport from heat dynamics, resulting, in the steady state, in the following diffusion equation for magnons:

$$\partial_x^2 \mu - (\mu - \hbar\omega)/\lambda_{cx}^2 - \mu/\lambda_n^2 = 0\,, \tag{2.10}$$

which is solved by

$$\mu = (\lambda_m/\lambda_{cx})^2 \hbar\omega + c_l e^{-x/\lambda_m} + c_r e^{(x-L)/\lambda_m}\,. \tag{2.11}$$

Here $\lambda_m^{-2} \equiv \lambda_n^{-2} + \lambda_{cx}^{-2}$, $\lambda_n \equiv \sqrt{\sigma/g_{n\mu}}$ is the thermal magnon diffusion length, and $\lambda_{cx} \equiv \sqrt{\hbar\sigma/2\eta n_c}$ is the condensate-cloud equilibration length (where $n_c$ is the condensate equilibrium density according to the phase diagram in Fig. 2.2). The boundary conditions are given by

$$j_x(0) = G_* c_l - \varsigma \Delta T/L = G[\mu_l - \mu(0)]\,, \tag{2.12a}$$
$$j_x(L) = -G_* c_r - \varsigma \Delta T/L = G[\mu(L) - \mu_r]\,, \tag{2.12b}$$

for the cloud (supposing $L \gg \lambda_m$), where $\mu(0, L) = (\lambda_m/\lambda_{cx})^2 \hbar\omega + c_{l,r}$, $G_* \equiv \sigma/\lambda_m$, and

$$v_c(0) = g^{\uparrow\downarrow}(\mu_l - \hbar\omega)/2\pi\hbar s, \tag{2.13a}$$
$$v_c(L) = g^{\uparrow\downarrow}(\hbar\omega - \mu_r)/2\pi\hbar s, \tag{2.13b}$$

for the condensate. The reservoir spin accumulations are $\mu_l = \mu_r = 0$ in the good spin sink case and are found according to $n_c v_c + j_x = 0$ (at both

interfaces) for the poor spin sinks. Integrating the steady-state version of Eq. (2.5a),

$$\partial_x v_c = 2\eta(\mu/\hbar - \omega) - 2\alpha\omega\,, \tag{2.14}$$

we get for $\Delta v_c \equiv v_c(L) - v_c(0)$:

$$\Delta v_c = \frac{2\eta\lambda_m(c_l + c_r)}{\hbar} - \left[2\alpha + 2\eta(\lambda_m/\lambda_n)^2\right]\omega L\,. \tag{2.15}$$

In the simpler, good spin sink case (where the spin Seebeck physics is manifested through the total spin currents injected into the metal reservoirs), we thus have 5 linear equations, (2.12), (2.13), and (2.15), for 5 unknowns: $c_{l,r}$, $\hbar\omega$, and $v_c$ at $x = 0, L$. For poor spin sinks (where the spin Seebeck physics is manifested through the spin accumulations induced in the metal reservoirs), we have two additional unknowns, $\mu_{l,r}$, and two more equations (for the vanishing total spin current at the interfaces). Note that the differential equation (2.5b) for $\delta n_c$ decouples in the linearized treatment. Adding and subtracting Eqs. (2.12), and substituting the difference of Eqs. (2.13) into Eq. (2.15) leads to

$$\begin{aligned}
(G + G_*)c_- - \varsigma\Delta T/L - G\mu_- &= 0\,,\\
(G + G_*)c_+ + G(\lambda_m/\lambda_{cx})^2\hbar\omega - G\mu_+ &= 0\,,\\
\frac{2\eta\lambda_m c_+}{\hbar} - \left[\alpha + \eta\left(\frac{\lambda_m}{\lambda_n}\right)^2 + \frac{g^{\uparrow\downarrow}}{2\pi sL}\left(1 - \frac{\mu_+}{\hbar\omega}\right)\right]\omega L &= 0\,,
\end{aligned} \tag{2.16}$$

where $c_\pm \equiv (c_l \pm c_r)/2$ and $\mu_\pm \equiv (\mu_l \pm \mu_r)/2$.

In the good spin sink case, $\mu_\pm = 0$, the last two equations above lead immediately to $\omega = 0$ and $c_+ = 0$. The remaining equation gives

$$c_l = \frac{\varsigma\Delta T/L}{G + G_*} = -c_r\,. \tag{2.17}$$

The spin currents at the two interfaces (which turn out to be purely thermal and equivalent) are thus given by

$$j_x = -\frac{\varsigma\Delta T/L}{1 + G_*/G}\,, \tag{2.18}$$

and vanish when either $\lambda_{cx} \to 0$ (strong condensate-cloud interaction regime, where $\lambda_m \to \lambda_{cx}$) or $\lambda_n \to 0$ (strong magnon damping regime, where $\lambda_m \to \lambda_n$), since $G_* \propto 1/\lambda_m \to \infty$. As, by decreasing field $B$, we go deeper into the condensate phase at a fixed $T$, and $n_c$ is monotonically increasing, $\lambda_{cx}$ decreases and thus the magnitude of $j_x$ is reduced (see Fig. 2.2), where

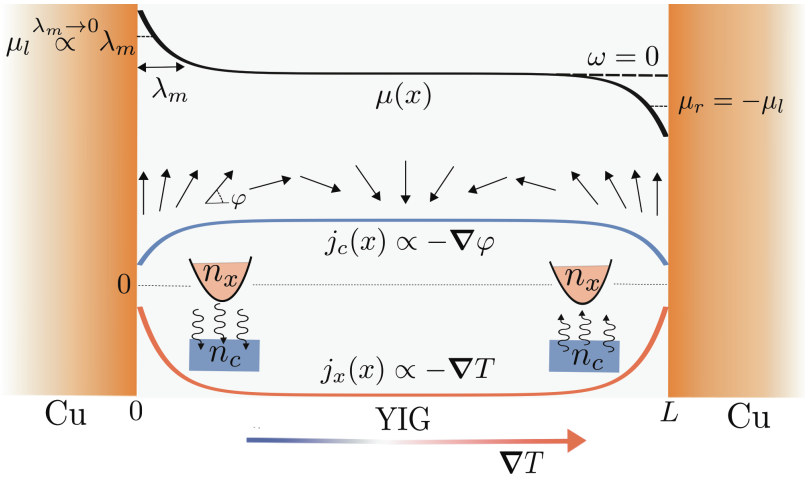


**Figure 2.3:** In the presence of a temperature gradient $\Delta T$, the magnon chemical potential $\mu(x)$ deviates near the interfaces from its zero bulk value in the ferromagnet (YIG). This is accompanied by the electronic spin accumulation build-up in adjacent metals (Cu, treated as a poor spin sink). The spin accumulation $\mu_l$ at the left interface exerts a torque on the magnetic order parameter, twisting it in the opposite direction with respect to the one induced by $\mu_r = -\mu_l$ at the right interface. In the mirror-symmetric case, the precession frequency $\omega$ vanishes. The condensate, $j_c$, and thermal, $j_x$, contributions to the spin currents are plotted for $\lambda_n = \lambda_{cx}$.

we took into account the dependence of $\lambda_m$ on $B$ but ignored the dependence of other quantities on $B$, which is valid as long as $T \gg K$ ). $j_x$ is largest at the transition point to the normal state and is given by Eq. (5.7) with $\lambda_m \to \lambda_n$. Note that although the superfluid velocity $v_c$ vanishes at both interfaces, it is nonzero inside the ferromagnet (at distances beyond $\lambda_m$ from the interfaces), according to Eq. (2.14):

$$v_c = \frac{2\eta\lambda_m c_l}{\hbar} = \frac{2\eta\lambda_m}{\hbar}\frac{\varsigma\Delta T/L}{G+G_*}\,. \tag{2.19}$$

Already in this simple case we encounter the *conveyor-belt* physics, as the superfluid spin current $n_c v_c$ in the bulk counteracts the diffusive thermal flux $-\varsigma\Delta T/L$ and reduces the net spin Seebeck effect as measured at interfaces.

In the opposite limit of the poor spin sinks, we still find $\omega = 0$ and $c_+ = 0$, so that $\mu_+ = 0$, while

$$\mu_l = \frac{\varsigma\Delta T/L}{G_* + (1+G_*/G)g^{\uparrow\downarrow}n_c/2\pi\hbar s} = -\mu_r\,. \tag{2.20}$$

This spin accumulation vanishes when either $\lambda_{cx} \to 0$ or $\lambda_n \to 0$ and decreases with decreasing field $B$, displaying an analogous behavior to the one of the spin current at the interfaces in the good spin sink case (see Fig. 2.2). While the total current now vanishes at the interfaces, $j_x$ and $v_c$ are both nonzero in the ferromagnet (see Fig. 2.3).

## 2.5 Experimental feasibility

Let us see if the superfluid characteristics in the spin Seebeck effect are detectable by sweeping $B$ across the equilibrium phase diagram at $T < T_c$.

To this end, we need first to estimate the transport and dissipation coefficients introduced in Eqs. (2.6a), (2.6b), (2.7), (2.9a) and (2.9b). The $g$ coefficients entering Eqs. (2.6a) and (2.6b) can be obtained according to the Gilbert-damping term $\propto \tau_\alpha^{-1}$ in Eq. (1.27), and go as $g_{n\mu} \sim g_{nT} \sim \alpha s (T/T_c)^{3/2}/\hbar$, $g_{uT} \sim g_{u\mu} = T g_{nT}$ (with the equality reflecting Onsager reciprocity).[2] We can similarly evaluate the coefficients appearing in Eqs. (2.9a) and (2.9b) as [102] $G = \partial_\mu M_1$, $S = \partial_T M_1$, $K = \partial_T M_2$, and $\Pi = \partial_\mu M_2$, in terms of

$$M_n \equiv \frac{g^{\uparrow\downarrow}}{\pi\hbar s} \int \frac{d^3p}{(2\pi\hbar)^3} \epsilon_{\mathbf{p}}^n f_B[(\epsilon_{\mathbf{p}} - \mu)/T]. \tag{2.21}$$

In equilibrium (in the condensate phase), $\epsilon_{\mathbf{p}} = p^2/2m + K n_c/s$. Approximating, furthermore, $\epsilon_{\mathbf{p}} \approx p^2/2m$ (which is justified as $T \gg U \to K n_c/s$), we get $(G, S, K, \Pi) = (g^{\uparrow\downarrow}/\pi\alpha s)(g_{n\mu}, g_{nT}, g_{uT}, g_{u\mu})$, using the above Gilbert-damping expressions for the $g$'s.

The transport coefficients in Eq. (2.7) are obtained following the integration of Eq. (1.27) over momentum subsequent to multiplication by $\mathbf{p}$. In the resulting integrals over the magnon energies, the integrands are inversely proportional to the scattering rate $\tau_\alpha^{-1} + \tau^{-1}$. Assuming an energy-independent scattering length $l$, the scattering rate $2\alpha\epsilon_{\mathbf{p}}/\hbar + \sqrt{2\epsilon_{\mathbf{p}}/ml^2}$ is dominated by momentum scattering at energies below $\epsilon^* \equiv T_c/s^{2/3}(\alpha l)^2$ and by Gilbert damping above $\epsilon^*$. With YIG in mind and taking $\alpha \sim 10^{-4}$, and $s \sim 10$ nm$^{-3}$, $\epsilon^* \lesssim T_c$ corresponds to $l \gtrsim 10$ $\mu$m, with shorter $l$ thus putting us in the scattering-dominated regime (due to disorder and phonons). Therefore, $\varsigma \sim (T/T_c)(s^{2/3}l)/\hbar$, $\kappa \sim \rho = T\varsigma$, and $\sigma \sim (T/T_c)(s^{2/3}l)/\hbar$ (omitting a logarithmic factor for $\sigma$, which depends on the

[2] In practice, however, the magnon energy relaxation $\propto g_{uT}$ driven by the magnon-phonon temperature mismatch, $T - T_p$, can be dominated by nonrelativistic spin-preserving magnon-phonon scattering (which is clearly outside the Gilbert damping phenomenology).

low-energy cutoff for our treatment of magnon transport). It is important, for our purposes, to remark that the bulk spin Seebeck coefficient $\varsigma$ may in practice be strongly enhanced (compared to the above treatment) by the magnon-phonon drag.

Let us now consider the spin Seebeck current (5.7):

$$j_x \propto \frac{1}{1+G^*/G}, \tag{2.22}$$

where

$$G \sim \frac{g^{\uparrow\downarrow}}{\pi\hbar}\left(\frac{T}{T_c}\right)^{3/2}. \tag{2.23}$$

For highest-quality Pt/YIG interfaces, $g^{\uparrow\downarrow} \sim 5$ nm$^{-2}$, which could be significantly reduced depending on the growth conditions and quality of the interface [101].

In the limit $G \gg G^*$, the $G^*$ dependence in $j_x$ drops out altogether (as in this regime the diffusive bulk spin Seebeck current is fully transmitted across the interface inducing only a very small spin accumulation), while in the opposite regime $j_x \propto G/G^*$, which is thus most favorable for manifesting the superfluid characteristics contained in $G^*$.

The relevant bulk conductance

$$G^* = \frac{\sigma}{\lambda_m} = \sigma\sqrt{\lambda_n^{-2} + \lambda_{cx}^{-2}} \tag{2.24}$$

needs to be comparable to $G$ at the transition point and $\lambda_{cx}$ needs to become comparable to $\lambda_n$ below the transition point (in the superfluid regime), for $j_x$ to readily exhibit the two-fluid aspects. The normal-phase $G^*$, which governs the ordinary spin Seebeck effect is

$$G_n^* = \frac{\sigma}{\lambda_n} = \sqrt{\sigma g_{n\mu}} \sim \frac{1}{\hbar}\sqrt{\alpha s^{5/3} l}\left(\frac{T}{T_c}\right)^{5/4}. \tag{2.25}$$

For the spin-diffusion length:

$$\lambda_n = \sqrt{\frac{\sigma}{g_{n\mu}}} \sim \sqrt{\frac{l}{\alpha s^{1/3}}\sqrt{\frac{T_c}{T}}}. \tag{2.26}$$

At room temperature, $T \sim T_c/2$, where $T_c \approx 560$ K, and taking $\alpha \sim 10^{-4}$, we need to set $l \sim 10$ $\mu$m in order to get the experimental $\lambda_n \sim 10$ $\mu$m [35]. These parameters then give $\hbar G_n^* \sim 3$ nm$^{-2}$, so that $G_n^* \gtrsim G$ even for good interfaces. If, e.g., for another material, the opposite regime of

$G_n^* \ll G$ is realized, the two-fluid aspects may be more clearly observed by the measurement of the spin accumulation, Eq. (19), in the poor spin sink regime, rather than the spin current in the good spin sink regime.

The superfluid conveyor-belt characteristics can thus be manifested below the transition temperature so long as $\lambda_{cx}$ is not too large compared to $\lambda_n$. Basing the estimates on our kinetic theory,

$$\left(\frac{\lambda_n}{\lambda_{cx}}\right)^2 = \frac{2\eta n_c}{\hbar g_{n\mu}} \sim \frac{\eta}{\alpha}\frac{n_c}{s}\left(\frac{T_c}{T}\right)^{3/2}. \tag{2.27}$$

At low temperatures (say $T \lesssim T_c/2$), $n_c/s \sim 1 - B/\tilde{B}$, below the transition field $\tilde{B}(T)$, and thus

$$\left(\frac{\lambda_n}{\lambda_{cx}}\right)^2 \sim \frac{\eta}{\alpha}\left(1 - \frac{B}{\tilde{B}}\right)\left(\frac{T_c}{T}\right)^{3/2}. \tag{2.28}$$

For YIG, $\tilde{B} = K \sim 2$ kG at zero temperature. Equation (2.4) can be evaluated in equilibrium ($U \to Kn_c/s$ and $\mu \to 0$), in which case $\eta \propto (T/T_c)^3(K/T)^2$ [51]. We estimate thus that sweeping the field across the condensate phase (i.e., below $\tilde{B}$) results in an observable drop of the spin current $j_x$ of order 1% at room temperature and 10% at the liquid helium temperature, due to the superfluid spin counterflow.

One key remaining issue is the exact estimate for the ratio $\eta/\alpha$. The above expression for $\eta$ underestimates the potentially dominant contribution of the low-energy subthermal magnons [51]. The question of the relevant $\alpha$ for thermal magnons is also still open, as the experimentally known $\alpha$ pertains to the Gilbert damping in the ferromagnetic resonance. Studying the conveyor-belt physics can become a useful practical tool for addressing these issues in YIG and other (ferro- and antiferro-)magnetic insulators.

It is worthwhile to remark that the spin Seebeck effect in our setup should clearly vanishes when $B \to 0$, at any temperature and irrespective of the spin superfluidity, according to the reflection symmetry in the $xz$ plane. Below $T_c$ and when $B$ is reduced below the transition field $\tilde{B}$, the spin Seebeck effect (corresponding to the spin current polarized along the $z$ axis) is gradually reduced due simply to the tilt of the magnetic order parameter away from the $z$ axis, even in the absence of the superfluid (which could, for example, be pinned by a small anisotropy within the easy plane). Our theory does not capture this, unless we properly expand the exchange term in the Hamiltonian (2.1) in terms of the higher-order terms that couple the thermal and condensate fields, which would lead to a Bogolyubov structure modifying both the spectrum and the spin character of magnons. This trivial geometric reduction $\propto \cos\theta \sim 1 - n_c/s$ (where

$\theta$ is the polar angle of the magnetic order parameter relative to $-z$) of the spin Seebeck effect can mask the conveyor-belt physics. One way to overcome it is to actually utilize the (otherwise parasitic) weak anisotropy within the easy plane. The latter sets a critical bias $\Delta T_c/L$ above which the conveyor belt is activated. The geometric contribution would be essentially the same below and above this threshold, while the superfluid-mediated conveyor belt would result in a steplike reduction of the spin Seebeck effect (as described by our theory) just above the threshold bias.

## 2.6 Discussion and conclusions

In this Chapter, we constructed a hydrodynamic theory which describes the interactions between thermal and condensed magnons in an easy-plane magnetic insulator in the presence of a thermal gradient. We predicted that spin superfluidity can be induced by sweeping the external magnetic field and experimentally probed via spin Seebeck effect. We estimate that for YIG this drop should be observable. Although we have explicitly considered a ferromagnetic insulator, we anticipate, according to Refs. [52] and [53], qualitatively similar behavior also for antiferromagnets.

Future works should more systematically address the magnon-phonon relaxation mechanisms and study the role of magnons in the net heat transport. Nonlinear response, in the contexts of dynamic instabilities [12] and pinning by parasitic in-plane anisotropies [4] have been partially addressed in Ref. [54].

# 3 Local thermomagnonic torques in two-fluid spin dynamics

We develop a general phenomenology describing the interplay between coherent and incoherent dynamics in ferromagnetic insulators. Using the Onsager reciprocity and Neumann's principle, we derive expressions for the local thermomagnonic torques exerted by thermal magnons on the order-parameter dynamics and the reciprocal pumping processes, which are in close analogy to the spin-transfer torque and spin pumping at metallic interfaces. Our formalism is applicable to general long-wavelength dynamics and, although here we explicitly focus on ferromagnetic insulators possessing $U(1)$ symmetry, our approach can be easily extended to other classes of magnetic materials. As an illustrative example, we apply our theory to investigate a domain wall floating over a spin superfluid, whose dynamics is triggered thermally at the system's edge. Our results demonstrate that the local pumping of coherent spin dynamics by a thermal magnon gas offers an alternative route - with no need for conducting components and thus devoid of Ohmic losses - for the control and manipulation of topological solitons.[1]

## 3.1 Introduction

The interaction between spin-polarized electron transport and magnetization dynamics via spin-transfer torques [13, 14] and spin pumping [18] has been investigated for almost two decades now. It paved the way for the manipulation of magnetization textures and dynamics without the deployment of external magnetic fields [55]. Recently, much enthusiasm has been

[1] This Chapter is directly based on *Local thermomagnonic torques in two-fluid spin dynamics*, B. Flebus, P. Upadhyaya, R. A. Duine, and Y. Tserkovnyak, Phys. Rev. B., in press. For this paper, B. Flebus performed all analytical calculations with the help of P. Upadhyaya. Y. Tserkovnyak conceived the project. B. Flebus drafted the paper, all other authors contributed to the text.

bolstered by the possibility of attaining similar outcomes by means of thermal control. Thermally-driven magnetization dynamics could be achieved through laser pulsing, as well as through heat diffusion, thereby removing the need for an electronic medium altogether [34].

In magnetic insulators, a thermal bias triggers a pileup of thermal magnons via the spin Seebeck effect [30–32]. This incoherent magnon cloud can relax by transferring spin angular momentum to the magnetic order parameter and thus resulting in a local (thermomagnonic) spin-transfer torque [51, 54]. The latter may then launch nonequilibrium spin textures, opening up new prospects for thermally-driven nonvolatile magnetic memories and logic with potentially little net dissipation.

In this Chapter, via Neumann's principle and the Onsager reciprocity relations, we develop a general formalism describing the local thermomagnonic torques exerted on the magnetic order parameter and the backaction of the coherent dynamics on the thermal magnons. These reciprocal phenomena are in close analogy to the spin-transfer torque and spin pumping in metallic multilayers [56]. Our phenomenology is suited to describe the interplay between diffusive and collective (Landau-Lifshitz–type) dynamics for general spin textures, providing a generalization of previous results [51, 54].

To simplify our discussion, we focus on the simplest nontrivial case yielding local thermomagnonic torques, i.e., axially-symmetric (either easy- or hard-axis) magnetic systems. The hard-axis case has been proposed for hosting a spin superfluid, which is rooted in the Goldstone mode associated with the spontaneous $U(1)$ symmetry breaking [4, 5, 57, 58]. In contrast to the exponentially-decaying flow of thermal magnons, the spin superfluid can transmit spin transport over long distances. This has been exploited recently by Upadhyaya *et al.* [59], who suggested that a hard-axis magnet can efficiently transfer spin angular momentum between a metallic spin reservoir and a distant domain wall. Here, we employ our phenomenology to extend their proposal to a domain wall driven by a thermally-activated superfluid dynamics.

## 3.2 Local thermomagnonic torques

In this section, we construct a general phenomenology describing the coupling between magnetic order-parameter dynamics and a quasi-equilibrium cloud of thermal magnons. Specifically, we consider a magnetic insulator, whose spin density is given in the ground state by $\mathbf{s} = s\mathbf{n}$, $s$ being the saturated spin density (in units of $\hbar$) and $\mathbf{n}$ the spin density orientation.

Finite temperature gives rise to the fluctuations $\delta\hat{\mathbf{s}} = \hat{\mathbf{s}} - \langle\hat{\mathbf{s}}\rangle$, where $\hat{\mathbf{s}}$ is the spin-density operator. These are composed of thermal magnons, whose density $\tilde{n}$ reduces the magnitude of the spin density to $\tilde{s} \equiv s - \tilde{n}$. Here, we will assume that the interactions within the thermal magnon cloud are fast enough (compared to the pumping and relaxation processes) to equilibrate them to a common temperature $T$ and chemical potential $\mu$. We are supposing the temperature to be large compared to the anisotropy fields, such that the magnons are of the exchange type and carry spin $-\hbar$ along $\mathbf{n}$.

If the coherent texture is smooth on the scale of the thermal - magnon wavelength, the hydrodynamic variables that describe the system are the orientation $\mathbf{n}$ of the order parameter and the thermal-magnon density $\tilde{n}$, which together parametrize the total (three-component) spin density $\langle\hat{\mathbf{s}}\rangle \equiv (s-\tilde{n})\mathbf{n}$. In terms of these variables, the instantaneous state of the magnet can be described by a free-energy functional $\mathcal{F}[\mathbf{n}, \tilde{n}]$. The effective (Landau-Lifshitz) transverse field $\mathbf{H} \equiv \delta_{\mathbf{n}}\mathcal{F}[\mathbf{n}, \tilde{n}]$ and the chemical potential $\mu \equiv \delta_{\tilde{n}}\mathcal{F}[\mathbf{n}, \tilde{n}]$ are the forces conjugate to the variables $\mathbf{n}$ and $\tilde{n}$, respectively.

Within the linear response, the relations between the rates $\dot{\mathbf{n}}$ and $\dot{\tilde{n}}$ and the forces can be written as

$$\begin{pmatrix} \dot{\mathbf{n}} \\ \dot{\tilde{n}} \end{pmatrix} = \begin{pmatrix} \mathbf{L}^{\mathbf{nn}} & \mathbf{L}^{\mathbf{n}\tilde{n}} \\ \mathbf{L}^{\tilde{n}\mathbf{n}} & \mathbf{L}^{\tilde{n}\tilde{n}} \end{pmatrix} \begin{pmatrix} \mathbf{H} \\ \mu \end{pmatrix} \equiv \mathbf{L} \begin{pmatrix} \mathbf{H} \\ \mu \end{pmatrix}, \tag{3.1}$$

where we have introduced the $3\times 3$ linear-response matrix $\mathbf{L}$, per each point in space. ($\mathbf{L}^{\mathbf{nn}}$ is a $2 \times 2$ block etc.) Leaving the relaxation processes aside for the moment, the decoupled orientational dynamics obey the Landau-Lifshitz equation [6]:

$$\hbar\dot{\mathbf{n}} = \frac{1}{\tilde{s}}\mathbf{H} \times \mathbf{n}\,. \tag{3.2}$$

The decoupled dynamics of the incoherent magnon cloud is treated diffusively:

$$\dot{\tilde{n}} = -\boldsymbol{\nabla} \cdot \tilde{\mathbf{j}}\,, \tag{3.3}$$

where we have defined (in the absence of thermal gradients, for now) $\tilde{\mathbf{j}} = -\sigma\boldsymbol{\nabla}\mu$ as the magnon flux, with $\sigma$ being the magnon conductivity [58, 60]. The kinetic (matrix-valued) coefficients $\mathbf{L}^{\mathbf{nn}}$ and $\mathbf{L}^{\tilde{n}\tilde{n}}$ can be easily read off from Eqs. (3.2) and (3.3). The off-diagonal coefficient $\mathbf{L}^{\mathbf{n}\tilde{n}}$ describes the thermomagnonic torque exerted by the thermal magnons on the orientational dynamics. Its reciprocal counterpart is the pumping of the magnon gas by the coherent magnetic precession, which is described by the coefficient $\mathbf{L}^{\tilde{n}\mathbf{n}}$.

The off-diagonal linear-response coefficients are connected via Onsager reciprocity [16], which dictates that

$$[\mathbf{L}^{\mathbf{n}\tilde{n}}(\mathbf{n})]_{ij} = -[\mathbf{L}^{\tilde{n}\mathbf{n}}(-\mathbf{n})]_{ji}\,, \tag{3.4}$$

where the minus signs stems from different time-reversal transformations of $\mathbf{n}$ and $\tilde{n}$. Let us next write the equation of motion for $\mathbf{n}$ due to thermomagnonic torques as

$$\hbar\dot{\mathbf{n}} = -\mathbf{h}(\mu, \mathbf{n}, \dot{\mathbf{n}}) \times \mathbf{n}\,, \tag{3.5}$$

where $\mathbf{h}(\mu, \mathbf{n}, \dot{\mathbf{n}}) \perp \mathbf{n}$ is a linear function of the nonequilibrium arguments $\mu$ and $\dot{\mathbf{n}}$. Terms $\propto \dot{\mathbf{n}}$ in Eq. (3.5) contribute to the coefficient $\mathbf{L}^{\mathbf{nn}}$. Their form is restricted by the Onsager reciprocal relations between the components of the transverse magnetization dynamics, i.e.,

$$\mathbf{L}^{\mathbf{nn}}(\mathbf{n}) = [\mathbf{L}^{\mathbf{nn}}(-\mathbf{n})]^{\mathrm{T}}\,, \tag{3.6}$$

where $^{\mathrm{T}}$ denotes matrix transpose. In addition to the requirements imposed by the reciprocity relations (3.4) and (3.6), the form of $\mathbf{h}(\mu, \mathbf{n}, \dot{\mathbf{n}})$ must be constrained by the structural symmetries of the system [61].

In the following, we restrict our attention to insulating magnets which retain $U(1)$ symmetry, typical examples of which are the simple easy-plane and easy-axis ferromagnets. In these systems, due to the rotational invariance around the $z$ axis, Neumann's principle requires that

$$\mathbf{h}(\mathcal{R}_z\mathbf{n}, \mathcal{R}_z\dot{\mathbf{n}}) = \mathcal{R}_z\{\mathbf{h}(\mathbf{n}, \dot{\mathbf{n}})\}\,, \tag{3.7}$$

where $\mathcal{R}_z(\theta)$ is the SO(3) rotation matrix by angle $\theta$ around the $z$ axis. The $U(1)$ symmetry, furthermore, enforces the conservation of the $z$-component of the total angular momentum associated with the total spin density, i.e.,

$$\tilde{s}\dot{n}_z - \dot{\tilde{n}}n_z = 0\,, \tag{3.8}$$

where $n_z \equiv \hat{\mathbf{z}}\cdot\mathbf{n}$. To derive explicitly the equations of motion (3.1), we start by expanding $\mathbf{h}$ in Eq. (3.5) up to linear order in $\mathbf{H}$, $\mu$ and $\dot{\mathbf{n}}$, which captures the Landau-Lifshitz torque, the static and the dynamic thermomagnonic torque, respectively. Utilizing structural symmetries (3.7), Onsager relations (3.4) to derive the reciprocal equation for $\dot{\tilde{n}}$, and the constraints (3.6) and (3.8), we finally arrive at

$$\begin{aligned}\hbar\dot{\mathbf{n}} =& \eta' n_z(\hbar n_z\dot{\mathbf{n}} - \mu\mathbf{n}\times\hat{\mathbf{z}}) - \eta n_z\mathbf{n}\times(\hbar n_z\dot{\mathbf{n}} - \mu\mathbf{n}\times\hat{\mathbf{z}}) \\ &+ \frac{1}{\tilde{s}}\mathbf{H}\times\mathbf{n}\,, \end{aligned} \tag{3.9}$$

$$\dot{\tilde{n}} = \eta'\tilde{s}n_z\dot{n}_z - \eta\frac{\tilde{s}}{\hbar}\hat{\mathbf{z}}\cdot\mathbf{n}\times(\hbar n_z\dot{\mathbf{n}} - \mu\mathbf{n}\times\hat{\mathbf{z}}) - \boldsymbol{\nabla}\cdot\tilde{\mathbf{j}}\,, \tag{3.10}$$

where $\eta$ and $\eta'$ are some even function of $n_z$. Since we are working at linear response, $\tilde{s}$ here can be taken to be the equilibrium spin density at the ambient temperature $T$.

We next proceed to restore the relaxation mechanisms, both for the precessional dynamics and the magnon density. Microscopically, these are rooted in the relativistic corrections, such as spin-orbit coupling, which would affect the conservation of the $z$-component of the spin angular momentum. We thus relax the constraint (3.8) when including the relaxation terms, while not revising our derivation of Eqs. (3.9) and (3.10). The underlying premise of such an approach is that the relaxation processes are usually weak enough that we can start by disregarding their role in the spin transfer between the coherent and incoherent dynamics.

The damping terms naturally appear in the Gilbert and Bloch forms for $\mathbf{n}$ and $\tilde{n}$, respectively, which append Eqs. (3.9) and (3.10) as follows:

$$\begin{aligned}\hbar\dot{\mathbf{n}} =&\eta' n_z(\hbar n_z\dot{\mathbf{n}} - \mu\mathbf{n}\times\hat{\mathbf{z}}) - \eta n_z\mathbf{n}\times(\hbar n_z\dot{\mathbf{n}} - \mu\mathbf{n}\times\hat{\mathbf{z}})\\ &+\frac{1}{\tilde{s}}\mathbf{H}\times\mathbf{n} - \alpha\hbar\mathbf{n}\times\dot{\mathbf{n}}\,, \qquad (3.11)\\ \dot{\tilde{n}} =&\eta'\tilde{s}n_z\dot{n}_z - \eta\frac{\tilde{s}}{\hbar}\hat{\mathbf{z}}\cdot\mathbf{n}\times(\hbar n_z\dot{\mathbf{n}} - \mu\mathbf{n}\times\hat{\mathbf{z}}) - \boldsymbol{\nabla}\cdot\tilde{\mathbf{j}}\\ &-\gamma\mu\,. \qquad (3.12)\end{aligned}$$

Here, $\alpha$ and $\gamma$ parametrize the Gilbert damping and the ($T_1$) Bloch relaxation of magnons, respectively. While $\alpha$ and $\gamma$ can generally depend on $n_z^2$ (and have a tensorial form, according to the axial symmetry), we will for simplicity be considering the limit when they are mere constants. Note that the general thermomagnonic torques $\propto\eta$ in Eqs. (3.11) and (3.12) reproduce the results of Ref. [54] for $n_z\approx -1$ (considered there).[2] The terms $\propto\eta'$ on the right-hand side of both equations have been omitted in Ref. [54], which we will similarly do hereafter. Indeed, in Eq. (3.11), the term $\propto\eta'\dot{\mathbf{n}}$ can be combined with the left-hand side, merely leading to a small rescaling of the equation if (which is natural to expect) $\eta'\ll 1$, while the term $\propto\eta'\mu$ gives rise to a field-like torque, which does not play a substantial role in the dynamics that we are interested in. The term $\propto\eta'\dot{n}_z$ in

[2]Note that the discussion of the large-angle dynamics in Ref. [54], when $n_z$ deviates significantly from $-1$, leading to their Eq. (9), is not reliable, as the appropriate factors of $n_z$ that are present in Eqs. 3.11 have not been taken into account. In particular, the reorientation of the magnetization subjected to a large antidamping torque $\propto\eta\mu>0$ does not switch between opposite directions along the $z$ axis, i.e., $n_z:\ \pm1\mapsto\mp1$, but rather pushes the magnetization towards the symmetry plane, i.e., $n_z:\ \pm1\mapsto 0$. ($\eta\mu<0$ pushes the magnetization away from the $xy$ plane.) This follows correctly from the present equations and is evident according to the structural symmetries as well as on physical grounds.

Eq. (3.12) is inoperative in a steady state with $n_z = \text{const}$, which is the case we will be focusing on. As a final simplification, we will take the remaining coefficient $\eta$ (which microscopically stems from the axial anisotropy [51]) to be a constant, in the spirit of our treatment of $\alpha$ and $\gamma$.

## 3.3 Domain wall floating on a superfluid

Let us now turn to a concrete application of the formalism derived in the previous section. Specifically, we will investigate the coupling between a domain wall and a spin superfluid. Our setup is similar to that of Ref. [59], except that the superfluid dynamics are here triggered thermally. It is accomplished by a thermomagnonic torque exerted by a pileup of thermal magnons, which is induced by a local heat source.

The key ingredient for the realization of a system supporting both zero modes, the spin superfluid and the domain wall, is the spontaneous breaking of the $U(1)\times Z_2$ composite symmetry, with $U(1)$ standing for the rotations around the $z$ axis (which would define a spin superfluid within, e.g., an easy-plane magnet) and $Z_2$ for the time reversal (which would govern domain walls within, e.g., an easy-axis magnet). A weakly exchange coupled bilayer of an easy-plane and an easy-axis magnetic films proposed in Ref. [59] is one such system that could be easily engineered. See Fig. 3.1 for a schematic.

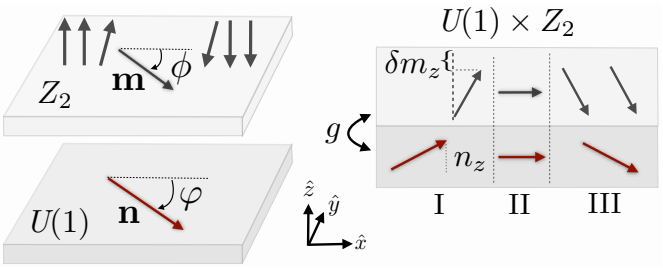


**Figure 3.1:** An easy-axis magnet exhibits an Ising-like order, with the global ground state oriented either up or down in spin space; a domain wall, resulting from this $Z_2$ symmetry breaking, separates the up and down domains (which are related by the time reversal). A superfluid arises in an easy-plane magnet from the spontaneous $U(1)$ symmetry breaking. When the layers are coupled together by a weak exchange interaction $\propto g$, the resulting bilayer displays a composite $U(1)\times Z_2$ symmetry breaking. The coupling induces a tilt $n_z$ ($\delta m_z$) of the order parameter $\mathbf{n}$ ($\mathbf{m}$) in regions I and III, while it locks together the orientations of the order parameters in region II. Here $\varphi$ ($\phi$) is the azimuthal angle of the easy-axis (easy-plane) order parameter $\mathbf{n}$ ($\mathbf{m}$).

While the easy-plane magnet hosts a spin superfluid, the ground state of an easy-axis magnet breaks the time-reversal ($Z_2$) symmetry, harboring a domain wall as a topologically-stable defect. The exchange coupling $\propto g$ between the two layers acts as an effective magnetic field on the easy-plane magnet: it tilts the order parameter, $\mathbf{n}$, out-of- plane, resulting in a finite $n_z$. The latter enables the conversion of thermal magnons into coherent spin dynamics via the thermomagnonic torques $\propto \eta\mu$ in Eq. (3.11). In the domain-wall region, the exchange coupling locks the orientations of the easy-plane and the easy-axis order parameters, allowing for an efficient transfer of angular momentum. This, finally, gives rise to the domain-wall motion, as argued in Ref. [59].

### 3.3.1 Model

We consider a bilayer of an easy-axis ferromagnet (of thickness $\bar{t}$) coupled to an easy-plane ferromagnet (of thickness $t$), as sketched in Fig. 3.2. Our analysis can also be straightforwardly generalized to an easy-axis ferromagnet| easy-plane antiferromagnet heterostructure [59] or essentially any $U(1)\times Z_2$-breaking system of the type sketched in Fig. 4.2.

A biased heat conductor at the left contact induces an accumulation of thermal magnons in the easy-plane layer, which is localized within the spin-diffusion length $\lambda_m \ll L$, with $L$ being the bilayer length in the $x$ direction [58]. The thermally-induced nonequilibrium magnon density $\tilde{n}$ exerts a torque $\propto \eta$ over the spin-diffusion length, triggering superfluid dynamics in the easy-plane magnet. The spin transport is subsequently carried along the $x$ axis by means of coherent precession of $\mathbf{n}$ in the $xy$ plane [59]. The thermal magnons hosted in the easy-axis magnet can also exert a torque on the superfluid across the interface. Here, however, in the limit of a weak interlayer coupling, we can neglect it, as it scales as $\propto g^2$.

The free-energy density (per unit of area in the $xy$ plane) describing our bilayer is

$$\begin{aligned}\mathcal{F}[\mathbf{m},\mathbf{n},\tilde{n}] =& \bar{A}\bar{t}(\partial_x\mathbf{m})^2/2 - \bar{K}\bar{t}m_z^2/2 \\ &+ At(\partial_x\mathbf{n})^2/2 + Ktn_z^2/2 \\ &+ U_{\rm int}[\mathbf{m},\mathbf{n}] + U[\tilde{n}]\,,\end{aligned} \tag{3.13}$$

where $\bar{A}$ ($A$) and $\bar{K}$ ($K$) are the exchange stiffness and the magnetic anisotropy of the easy-axis (easy-plane) magnet respectively, and we supposed quasi-one-dimensional textures along the $x$ axis. The interfacial exchange interaction $U_{\rm int} = -g\,\mathbf{m}\cdot\mathbf{n}$ couples the order parameters of the two

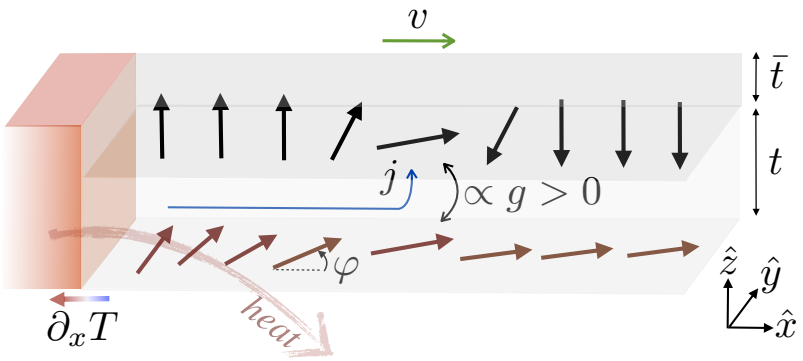


**Figure 3.2:** A bilayer of an easy-plane ferromagnet of thickness $t$, coupled (with coupling strength $g > 0$) to an easy-axis ferromagnet of thickness $\bar{t}$. At the left edge, a heat conductor induces the heat flux $\propto -\partial_x T$ (localized near the bilayer edge), which, in turn, activates the superfluid current $j \propto -\partial_x \varphi$. The coupling $\propto g$ locks the easy-plane and easy-axis orientations in the domain-wall region, interrupting the superfluid flow. The superfluid current is then absorbed by the domain wall, inducing its motion with velocity $v$. Note that we are assuming that the heat is drained out through a material that acts as a good spin sink (such as, e.g., a platinum contact). This would mitigate thermomagnonic torques that would counter those on the injection side.

magnets with the coupling strength $g$. $U[\tilde{n}]$ is the thermal-magnon free energy, taken to be decoupled from the order parameters, as our focus is on the dissipative spin torques. $\mathbf{m} = (\sin\theta\cos\phi, \sin\theta\sin\phi, \cos\theta)$ is the unit vector oriented along the direction of the spin density in the easy-axis ferromagnet, parametrized by the spherical angles $\theta$ and $\phi$. The spin-density orientation of the easy-plane ferromagnet $\mathbf{n} = (\sqrt{1-n_z^2}\cos\varphi, \sqrt{1-n_z^2}\sin\varphi, n_z)$ is parametrized by the azimuthal angle $\varphi$ and the $z$ projection $n_z$. The chemical potential $\mu$ is contained in the dependence $U[\tilde{n}]$.

Let us now suppose the easy-axis magnet to host a domain wall of width $\lambda = \sqrt{\bar{A}/\bar{K}} \ll L$. In the following, we account solely for the coupling between the domain wall and the coherent dynamics of the easy-plane ferromagnet. We neglect the interactions between the domain wall and thermal magnons, which are disturbed by the heat flux only in the vicinity of the bilayer edge (see Fig. 3.2). Taking $x = X$ as the domain wall location, we have $\theta \approx 0$ for $x \ll X$ (regions $\mathrm{I}_{i,b}$) and $\theta \approx \pi$ for $x \gg X$ (region III). Then, in regions $\mathrm{I}_{i,b}$, the exchange interaction $U_{\mathrm{int}} \approx -g n_z$ leads to a tilt of the $z$-component, $n_z^{\mathrm{I}}$, of the order parameter $\mathbf{n}$, with $n_z^{\mathrm{I}} \gtrless 0$ for $g \gtrless 0$. In region III, we have instead $U_{\mathrm{int}} \approx g n_z$, and the tilt, $n_z^{\mathrm{III}}$, reverses its

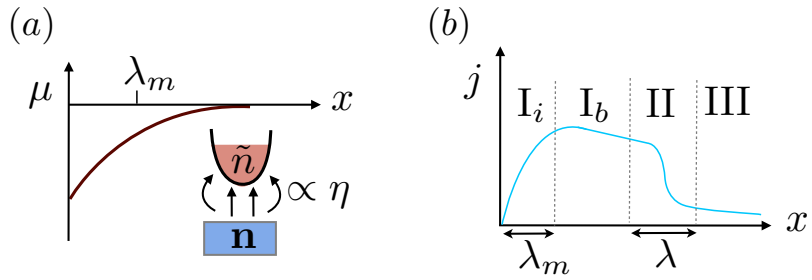


**Figure 3.3:** (a) Out-of-equilbrium chemical potential profile decaying away from the left edge with the diffusion length $\lambda_m$. The thermal magnon density $\tilde{n}$ equilibrates by exerting a torque $\propto \eta$ on the order parameter $\mathbf{n}$. (b) Superfluid current profile. The current increases and saturates exponentially in the interfacial region $\mathrm{I}_i$, decays linearly in the bulk region $\mathrm{I}_b$, is absorbed by the domain wall in region II, with the remaining current decaying linearly within region III.

sign. Note that, for simplicity, we are taking the coupling $g$ to be weak (compared to $Kt$ and $\bar{K}\bar{t}$), so that $|n_z^{\mathrm{I,III}}| \ll 1$; to linear order in $g$, we neglect the tilt $\delta m_z$ induced on $\mathbf{m}$. $n_z^{\mathrm{I,III}}$ are constant in regions $\mathrm{I}_{i,b}$ and III, respectively, with $n_z^{\mathrm{III}} = -n_z^{\mathrm{I}}$.

The static canting of the magnetization, $n_z^{\mathrm{I}}$, enables the two-fluid character for the out-of-plane polarized spin transport in the easy-plane magnet. [58] Namely, in the interfacial region $\mathrm{I}_i$, the heat flux at the left interface induces a pileup of thermal magnons with chemical potential $\mu$ [see Fig. 3.3(a)], which feed the superfluid current according to the term $\propto \eta n_z^{\mathrm{I}} \mu$ in Eq. (3.11). This gives rise to a $z$-polarized superfluid current density, which is proportional to the gradient of the azimuthal angle, i.e., $j \sim -\partial_x \varphi$ [4, 62]. In region II, the coupling $U_{\mathrm{int}}$ locks the azimuthal angles of the easy-axis and easy-plane magnets, $\phi = \varphi$ at $x = X$, impeding the superfluid current flow. Since the $U(1)$ symmetry demands the conservation of the $z$-component of the angular momentum, the superfluid current is absorbed by the domain wall [see Fig. 3.3(b)] and converted into its sliding motion (see Fig. 3.2).

### 3.3.2 Coupled dynamics

Within the Landau-Lifshitz-Gilbert phenomenology and by including the relevant thermomagnonic torques [see Eq. (3.11)], the orientational order-

parameter dynamics in our bilayer can be written as

$$\hbar(1+\bar{\alpha}\mathbf{m}\times)\dot{\mathbf{m}} = -\,\mathbf{m}\times\delta_{\mathbf{m}}\mathcal{F}/\bar{s}\bar{t}\,, \tag{3.14}$$

$$\hbar(1+\alpha\mathbf{n}\times)\dot{\mathbf{n}} = -\,\mathbf{n}\times\delta_{\mathbf{n}}\mathcal{F}/st - \eta n_z\mathbf{n}\times(\hbar n_z\dot{\mathbf{n}} - \mu\mathbf{n}\times\hat{\mathbf{z}})\,, \tag{3.15}$$

where $\alpha$ ($\bar{\alpha}$) parametrizes Gilbert damping of the easy-plane (easy-axis) ferromagnet, $s$ ($\bar{s}$) is the equilibrium spin density of the easy-plane (easy-axis) ferromagnet, and the functional derivatives $\delta$ are taken with respect to the $xy$ coordinates only. (We are hereafter dropping the tilde on $\tilde{s}$.) Soft dynamics of the easy-axis ferromagnet reduces to the dynamics of the domain-wall region, which, in the collective-coordinate approach [63,64] and using the Walker ansatz for the magnetization profile, i.e., $\ln\tan(\theta/2) = (x-X)/\lambda$, reads as

$$\bar{s}\dot{\Phi} - \bar{\alpha}\bar{s}\dot{X}/\lambda = 0\,, \quad \bar{s}\dot{X} + \bar{\alpha}\bar{s}\lambda\dot{\Phi} = \tau_\Phi/2\bar{t}\,. \tag{3.16}$$

Here, the soft-mode coordinates $X$ and $\Phi \equiv \phi(X)$ are the location of the domain wall and the azimuthal angle at its center, respectively, while $\hbar\tau_\Phi \equiv -\partial_\Phi \int dx\, U_{\rm int} = g\int_\lambda dx\, \sin\theta\sin(\varphi-\phi)$ is the torque arising from the exchange interaction with the easy-plane ferromagnetic sublayer.

To linear order in $n_z$, the $z$-projected dynamics of Eq. (3.15) become

$$\hbar s(\dot{n}_z + \alpha\dot{\phi}) = A\partial_x^2\varphi - \eta s n_z\mu + (g/t)\sin\theta\sin(\phi-\varphi)\,. \tag{3.17}$$

Viewing Eq. (3.17) as a continuity equation for the $z$- component of the spin density $s_z = sn_z$ allows us to identify $j = -A\partial_x\varphi$ as the $z$-polarized superfluid spin-current density flowing in the $x$ direction. The thermal-magnon density $\tilde{n}$ evolves according to Eq. (3.12) as

$$\dot{\tilde{n}} + \partial_x\tilde{j} + \sigma\mu/\lambda_m^2 = -\eta s n_z\dot{\varphi}\,, \tag{3.18}$$

where $\tilde{j} = -\sigma\partial_x\mu - \zeta\partial_x T$ (with $\zeta$ being the bulk magnon Seebeck coefficient) is the thermal-magnon flux and $\lambda_m = \sqrt{\sigma/(\gamma+\eta s/\hbar)}$ is the thermal-magnon diffusion length, which is reduced by the superfluid coupling $\eta$.[3] Note that so far, we are not including the direct thermomagnonic torques [65, 66] by the thermal gradient $\partial_x T$ onto the precessional order-parameter dynamics. We will comment on those below.

[3]The more general expression following from Eq. **??**EQ13) is $\lambda_m = \sqrt{\sigma/[\gamma+\eta s(1-n_z^2)/\hbar]}$, which reproduces the result derived in Ref. [58], $\lambda_m = \sqrt{\sigma/(\gamma+2\eta n_c/\hbar)}$, where $n_c = s(1+n_z)$ is their *magnon-condensate density,* in the limit opposite to the one taken in this Chapter: $n_z \to -1$.

In the following, we solve Eqs. (3.16)-(3.18), looking for solutions of the form $\dot{\Phi} = \Omega$, $\dot{X} = v$, $\varphi(x,t) = f(x) + \Omega t$, $\dot{n}_z = 0$ and $\dot{\hat{n}} = 0$, corresponding to a steady-state motion of the domain wall propelled by a superfluid spin flow. We impose hard-wall boundary conditions at $x = 0$ both for the superfluid and normal components of the spin current, i.e.,

$$\partial_x \varphi = 0\,, \quad \sigma \partial_x \mu + \zeta \partial_x T = 0\,. \tag{3.19}$$

Solving Eq. (3.18) with the boundary conditions (3.19) yields

$$\mu(x) = \mu_0 e^{-x/\lambda_m} - (\lambda_m/\lambda_{cx})^2\, n_z^{\rm I} \hbar\Omega\,, \tag{3.20}$$

in region I. Here, $\mu_0 = \lambda_m \zeta \partial_x T/\sigma$ and $\lambda_{cx} = \sqrt{\hbar\sigma/\eta s}$ is the superfluid-thermal magnon equilibration length [58]. Integrating Eq. (3.17) in regions I and III, with $\lambda_m, \lambda \ll X, L$, leads us to [4]

$$j_- = -\eta s n_z^{\rm I} \mu_0 \lambda_m - \alpha s \hbar \Omega X\,, \tag{3.21}$$

$$j_+ = \alpha s \hbar \Omega (L - X)\,, \tag{3.22}$$

where $j_\mp$ are the superflow spin currents just before and after the domain wall (i.e., region II). On the other hand, the spin-current loss within the domain-wall region, $\Delta j = j_- - j_+$, equals

$$\Delta j = \alpha s \hbar \Omega \lambda + \hbar \tau_\Phi / t\,. \tag{3.23}$$

Combining Eqs. (3.21)-(3.23) yields

$$\tau_\Phi/t = -\eta s n_z^{\rm I} \mu_0 \lambda_m/\hbar - s\alpha\Omega L\,. \tag{3.24}$$

The physical interpretation of Eq. (3.24) is straightforward: The amount of the angular momentum transferred from the superfluid to the domain wall is proportional to the spin current fed into the superfluid by the thermal cloud, minus the net current loss due to Gilbert damping.

Using Eqs. (3.16) and (3.24), we can determine the velocity $v$ at which the domain wall moves as

$$v \equiv \dot{X} = -\frac{\eta n_z^{\rm I} \lambda_m^2 (s/\bar{s})(\zeta/\sigma)/2\hbar}{(\bar{t}/t)(1+\bar{\alpha}^2) + \alpha\bar{\alpha}L/2\lambda} \partial_x T\,. \tag{3.25}$$

Equation (3.25) is the central result of our calculation. The numerator is proportional to the torque exerted by the thermally-induced magnon pileup

[4] We are neglecting the last term in Eq. 3.20, $\propto n_z^{\rm I}$, which would result in a higher-order, $\propto (n_z^{\rm I})^2$, correction to the velocity below.

at the left edge of the bilayer, while the denominator is augmented by the Gilbert-damping spin leakage associated with the domain-wall dynamics in the easy-axis layer and the superfluid dynamics in the easy-plane layer. When a ferromagnetic (antiferromagnetic) exchange coupling between the two layers is switched on, $g \gtrless 0$, the superfluid induces a domain-wall motion towards the right (left) end, with a driving force proportional to the interfacial temperature gradient $\partial_x T < 0$ and to the strength of the interaction between the superfluid and the thermal cloud within the easy-plane magnet, $\eta$.

Let us compare, in the limit of small damping, i.e., $\alpha, \bar{\alpha} \ll 1$, Eq. (3.25) with the result of Ref. [66] for the domain-wall velocity subject to the bulk thermomagnonic torques $\propto \partial_x T$. The latter concerns the domain-wall motion induced by a thermal-magnon flux traversing its profile (which should be contrasted with our superfluid-mediated torques that are induced nonlocally). Within the stochastic Landau-Lifshitz-Gilbert phenomenology, the corresponding velocity is [66]

$$v \sim 0.1 \frac{\partial_x T}{\bar{\alpha} \hbar \bar{s} \bar{\lambda}} , \tag{3.26}$$

where $\bar{\lambda} = \sqrt{\bar{A}/\bar{s}T}$ is the thermal-magnon wavelength (in units such that the Boltzmann constant is $k_B = 1$). With YIG in mind, taking $\bar{s} = 1/\mathrm{nm}^3$, $\bar{\alpha} = 10^{-4}$, $\bar{\lambda} = 10$ nm, and $\partial_x T = 20$ K/mm, the domain-wall velocity (3.26) is $v \simeq 0.1$ m/s. The superfluid-induced domain-wall velocity (3.25) exceeds Eq. (3.26) when

$$\eta \gtrsim \frac{0.1}{n_z^{\mathrm{I}}} \frac{1}{\bar{\alpha}\bar{\lambda}} \frac{\bar{t}}{t} \frac{1}{s\lambda_m^2} \frac{\sigma}{\zeta} , \tag{3.27}$$

supposing that $\alpha\bar{\alpha} \ll (\lambda/L)(\bar{t}/t)$. Let us take, consistently with our approximations, $n_z \sim 0.1$. Following the transport theory of Ref. [58], we can set $\sigma/\zeta \sim 1$ in the simplest diffusive limit. Rewriting $s \sim 1/a^3$, with $a$ being the atomic-lattice constant, Eq. (3.27) reads as

$$\eta \gtrsim \underbrace{\left(\frac{1}{\bar{\alpha}}\right)}_{\gg 1} \underbrace{\left(\frac{a^3}{\bar{\lambda}\lambda_m^2}\right)}_{\ll 1} \frac{\bar{t}}{t} . \tag{3.28}$$

This show that it is in principle possible to achieve domain-wall motion with the superfluid-mediated spin transfer, which is faster than the motion in response to the direct thermal gradient. Taking $\bar{\alpha}/\eta \sim 10$ and $\lambda_m \sim 10$ $\mu$m, the superfluid-induced (3.25) and the thermally-driven DW velocities (3.26)

are comparable for films of the same thickness. We note, however, that the dissipation of energy in the superfluid case scales more favorably with the geometric dimensions of the structure, as the spin current can be supplied predominantly to the domain wall, without the diffusive/Ohmic losses throughout the entire system.

## 3.4 Discussion and conclusion

In this work, we have outlined a phenomenological approach to derive local thermomagnonic torques and pumping allowed by the symmetries of a magnetic system, using axially-symmetric $U(1)$ magnets as a concrete illustrative example. Our formalism, which relies on the Onsager and Neumann's principles, can be extended to other classes of magnetic systems, as well as the nonlocal torque/pumping phenomena. For simplicity, we have included the dissipative spin angular-momentum losses perturbatively, disregarding their effect on the torque/pumping process. In the opposite regime of a very strong spin relaxation, this assumption can also be easily relaxed.

As a possible practical application, we have discussed the coupling between a superfluid and a domain-wall in an easy-plane|easy-axis ferromagnetic heterostructure. We have shown that a local heat flux can induce a distant motion of a domain wall via a spin superfluid. Furthermore, we have established that the transfer of angular momentum in our set-up can be more efficient than the one involving bulk temperature gradients and the direct interaction between thermal magnons and the domain wall.

Our findings allow to bridge thermal biases with collective spin dynamics, paving a way for the conversion of heat into long-ranged spin transport that suffers little dissipation. In particular, this can be used for channeling spin currents into topological soliton motion from featureless heat sources. A possible future application is the injection of chiral domain walls by means of a local thermal bias, as a natural extension of the proposal put forward in Ref. [67].

# 4 Magnon-polaron transport in magnetic insulators

We theoretically study the effects of strong magnetoelastic coupling on the transport properties of magnetic insulators. We develop a Boltzmann transport theory for the mixed magnon-phonon modes ("magnon polarons") and determine transport coefficients and spin diffusion length. Magnon-polaron formation causes anomalous features in the magnetic field and temperature dependence of the spin Seebeck effect when the disorder scattering in the magnetic and elastic subsystems is sufficiently different. Experimental data by Kikkawa *et al.* [20] on yttrium iron garnet films can be explained by an acoustic quality that is much better than the magnetic quality of the material. We predict similar anomalous features in the spin and heat conductivity and non-local spin transport experiments.[1]

## 4.1 Introduction

The magnetoelastic coupling (MEC) between magnetic moments and lattice vibrations in ferromagnets stems from spin-orbit, dipole-dipole and exchange interactions. This coupling gives rise to magnon-polarons, i.e., hybridized magnon and phonon modes in proximity of the intersection of the uncoupled elastic and magnetic dispersions [21–24]. Interest in the coupling of magnetic and elastic excitations emerged recently in the field of spin caloritronics [34], since it affects thermal and spin transport properties of magnetic insulators such as yttrium iron garnet (YIG) [68–71].

In this work we address the spin Seebeck effect (SSE) at low temperatures – which provides an especially striking evidence for magnon-polarons

[1] This Chapter is directly based on *Magnon-polaron transport in magnetic insulators*, B. Flebus, K. Shen, T. Kikkawa, K. Uchida, Z. Qiu, E. Saitoh, R. A. Duine, and G. E. W. Bauer, submitted to PRB. For this paper, B. Flebus performed all analytical calculations while the numerical calculations were carried out by K. Shen. R. Duine, G. E. W. Bauer, and E. Saitoh conceived the project. B. Flebus drafted the paper, all other authors contributed to the text.

in the form of asymmetric spikes in the magnetic field dependence [20]. The enhancement emerges at the magnetic fields corresponding to the tangential intersection of the magnonic dispersion with the acoustic longitudinal and transverse phonon branches that we explain by phase-space arguments and an unexpected high acoustic quality of YIG.

Here we present a Boltzmann transport theory for coupled magnon and phonon transport in bulk magnetic insulators and elucidate the anomalous field and temperature dependencies of the SSE in terms of the composite nature of the magnon-polarons. The good agreement between theory and the experiments generates confidence that the SSE can be used as an instrument to characterize magnons vs. phonon scattering in a given material. We derive the full Onsager matrix, including spin and heat conductivity as well as the spin diffusion length. We predict magnon-polaron signatures in all transport coefficients that await experimental exposure.

This Chapter is organized as follows: In Sec. 4.2 we start by introducing the standard model for spin wave and phonon band dispersions of a magnetic insulator and the magnetoelastic coupling. In Sec. 4.3, we describe the magnon-polaron modes and their field-dependent behavior in reciprocal space. The linearized Boltzmann equation is shown to lead to expressions for the magnon-polaron transport coefficients. In Sec. 4.4, we present numerical results for the spin Seebeck coefficient, spin and heat conductivity, and spin diffusion length for YIG. We also derive approximate analytical expressions for the field and temperature dependence of the anomalies emerging in the transport coefficients and compare our results with the experiments. In Sec. 4.5 we present our conclusions and an outlook.

## 4.2 Model

In this section we introduce the Hamiltonian describing the coupling between magnons and phonons in magnetic insulators. The experimentally relevant geometry is schematically depicted in Fig. 4.1.

### 4.2.1 Magnetic Hamiltonian

We consider a magnetic insulator with spins $\mathbf{S}_p = \mathbf{S}(\mathbf{r}_p)$ localized on lattice sites $\mathbf{r}_p$. The magnetic Hamiltonian consists of dipolar and (Heisenberg) exchange interactions between spins and of the Zeeman interaction due to

an external magnetic field $\mathbf{B} = \mu_0 H \hat{\mathbf{z}}$ [?, 72, 73]. It reads as

$$\begin{aligned}\mathcal{H}_{\text{mag}} = & \frac{\mu_0 (g\mu_B)^2}{2} \sum_{p \neq q} \frac{|\mathbf{r}_{pq}|^2 \mathbf{S}_p \cdot \mathbf{S}_q - 3\,(\mathbf{r}_{pq} \cdot \mathbf{S}_p)\,(\mathbf{r}_{pq} \cdot \mathbf{S}_q)}{|\mathbf{r}_{pq}|^5} \\ & - J \sum_{p \neq q} \mathbf{S}_p \cdot \mathbf{S}_q \; - g\mu_B B \sum_p S_p^z \,. \end{aligned} \tag{4.1}$$

Here, $g$ is the g-factor, $\mu_0$ the vacuum permeability, $\mu_B$ the Bohr magneton, $J$ the exchange interaction strength, and $\mathbf{r}_{pq} = \mathbf{r}_p - \mathbf{r}_q$. By averaging over the complex unit cell of a material such as YIG, we define a coarse-grained, classical spin $S = |\mathbf{S}_p| = a_0^3 M_s/(g\mu_B)$ on a cubic lattice with unit cell lattice constant $a_0$, with $M_s$ being the zero temperature saturation magnetization density. The crystal anisotropy is disregarded, while the dipolar interaction is evaluated for a magnetic film in the $yz$-plane, see Fig. 4.1. We employ the Holstein-Primakoff transformation and expand the spin operators as [9]

$$\begin{aligned} S_p^- &= \sqrt{2S} a_p^\dagger \sqrt{1 - \frac{a_p^\dagger a_p}{2S}} \approx \sqrt{2S} \left[ a_p^\dagger - \frac{a_p^\dagger a_p^\dagger a_p}{4S} \right] , \\ S_p^z &= S - a_p^\dagger a_p \,, \end{aligned} \tag{4.2}$$

where $S_p^- = S_p^x - i S_p^y$, and $a_p / a_p^\dagger$ annihilate/create a magnon at the lattice site $\mathbf{r}_p$ and obey Boson commutation rules $[a_p, a_q^\dagger] = \delta_{pq}$. Substituting the Fourier representation

$$a_p = \frac{1}{\sqrt{N}} \sum_{\mathbf{k}} e^{i\mathbf{k}\cdot\mathbf{r}_p} a_{\mathbf{k}} \,, \quad a_p^\dagger = \frac{1}{\sqrt{N}} \sum_{\mathbf{k}} e^{-i\mathbf{k}\cdot\mathbf{r}_p} a_{\mathbf{k}}^\dagger \,, \tag{4.3}$$

where $N$ is the number of lattice sites, and retaining only quadratic terms in the bosonic operators and disregarding a constant, the Hamiltonian (4.1) becomes

$$\mathcal{H}_{\text{mag}} = \sum_{\mathbf{k}} A_{\mathbf{k}} a_{\mathbf{k}}^\dagger a_{\mathbf{k}} + \frac{1}{2} \left( B_{\mathbf{k}} a_{-\mathbf{k}} a_{\mathbf{k}} + B_{\mathbf{k}}^* a_{\mathbf{k}}^\dagger a_{-\mathbf{k}}^\dagger \right) , \tag{4.4}$$

with

$$\begin{aligned} \frac{A_{\mathbf{k}}}{\hbar} &= D_{\text{ex}} \mathcal{F}_{\mathbf{k}} + \gamma \mu_0 H + \frac{\gamma \mu_0 M_s \sin^2 \theta_{\mathbf{k}}}{2} \,, \\ \frac{B_{\mathbf{k}}}{\hbar} &= \frac{\gamma \mu_0 M_s \sin^2 \theta_{\mathbf{k}}}{2} e^{-2i\phi_{\mathbf{k}}} \,. \end{aligned} \tag{4.5}$$

Here, $D_{\text{ex}} = 2SJa_0^2$ is the exchange stiffness, $\gamma = g\mu_B/\hbar$ the gyromagnetic ratio, $\theta_{\mathbf{k}} = \arccos(k_z/k)$ the polar angle between wave-vector $\mathbf{k}$ with $k =$

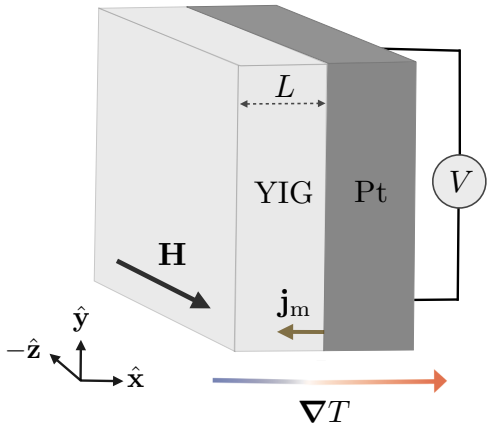


**Figure 4.1:** Pt|YIG bilayer subject to a thermal gradient $\boldsymbol{\nabla} T \parallel \hat{\mathbf{x}}$ and a magnetic field $\mathbf{H} \parallel \hat{\mathbf{z}}$. The thermal bias gives rise to a flow of magnons, i.e., a magnonic spin current $\mathbf{j}_\mathrm{m}$, in the YIG film of thickness $L$. In the Pt lead, the spin current is then converted into a measurable voltage $V$ via the inverse Spin Hall effect.

$|\mathbf{k}|$ and the magnetic field along $\hat{\mathbf{z}}$ and $\phi_\mathbf{k}$ the azimuthal angle of $\mathbf{k}$ in the $xy$ plane. The form factor $\mathcal{F}(\mathbf{k}) = 2(3 - \cos k_x a_0 - \cos k_y a_0 - \cos k_z a_0)/a_0^2$ can be approximated as $\mathcal{F}(\mathbf{k}) \approx k^2$ in the long-wavelength limit ($ka_0 \ll 1$). Equation (4.4) is diagonalized by the Bogoliubov transformation [74]

$$\begin{bmatrix} a_\mathbf{k} \\ a^\dagger_{-\mathbf{k}} \end{bmatrix} = \begin{bmatrix} u_\mathbf{k} & -v_\mathbf{k} \\ -v^*_\mathbf{k} & u_\mathbf{k} \end{bmatrix} \begin{bmatrix} \alpha_\mathbf{k} \\ \alpha^\dagger_{-\mathbf{k}} \end{bmatrix} , \tag{4.6}$$

with parameters

$$u_\mathbf{k} = \sqrt{\frac{A_\mathbf{k} + \hbar\omega_\mathbf{k}}{2\hbar\omega_\mathbf{k}}} , \quad v_\mathbf{k} = \sqrt{\frac{A_\mathbf{k} - \hbar\omega_\mathbf{k}}{2\hbar\omega_\mathbf{k}}} e^{2i\phi_\mathbf{k}} . \tag{4.7}$$

The Hamiltonian (4.4) is then simplified to

$$\mathcal{H}_\mathrm{mag} = \sum_\mathbf{k} \hbar\omega_\mathbf{k} \alpha^\dagger_\mathbf{k} \alpha_\mathbf{k} , \tag{4.8}$$

where $\hbar\omega_\mathbf{k} = \sqrt{A_\mathbf{k}^2 - |B_\mathbf{k}|^2}$ is the magnon dispersion. For bulk magnons in the long-wavelength limit [75, 76]

$$\omega_\mathbf{k} = \sqrt{D_\mathrm{ex} k^2 + \gamma\mu_0 H} \sqrt{D_\mathrm{ex} k^2 + \gamma\mu_0 (H + M_s \sin^2\theta_\mathbf{k})}. \tag{4.9}$$

We disregard Damon-Eshbach modes [77] localized at the surface since, in the following, we focus on transport in thick films normal to the plane, i.e., in the $x$-direction in Fig. 4.1. For thick films the backward moving volume modes are relevant only for wave numbers $k$ very close to the origin and are disregarded as well. Higher order terms in the magnon operators that encode magnon-magnon scattering processes have been disregarded as well in Eq. (4.4), which is allowed for sufficiently low magnon-densities or temperatures (for YIG $\lesssim 100\,\mathrm{K}$ [78]). In this regime, the main relaxation mechanism is magnon scattering by static disorder [68] with Hamiltonian

$$\mathcal{H}_{\text{mag-imp}} = \sum_{\mathbf{k},\mathbf{k}'} v^{\text{mag}}_{\mathbf{k},\mathbf{k}'} \alpha^\dagger_{\mathbf{k}} \alpha_{\mathbf{k}'} \,, \tag{4.10}$$

where $v^{\text{mag}}_{\mathbf{k},\mathbf{k}'}$ is an impurity-scattering potential. In the following, we employ the isotropic, short-range scattering approximation $v^{\text{mag}}_{\mathbf{k},\mathbf{k}'} = v^{\text{mag}}$.

### 4.2.2 Mechanical Hamiltonian

We focus on lattice vibrations or sound waves with wavelengths much larger than the lattice constant that are well-described by continuum mechanics. The Hamiltonian of an elastically isotropic solid reads [79]

$$\begin{aligned}\mathcal{H}_{\text{el}} = \int d^3r \sum_{i,j} \frac{\Pi_i^2(\mathbf{r})}{2\bar{\rho}} \delta_{ij} + (c_\parallel^2 - c_\perp^2) \frac{\bar{\rho}}{2} \frac{\partial R_i(\mathbf{r})}{\partial x_i} \frac{\partial R_j(\mathbf{r})}{\partial x_j} \\ + c_\parallel^2 \frac{\bar{\rho}}{2} \frac{\partial R_i(\mathbf{r})}{\partial x_j} \frac{\partial R_i(\mathbf{r})}{\partial x_j},\end{aligned} \tag{4.11}$$

where $\bar{\rho}$ is the average mass density, $R_i$ is the $i$-th component of the displacement vector $\mathbf{R}$ of a volume element at $\mathbf{r}$ with respect to its equilibrium position, $\Pi_i$ is the conjugate phonon momentum and $c_\parallel$ and $c_\perp$ are the velocities of the longitudinal acoustic (LA) and transverse acoustic (TA) lattice waves, respectively. The Hamiltonian (4.11) can be quantized by the phonon creation (annihilation) operators $c^\dagger_{\lambda\mathbf{k}}$ ($c_{\lambda\mathbf{k}}$) as

$$R_i(\mathbf{r},t) = \sum_{\mathbf{k},\lambda} \epsilon_{i\lambda}(\mathbf{k}) \left(\frac{\hbar}{2\bar{\rho}V\omega_{\lambda\mathbf{k}}}\right)^{1/2} (c^\dagger_{\lambda\mathbf{k}} + c_{\lambda-\mathbf{k}}) e^{i\mathbf{kr}} \,, \tag{4.12}$$

$$\Pi_i(\mathbf{r},t) = i \sum_{\mathbf{k},\lambda} \epsilon_{i\lambda}(\mathbf{k}) \left(\frac{\bar{\rho}\hbar\omega_{\lambda\mathbf{k}}}{2V}\right)^{1/2} \left(c^\dagger_{\lambda\mathbf{k}} - c_{\lambda-\mathbf{k}}\right) e^{-i\mathbf{kr}} \,, \tag{4.13}$$

where $\lambda = 1, 2$ labels the shear waves polarized normal to the wave-vector $\mathbf{k}$ (TA phonons), while $\lambda = 3$ represents a pressure wave (LA phonons). Here

$\omega_{\lambda\mathbf{k}} = c_\lambda|\mathbf{k}|$ is the phonon dispersion and $\epsilon_{i\lambda}(\mathbf{k}) = \hat{\mathbf{x}}_i \cdot \hat{\epsilon}(\mathbf{k},\lambda)$ are Cartesian components $i = x, y, z$ of the unit polarization vectors

$$\hat{\epsilon}(\mathbf{k},1) = (\cos\theta_\mathbf{k}\cos\phi_\mathbf{k}, \cos\theta_\mathbf{k}\sin\phi_\mathbf{k}, -\sin\theta_\mathbf{k})\,, \tag{4.14a}$$

$$\hat{\epsilon}(\mathbf{k},2) = i(-\sin\phi_\mathbf{k}, \cos\phi_\mathbf{k}, 0)\,, \tag{4.14b}$$

$$\hat{\epsilon}(\mathbf{k},3) = i(\sin\theta_\mathbf{k}\cos\phi_\mathbf{k}, \sin\theta_\mathbf{k}\sin\phi_\mathbf{k}, \cos\theta_\mathbf{k})\,, \tag{4.14c}$$

that satisfy $\hat{\epsilon}^*(\mathbf{k},\lambda) = \hat{\epsilon}(-\mathbf{k},\lambda)$ [68]. In terms of the operators $c_{\lambda\mathbf{k}}$ and $c^\dagger_{\lambda\mathbf{k}}$, Eq. (4.11) becomes

$$\mathcal{H}_\mathrm{el} = \sum_{\mathbf{k},\lambda} \hbar\omega_{\lambda\mathbf{k}} \left(c^\dagger_{\lambda\mathbf{k}} c_{\lambda\mathbf{k}} + \tfrac{1}{2}\right)\,. \tag{4.15}$$

Analogous to magnons, at low temperatures phonon relaxation is dominated by static disorder

$$\mathcal{H}_\mathrm{imp} = \sum_\lambda \sum_{\mathbf{k},\mathbf{k}'} v^\mathrm{ph}_{\mathbf{k},\mathbf{k}'} c^\dagger_{\lambda\mathbf{k}} c_{\lambda\mathbf{k}'}\,, \tag{4.16}$$

where $v^\mathrm{ph}_{\mathbf{k},\mathbf{k}'}$ is the phonon impurity-scattering potential, in the following assumed to be isotropic and short-range, i.e., $v^\mathrm{ph}_{\mathbf{k},\mathbf{k}'} = v^\mathrm{ph}$.

### 4.2.3 Magnetoelastic coupling

The magnetic excitations are coupled to the elastic displacement via magnetoelastic interactions. In the long-wavelength limit, to leading order in the magnetization $M_i = ng\mu_B S_i$ ($n = 1/a_0^3$) and displacement field $R_i$, the magnetoelastic energy reads as [22, 74]

$$\begin{aligned}\mathcal{H}_\mathrm{mec} = \frac{\hbar n}{M_s^2} \int d^3r \sum_{ij} \Big[ & B_{ij} M_i(\mathbf{r}) M_j(\mathbf{r}) \\ & + B'_{ij} \frac{\partial \mathbf{M}(\mathbf{r})}{\partial r_i} \cdot \frac{\partial \mathbf{M}(\mathbf{r})}{\partial r_j} \Big] R_{ij}(\mathbf{r})\,,\end{aligned} \tag{4.17}$$

where $B_{ij} = \delta_{ij}B_\parallel + (1-\delta_{ij})B_\perp$ and $B'_{ij} = \delta_{ij}B'_\parallel + (1-\delta_{ij})B'_\perp$ are the phenomenological magnetoelastic constants and

$$R_{ij}(\mathbf{r}) = \frac{1}{2}\left[\frac{\partial R_i(\mathbf{r})}{\partial r_j} + \frac{\partial R_j(\mathbf{r})}{\partial r_i}\right]\,, \tag{4.18}$$

is the displacement gradient $R_{ij}$.

The exchange term $\sim B'_{ij}$ in Eq. (4.17) contains magnetization gradients and predominantly affects short wavelength magnons. We disregard

this term since we are interested in capturing low temperature features. Linearizing with respect to small nonequilibrium variables – $R_i$, $M_x, M_y$ – Eq. (4.17) then becomes

$$\mathcal{H}_{\rm mec} = \hbar n B_\perp \left(\frac{\gamma\hbar^2}{4M_s\bar{\rho}}\right)^{1/2} \sum_{\mathbf{k},\lambda} k\omega_{\mathbf{k}\lambda}^{-1/2} e^{-i\phi} a_{\mathbf{k}} (c_{\lambda-\mathbf{k}} + c_{\lambda\mathbf{k}}^\dagger) \times (-i\delta_{\lambda 1}\cos 2\theta_{\mathbf{k}} + i\delta_{\lambda 2}\cos\theta_{\mathbf{k}} - \delta_{\lambda 3}\sin 2\theta_{\mathbf{k}}) + \text{H.c.}\,, \tag{4.19}$$

where $\delta_{\lambda i}$ is the Kronecker delta.

## 4.3 Magnon-polarons

Here we introduce magnon-polarons and formulate their semiclassical transport properties.

### 4.3.1 Magnon-polaron modes

We rewrite the Hamiltonian $\mathcal{H} = \mathcal{H}_{\rm mag} + \mathcal{H}_{\rm el} + \mathcal{H}_{\rm mec}$ as

$$\mathcal{H} = \frac{1}{2}\sum_{\mathbf{k}} \left[\boldsymbol{\beta}_{\mathbf{k}}^\dagger \quad \boldsymbol{\beta}_{-\mathbf{k}}\right] \cdot \boldsymbol{H}_{\mathbf{k}} \cdot \left[\boldsymbol{\beta}_{\mathbf{k}} \quad \boldsymbol{\beta}_{-\mathbf{k}}^\dagger\right]^T \tag{4.20}$$

where $\boldsymbol{\beta}_{\mathbf{k}}^\dagger \equiv \left(\alpha_{\mathbf{k}}^\dagger\ c_{1\mathbf{k}}^\dagger\ c_{2\mathbf{k}}^\dagger\ c_{3\mathbf{k}}^\dagger\right)$ and the Bogoliubov-de Gennes Hamiltonian $\boldsymbol{H}_{\mathbf{k}}$ is an $8\times 8$ Hermitian matrix. Following Ref. [80], we introduce the para-unitary matrix $\boldsymbol{\mathcal{T}}_{\mathbf{k}}$ that diagonalizes $\boldsymbol{H}_{\mathbf{k}}$ as

$$\boldsymbol{H}_{\mathbf{k}}\boldsymbol{\mathcal{T}}_{\mathbf{k}} = \boldsymbol{\nu}\boldsymbol{\mathcal{T}}_{\mathbf{k}} \begin{bmatrix} \boldsymbol{E}_{\mathbf{k}} & \mathbf{0} \\ \mathbf{0} & -\boldsymbol{E}_{-\mathbf{k}} \end{bmatrix}, \tag{4.21}$$

where $[\boldsymbol{\nu}]_{jm} = \delta_{jm}\nu_j$ with $\nu_j = +1$ for $j = 1,..,4$ and $\nu_j = -1$ for $j = 5,..,8$, and $\boldsymbol{E}_{\mathbf{k}}$ is a diagonal matrix, whose $i$-th element $\hbar\Omega_{i\mathbf{k}}$ represents the dispersion relation of the hybrid mode with creation operator $\Gamma_{i\mathbf{k}}^\dagger = \sum_{j=1}^{8} [\boldsymbol{\beta}_{\mathbf{k}}^\dagger\ \boldsymbol{\beta}_{-\mathbf{k}}]_j (\boldsymbol{\mathcal{T}}_{\mathbf{k}}^{-1})_{ij}^*$ that is neither a pure phonon or magnon, but a magnon-polaron.

Let us focus our attention to waves propagating perpendicularly to the magnetic field, i.e., $\mathbf{k} = k\hat{\mathbf{x}}$ (see Fig. 4.1). It follows from Eq. (4.19) that magnon-polarons involve only TA phonons. Disregarding the dipolar interactions, the TA phonon branch is tangent to the magnon dispersion for $\mu_0 H_\perp = c_\perp^2/4D_{ex}\gamma$ at $k_\perp = c_\perp/2D_{ex}$. This estimate holds for $M_s \ll H_\perp$; otherwise the dipolar interaction shifts the magnon dispersion to higher values, leading to a smaller critical field $H_\perp$. For $H < H_\perp$, the TA phonon

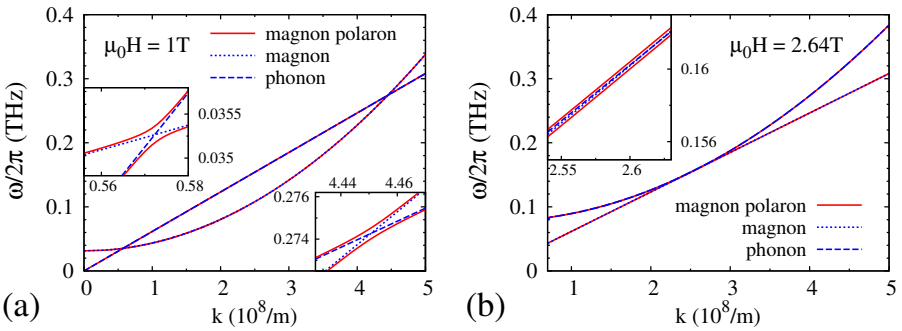


**Figure 4.2:** Magnon, TA phonon ($\lambda = 1$), and magnon-polaron mode dispersions for YIG (see Table 4.1 for parameters) with $\mathbf{H} \parallel \hat{\mathbf{z}}$ and $\mathbf{k} \parallel \hat{\mathbf{x}}$ ($\theta = \pi/2$ and $\phi = 0$). (a) For $\mu_0 H = 1\,\mathrm{T}$, the magnon and transverse phonon dispersions intersect at two crossing points $\mathrm{k}_{1,2}$. The mixing between magnons and phonons (see insets) is maximized at these crossings. (b) For $\mu_0 H_\perp = 2.64\,\mathrm{T}$, the phonon dispersion becomes a tangent to the magnon dispersion which maximizes the phase space of magnon-polaron formation (see inset).

dispersion intersects the spin wave spectrum at two crossing points, $k_1$ and $k_2$,

$$k_{1,2} = k_\perp \mp \sqrt{k_\perp^2 - \frac{\gamma \mu_0 H}{D_{ex}}}\,, \tag{4.22}$$

where the minus (plus) corresponds to the label 1 (2). In the vicinity of $k_{1,2}$, the modes corresponding to the dispersions $\Omega_{1,2k}$ are strongly coupled, as shown in the inset of Fig. 4.2(a). The magnetoelastic coupling changes the crossing at $k_{1,2}$ into an anti-crossing with energy splitting $\Delta\Omega_{k_{1,2}} = \Omega_{2k_{1,2}} - \Omega_{1k_{1,2}}$. For $k \ll k_1$, the $\Gamma_{1k}^\dagger$ ($\Gamma_{2k}^\dagger$) mode resembles closely a pure spin wave (lattice vibration) whilst for $k_1 \ll k \ll k_2$ these roles are reversed, returning to their original character for $k \gg k_2$. At the critical magnetic field $H_\perp$, the magnon dispersion shifts upwards such that the TA phonon branch becomes tangential. Figure 4.2(b) shows that this "touching" condition generates the strongest effects of the MEC, since the magnon and phonon modes are strongly coupled over a relatively large volume in momentum space. At higher magnetic fields, the uncoupled magnonic and TA phononic curves no longer cross, hence the MEC does not play a significant role, and $\boldsymbol{\mathcal{T}}_k$ reduces to the identity matrix. An analogous physical picture holds when considering the magnon-polaron modes arising from the coupling between magnons and LA phonons for $\sin 2\theta_{\mathbf{k}} \neq 0$, with critical field $\mu_0 H_\parallel = c_\parallel^2 / 4 D_{ex} \gamma$ and touch point $k_\parallel = c_\parallel / 2 D_{ex}$ (for $M_s \ll H_\parallel$).

**Table 4.1:** Selected YIG parameters [84–91].

| | Symbol | Value | Unit |
|---|---|---|---|
| Macrospin | S | 20 | - |
| g-factor | g | 2 | - |
| Lattice constant | $a_0$ | 12.376 | Å |
| Gyromagnetic ratio | $\gamma$ | $2\pi \times 28$ | GHz/T |
| Saturation magnetization | $\mu_0 M_s$ | 0.2439 | T |
| Exchange stiffness | $D_{ex}$ | $7.7 \times 10^{-6}$ | $m^2/s$ |
| LA-phonon sound velocity | $c_{\parallel}$ | $7.2 \times 10^3$ | m/s |
| TA-phonon sound velocity | $c_{\perp}$ | $3.9 \times 10^3$ | m/s |
| Magnetoelastic coupling | $B_{\perp}$ | $2\pi \times 1988$ | GHz |
| Average mass density | $\bar{\rho}$ | $5.17 \times 10^3$ | $Kg/m^3$ |
| Gilbert damping | $\alpha$ | $10^{-4}$ | - |

### 4.3.2 Magnon-polaron transport

We proceed to assess the magnetoelastic coupling effects on the transport properties of a magnetic insulator in order to model the spin Seebeck effect and magnon injection by heavy metal contacts.

A non-equilibrium state at the interface between the magnetic insulator and the normal metal generates a spin current that can be detected by the inverse spin Hall effect, as shown in Fig. 4.1. The spin current and spin-mediated heat currents are then proportional to the interface spin mixing conductance that is governed by the exchange interaction between conduction electrons in the metal and the magnetic order in the ferromagnet. In the presence of magnon-polarons, the excitations at the interface have mixed character. Since the spin-pumping and spin torque processes are mediated by the exchange interaction, only the magnetic component of the magnon-polaron in the metal interacts with the conduction electrons. We focus here on the limit in which the smaller of the magnon spin diffusion length and magnetic film thickness is sufficiently large such that the spin current is dominated by the bulk transport and the interface processes may be disregarded. We therefore calculate in the following the spin-projected angular momentum and heat currents in the bulk of the ferromagnet, assuming that the interface scattering processes and subsequent conversion into an inverse spin Hall voltage do not change the dependence of the observed signals on magnetic field, temperature gradient, material parameters, etc..

Since the phonon specific heat is an order of magnitude larger than

the magnon one at low temperatures [81], we may assume that the phonon temperature and distribution is not significantly perturbed by the magnons. $T$ is the phonon temperature at equilibrium and we are interested in the response to a constant gradient $\boldsymbol{\nabla} T \| \hat{\mathbf{x}}$. The spin-conserving relaxation of the magnon distribution towards the phonon temperature is assumed to be so efficient that the magnon temperature is everywhere equal to the phonon temperature. Also the magnon-polaron temperature profile is then $T(x) = T + |\boldsymbol{\nabla} T|\, x$. Assuming efficient thermalization of both magnons and phonons and weak spin-non-conserving processes as motivated by the small Gilbert damping, a non-equilibrium distribution as injected by a metallic contact can be parameterized by a single parameter, viz. the effective magnon-polaron chemical potential $\mu$ [60]. This approximation might break down at a very low temperatures, but to date there is no evidence for that.

In equilibrium the chemical potential of magnons and phonons vanishes since their number is not conserved. The occupation of the $i$-th magnon-polaron in equilibrium is therefore given by the Planck distribution function

$$f_{i\mathbf{k}}^{(0)} = \left( \exp \frac{\hbar \Omega_{i\mathbf{k}}}{k_B T} - 1 \right)^{-1} . \tag{4.23}$$

Note that here we have assumed the $i$-th magnon polaron scattering rate to be sufficiently smaller than the gap between the magnon-polaron mode dispersions, i.e., $\tau_{i\mathbf{k}_i}^{-1} \ll \Delta\Omega_{\mathbf{k}_i}$ for every $\mathbf{k}_i$, which guarantees the $i$-th magnon-polaron to not dephase and hence its distribution function to be well-defined. We focus on films with thickness $L \gg \Lambda_{\mathrm{mag}}, \Lambda_{\mathrm{ph},\lambda}, \ell_{\mathrm{m}}, \ell_{\mathrm{ph},\lambda}$, where $\Lambda_{\mathrm{mag}} = (4\pi\hbar D_{ex}/k_B T)^{1/2}$ and $\Lambda_{\mathrm{ph},\lambda} = \hbar c_\lambda / k_B T$ are the thermal magnon and phonon (de Broglie) wavelengths, respectively, and $\ell_{\mathrm{m}}$ ($\ell_{\mathrm{ph},\lambda}$) the magnon (phonon) mean free path. The bulk transport of magnon-polarons is then semiclassical and can be treated by means of Boltzmann transport theory. In the relaxation time approximation to the collision integral, the Boltzmann equation for the out-of-equilibrium distribution function $f_{i\mathbf{k}}(\mathbf{r}, t)$ reads

$$\partial_t f_{i\mathbf{k}} + \partial_{\mathbf{r}} f_{i\mathbf{k}} \cdot \partial_{\mathbf{k}} \Omega_{i\mathbf{k}} = -(f_{i\mathbf{k}} - f_{i\mathbf{k}}^{(0)})/\tau_{i\mathbf{k}} , \tag{4.24}$$

where $\tau_{i\mathbf{k}}$ is the relaxation time towards equilibrium. In the steady state, the deviation $\delta f_{i\mathbf{k}}(\mathbf{r}) = f_{i\mathbf{k}}(\mathbf{r}) - f_{i\mathbf{k}}^{(0)}$ encodes the magnonic spin, $\mathbf{j}_{\mathrm{m}}$, and heat, $\mathbf{j}_{Q,\mathrm{m}}$, current densities

$$\mathbf{j}_{\mathrm{m}} = \int \frac{d^3\mathbf{k}}{(2\pi)^3} \sum_i W_{i\mathbf{k}} (\partial_{\mathbf{k}} \Omega_{i\mathbf{k}}) \delta f_{i\mathbf{k}} , \tag{4.25}$$

$$\mathbf{j}_{Q,\mathrm{m}} = \int \frac{d^3\mathbf{k}}{(2\pi)^3} \sum_i W_{i\mathbf{k}} (\partial_{\mathbf{k}} \Omega_{i\mathbf{k}}) (\hbar \Omega_{i\mathbf{k}}) \delta f_{i\mathbf{k}} . \tag{4.26}$$

Here, $W_{i\mathbf{k}} = |(\boldsymbol{U}_{\mathbf{k}})_{i1}|^2 + |(\boldsymbol{U}_{\mathbf{k}})_{i5}|^2$ is the magnetic amplitude of the $i$-th quasi-particle branch with $\boldsymbol{U}_{\mathbf{k}} = \boldsymbol{\mathcal{T}}_{\mathbf{k}}^{-1}$. For small temperature gradients, Eqs. (4.25) and (4.26) can be linearized

$$\mathbf{j}_{\mathrm{m}} \simeq -\boldsymbol{\sigma} \cdot \boldsymbol{\nabla}\mu - \boldsymbol{\zeta} \cdot \boldsymbol{\nabla} T \,, \tag{4.27}$$

$$\mathbf{j}_{Q,\mathrm{m}} \simeq -\boldsymbol{\rho}^{(\mathrm{m})} \cdot \boldsymbol{\nabla}\mu - \boldsymbol{\kappa}^{(\mathrm{m})} \cdot \boldsymbol{\nabla} T \,, \tag{4.28}$$

where the tensors $\boldsymbol{\sigma}$, $\boldsymbol{\kappa}^{(\mathrm{m})}$ , $\boldsymbol{\zeta}$, and $\boldsymbol{\rho}^{(\mathrm{m})}(= T\boldsymbol{\zeta}$ by the Onsager-Kelvin relation) are, respectively, the spin and (magnetic) heat conductivities, and the spin Seebeck and Peltier coefficients. In the absence of magnetoelastic coupling, Eqs. (4.27) and (4.28) reduce to the spin and heat currents of magnon diffusion theory [60].

The total heat current $\mathbf{j}_Q$ carried by both magnon and phonon systems does not invoke the spin projection $W_{i\mathbf{k}}$, i.e.,

$$\begin{aligned} \mathbf{j}_Q &= \int \frac{d^3\mathbf{k}}{(2\pi)^3} \sum_i (\partial_{\mathbf{k}} \Omega_{i\mathbf{k}})(\hbar\Omega_{i\mathbf{k}}) \delta f_{i\mathbf{k}} \,, \\ &\simeq -\boldsymbol{\kappa} \cdot \boldsymbol{\nabla} T \,, \end{aligned} \tag{4.29}$$

where $\boldsymbol{\kappa}$ is the total heat conductivity.

In terms of the general transport coefficients

$$\begin{aligned} L_{\alpha\gamma}^{mn} = \beta \int \frac{d^3\mathbf{k}}{(2\pi)^3} \sum_i (W_{i\mathbf{k}})^m \tau_{i\mathbf{k}} (\partial_{k_\alpha} \Omega_{i\mathbf{k}})(\partial_{k_\gamma} \Omega_{i\mathbf{k}}) \\ \times \frac{e^{\beta\hbar\Omega_{i\mathbf{k}}}}{(e^{\beta\hbar\Omega_{i\mathbf{k}}} - 1)^2} (\hbar\Omega_{i\mathbf{k}})^n \,, \end{aligned} \tag{4.30}$$

(with $\beta = 1/k_B T$), we identify $\sigma_{\alpha\gamma} = L_{\alpha\gamma}^{10}$, $\zeta_{\alpha\gamma} = L_{\alpha\gamma}^{11}/T$, $\kappa_{\alpha\gamma}^{(\mathrm{m})} = L_{\alpha\gamma}^{12}/T$ and $\kappa_{\alpha\gamma} = L_{\alpha\gamma}^{02}/T$.

At low temperatures, the excitations relax dominantly by elastic magnon- and phonon-disorder scattering as modelled here by Eqs. (4.10) and (4.16), respectively. The Fermi Golden Rule scattering rate $\tau_{i\mathbf{k}}^{-1}$ of the $i$-th magnon-polaron reads

$$\begin{aligned} \tau_{i\mathbf{k}}^{-1} = \frac{2\pi}{\hbar} \sum_{l=1}^{4} \sum_{j\mathbf{k}'} \Big[ (\boldsymbol{U}_{\mathbf{k}'})_{jl}^* (\boldsymbol{U}_{\mathbf{k}})_{il} \\ + (\boldsymbol{U}_{\mathbf{k}'})_{jl+4}^* (\boldsymbol{U}_{\mathbf{k}})_{il+4} \Big]^2 |v_l|^2 \delta(\hbar\Omega_{i\mathbf{k}} - \hbar\Omega_{j\mathbf{k}'}) \,, \end{aligned} \tag{4.31}$$

where $v_1 = v^{\mathrm{mag}}$ and $v_{2,3,4} = v^{\mathrm{ph}}$, while the purely magnonic and phononic scattering rates are given by

$$\tau_{\mathbf{k},\mathrm{mag}}^{-1} = \frac{L^3 |v^{\mathrm{mag}}|^2}{2\pi\hbar^2 D_{ex}} k \,, \qquad \tau_{\mathbf{k},\mathrm{ph}_\lambda}^{-1} = \frac{L^3 |v^{\mathrm{ph}}|^2}{\pi\hbar^2 c_\lambda} k^2 \,. \tag{4.32}$$

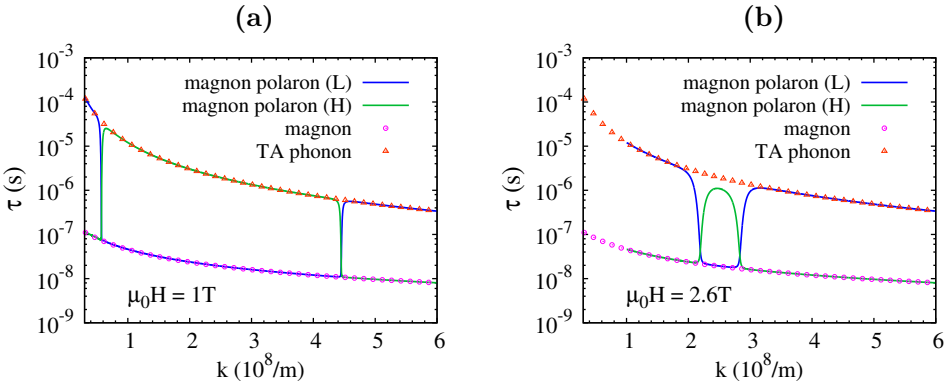


**Figure 4.3:** (a) Scattering times of magnons, TA phonons ($\lambda = 1$), and lower (L)/upper (H) branch magnon-polarons in YIG for $\mu_0 H = 1\,\mathrm{T}$ ($\mathbf{H} \parallel \hat{\mathbf{z}}$) as a function of wave vector $\mathbf{k} \parallel \hat{\mathbf{x}}$ for $\eta = 100$. (b) Same as (a) but $\mu_0 H_\perp = 2.64\,\mathrm{T}$.

## 4.4 Results

In this section we discuss our numerical results for the transport coefficients, in particular the emergence of field and temperature dependent anomalies, and we compare the thermally induced spin current with measured spin Seebeck voltages [20].

### 4.4.1 Spin and heat transport

We consider a sufficiently thick ($> 1\,\mu$m) YIG film subject to a temperature gradient $\boldsymbol{\nabla} T \parallel \hat{\boldsymbol{x}}$ and magnetic field $\mathbf{H} \parallel \hat{\boldsymbol{z}}$, as illustrated in Fig. 4.1. The parameters we employ are summarized in Table 4.1. A scattering potential $|v^{\mathrm{mag}}|^2 = 10^{-5}\ \mathrm{s}^{-2}$ (with $v^{\mathrm{mag}}$ in units of $\hbar$) reproduces the observed low-temperature magnon mean free path [81]. We treat the ratio between magnetic and non-magnetic impurity-scattering potentials, $\eta = |v^{\mathrm{mag}}/v^{\mathrm{ph}}|^2$, as an adjustable parameter. With the deployed scattering potentials $\tau_{\mathbf{k}_i}^{-1} \ll \Delta\Omega_{\mathbf{k}_i}$ for all magnon-polaron modes, ensuring the validity of our treatment. We compute the integrals appearing in Eq. (4.30) numerically on a fine grid ($\sim 10^6$ $k$-points) to guarantee accurate results.

Figure 4.3(a) shows the magnon-polaron scattering times and how they deviate from the purely phononic and magnonic ones close to the anti-crossings. At the "touching" fields the phase space portion over which the scattering times are modified with respect to the uncoupled situation is maximal (see Fig. 4.2(b)) as are the effects on spin and heat transport properties as discussed below.

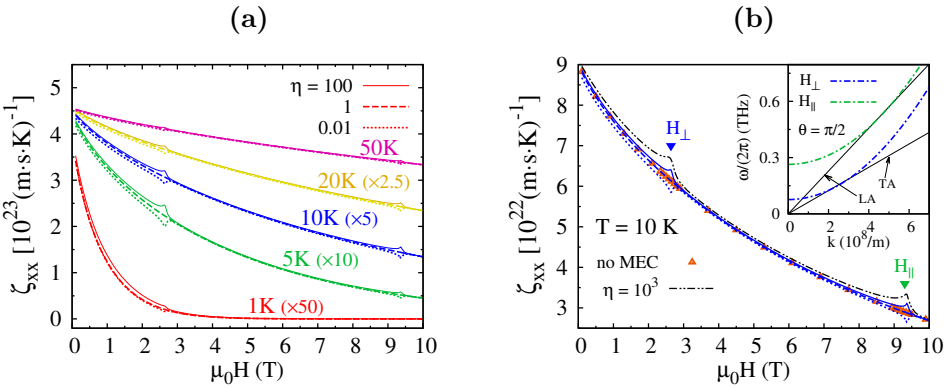


**Figure 4.4:** (a) The magnetic field and temperature dependence of longitudinal spin Seebeck coefficient $\zeta_{xx}$ for different values of the ratio $\eta$ between magnon and phonon impurity-scattering potentials. (b) Longitudinal spin Seebeck coefficient $\zeta_{xx}$ as a function of magnetic field at $T = 10$ K. The solid, dashed, dotted blue lines are computed for, respectively, $\eta = 100, 1, 0.01$, while the black dash-dotted curve is calculated for $\eta = 10^3$. The triangled curve corresponds to the LLSC in the absence of MEC. The inset shows the dispersions of uncoupled magnons, transverse (TA) and longitudinal (LA) acoustic phonons at $H_{\parallel}$ and $H_{\perp}$.

In Fig. 4.4(a), , we plot the (bulk) spin Seebeck coefficient $\zeta_{xx}$ as a function of magnetic field for different values of $\eta$. For $\eta = 1$, $\zeta_{xx}$ decreases monotonously with increasing magnetic field, while for $\eta \neq 1$ two anomalies are observed at $\mu_0 H_{\perp} \sim 2.64\,\mathrm{T}$ and $\mu_0 H_{\parallel} \sim 9.3\,\mathrm{T}$. More precisely, peaks (dips) appear for $\eta = 100(0.01)$ at the same magnetic fields but with amplitudes that depend on temperature. The underlying physics can be understood in terms of the dispersion curves plotted in the inset of Fig. 4.4(b). The first (second) anomaly occurs when the TA (LA) phonon branch becomes a tangent of the magnon dispersion, which maximizes the integrated magnon-polaron coupling.

The group velocity of the resulting magnon-polaron does not differ substantially from the purely magnonic one, but its scattering time can be drastically modified, depending on the ratio between the magnonic and phononic scattering potentials (see Fig. 4.3(b)). The spin currents can therefore be both enhanced or suppressed by the MEC. When the magnon-impurity scattering potential is larger than the phonon-impurity one, the hybridization induced by the MEC lowers the effective potential perceived by magnons, giving rise to an enhanced scattering time and hence larger currents. This can be confirmed by comparing the blue solid ($\eta = 100$) and the black dash-dotted ($\eta = 10^3$) lines in Fig. 4.4(b), showing that the

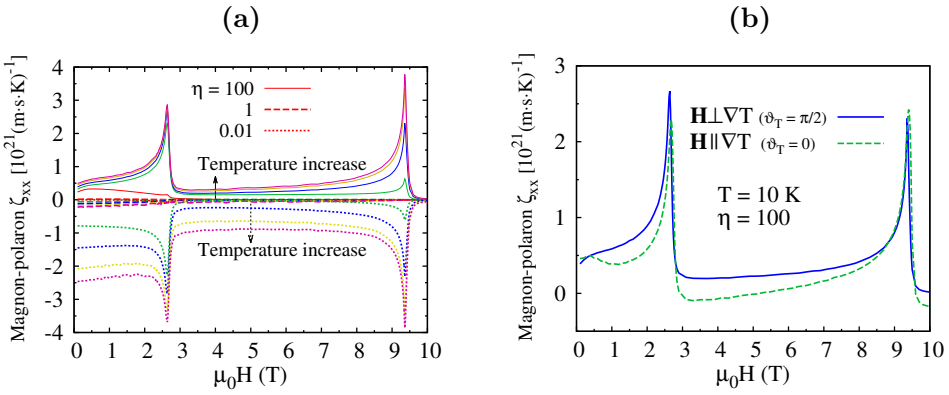


**Figure 4.5:** (a) The magnetic field and temperature dependence of the magnon-polaron contribution to $\zeta_{xx}$ for different values of the ratio $\eta$ between magnon and phonon impurity-scattering potentials. (b) $\zeta_{xx}$ as function of magnetic field for $\mathbf{H} \perp \boldsymbol{\nabla} T$ (blue solid line) and $\mathbf{H} \| \boldsymbol{\nabla} T$ (green dashed line) at $T = 10$ K for $\eta = 100$.

magnitude of the peaks increases with increasing $\eta$. When magnetic and non-magnetic scattering potentials are the same, i.e., $\eta = 1$, the anomalies vanish as illustrated by the dashed blue line in Fig. 4.4(b), and agrees with the results obtained in the absence of MEC (triangles).

The frequencies at which magnon and phonon dispersions are tangential for uncoupled transverse and longitudinal modes are 0.16 THz ($\hat{=}$8 K)and 0.53 THz ($\hat{=}$26 K). Far below these temperatures, the magnon-polaron states are not populated, which explains the disappearance of the second anomaly and the strongly reduced magnitude of the first one at 1 K inFig. 4.4(a). In the opposite limit, the higher energy anomaly becomes relatively stronger [see the solid curve at 50 K in Fig. 4.4(a)]. The overall decay of the spin Seebeck coefficient with increasing magnetic field is explained by the freeze-out caused by the increasing magnon gap opened by the magnetic field [see the inset of Fig. 4.4(b)].

This strong decrease has been observed in single YIG crystals [82, 92], but it is suppressed in thinner samples or even enhanced at low temperatures [20]. The effect is tentatively ascribed to the paramagnetic GGG substrate that becomes magnetically active a low temperatures [20] and is beyond the scope of the present theory. We therefore subtract the pure magnonic background (triangles in Fig. 4.4(b)) from the magnon-polaron spin currents, which leads to the net magnon-polaron contribution shown in Fig. 4.5(a).

The dipolar interaction is responsible for the anisotropy in the magnon

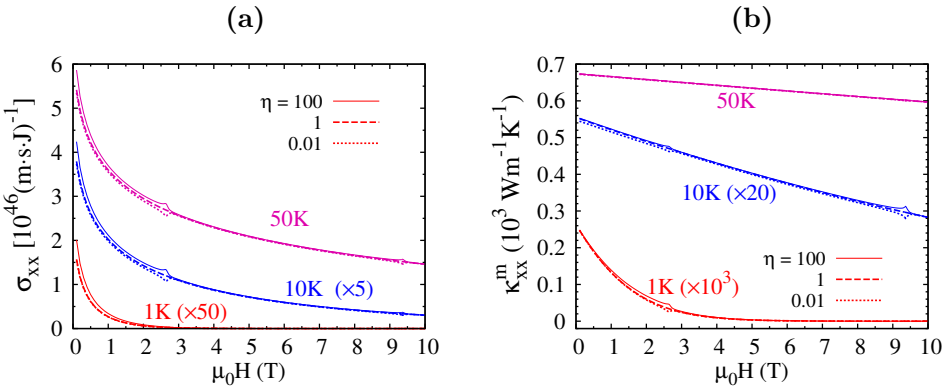


**Figure 4.6:** (a) The magnetic field and temperature dependence of the magnon spin conductivity $\sigma_{xx}$ for different values of the ratio $\eta$ between magnon and phonon impurity-scattering potentials. (b) The magnetic field and temperature dependence of the magnon heat conductivity $\kappa^{\mathrm{m}}_{xx}$ for different values of the ratio $\eta$ between magnon and phonon impurity-scattering potentials.

dispersion in Eq. (4.9), which is reflected in the magnetic field dependence of the heat and spin currents. In Fig.. 4.5(b) we plot $\zeta_{xx}$ as function of the angle $\vartheta_T$ between magnetic field and transport direction for $\eta = 100$ and $T = 10$ K. The magnon-polaron contributions for magnetization parallel and perpendicular to the transport are plotted as the green dashed and blue solid curves, respectively. The anisotropy shifts the magnon-polaron peak positions, but does not substantially modify their amplitude. On these grounds, we proceed with computing other transport coefficients for the configuration $\mathbf{H}\perp\boldsymbol{\nabla}T$ only.

Figure 4.6(a) shows the magnon spin conductivity $\sigma_{xx}$ as function of the magnetic field and temperature for different values of $\eta$. Two peaks (dips) appear at $H_\perp$ and $H_\parallel$ for $\eta = 100$ ($\eta = 0.01$) at 10 K and 50 K, while they disappear for $\eta = 1$. At very low temperatures, $T = 1\,\mathrm{K}$, the anomalies are not visible anymore. The dependence of the spin conductivity on the temperature, on the angle between the magnetic field and temperature gradient, and on the scattering potentials ratio $\eta$ is the same as reported for the spin Seebeck coefficient $\zeta_{xx}$.

In Fig. 4.6(b), we plot the dependence of the magnon heat conductivity $\kappa^{(\mathrm{m})}_{xx}$ on the magnetic field and on the temperature for different values of $\eta$. The only difference with respect to the coefficient $\zeta_{xx}$ is in the ratio between the amplitudes of the two anomalies at $T = 10$ K, at which the magnon modes contributing to the low-field ($H_\perp$) anomaly are thermally excited, in contrast to high field $\left(H_\parallel\right)$ modes. In $\zeta_{xx}$ the anomaly at $H_\perp$

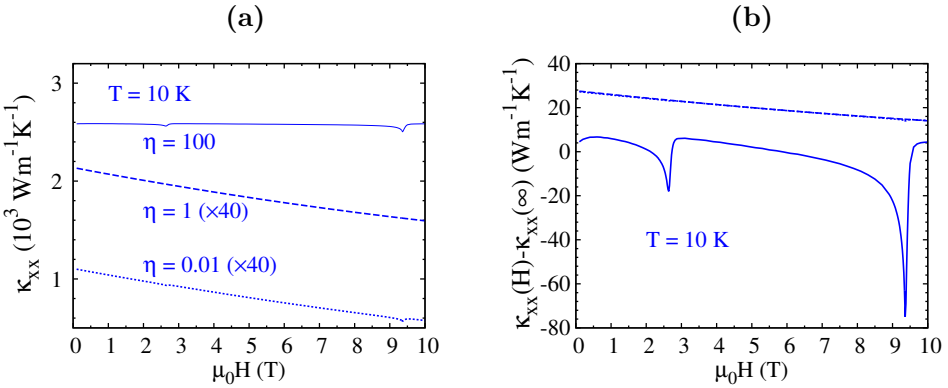


**Figure 4.7:** (a) The magnetic field dependence of the heat conductivity $\kappa_{xx}$ at $T = 10$ K for different values of the ratio $\eta$ between magnon and phonon impurity-scattering potentials. (b) Magnetic field dependence of the experimental magnon heat conductivity $\kappa_{xx} - \kappa_{xx}(\infty)$ at $T = 10$ K for different values of the ratio $\eta$ between magnon and phonon impurity-scattering potentials.

should therefore by better visible, as is indeed the case. The magnon heat conductivity from Eq. (4.30) contains an additional factor in the integrand which is proportional to the energy of the magnon-polaron modes. The latter compensates for the lower thermal occupation, which explains why the anomaly at $H_{\parallel}$ is more pronounced in comparison with the spin Seebeck effect.

Perhaps surprisingly, the total heat conductivity $\kappa_{xx}$ in Fig. 4.7(a) displays only *dips* for $\eta \neq 1$ at the special fields $H_{\perp,\parallel}$. This can be explained as follows. For $\eta \gg 1$, the phonon contribution to the heat conductivity is larger than the magnon contribution. Except at the critical fields $H_{\perp,\parallel}$, the magnetic field dependence of $\kappa_{xx}$ is therefore very weak (solid blue line). When phonons mix with magnons with a short scattering time, the thermal conductivity is suppressed, causing the dips close to $H_{\perp,\parallel}$. For $\eta \ll 1$, on the other hand, the magnon contribution to heat conductivity prevails, as is seen by the strong magnetic field dependence of $\kappa_{xx}$ (dotted blue line). Since now $|v^{\mathrm{mag}}| < |v^{\mathrm{ph}}|$, the heat conductivity of the resulting magnon-polaron mode is lower than the purely magnonic one. Again dips appear close to the "touching" magnetic fields.

Experimentally, the magnon heat conductivity $\kappa_{xx}^{(\mathrm{m,exp})}$ at a given temperature was referred to the difference between finite-field value $\kappa_{xx}(H)$ and $\kappa_{xx}(\infty)$, i.e., $\kappa_{xx}^{(\mathrm{m,exp})}(H) = \kappa_{xx}(H) - \kappa_{xx}(\infty)$ [81]. The latter, $\kappa_{xx}(\infty)$, corresponds to the saturation value of the heat conductivity at high-field

limit, above which it becomes a constant function of the magnetic field, suggesting that the magnon contribution has been completely frozen out and only the phonon contribution remains. In general, $\kappa_{xx}^{(\mathrm{m})}$ and $\kappa_{xx}^{(\mathrm{m,exp})}$ differ in the presence of magnetoelasticity. The magnon heat conductivity $\kappa_{xx}^{(\mathrm{m,exp})}$ in Fig. 4.7(b), evaluated by subtracting the high-field limit for $T = 10$ K, shows dips for both $\eta = 0.01$ and $\eta = 100$, in contrast to the magnon heat conductivity $\kappa_{xx}^{(\mathrm{m})}$ in Fig. 4.6(b) with peaks for $\eta = 100$. The disagreement stems from $\kappa_{xx}(\infty)$, which is the (pure) phonon contribution to the heat conductivity at infinite magnetic fields, but is not the same as the phonon heat conductivity at ambient magnetic fields when the MEC is significant. In the latter case, the phonon heat conductivity itself depends on the magnetic field and displays anomalies at $H_{\perp,\parallel}$; hence $\kappa_{xx}^{(\mathrm{m,exp})} \neq \kappa_{xx}^{(\mathrm{m})}$.

Nonetheless $\kappa_{xx}^{(\mathrm{m,exp})}$ can be useful since its fine structure contains information about the ratio between the magnon-impurity and phonon-impurity scattering potentials $|v^{\mathrm{mag}}|$ and $|v^{\mathrm{ph}}|$. Also, $\kappa_{xx}(\infty)$ for $\eta = 100$ is much larger than for $\eta = 0.01$, and its value gives additional information about the relative acoustic and magnetic quality of the sample. For example, the results reported by Ref. [81] can be interpreted, within our theory, as suggesting a much higher acoustic than magnetic quality of the samples, i.e., $\eta \gg 1$. The authors, however, have not investigated the magnetic field dependence of the heat conductivity but rather the temperature dependence, which is beyond the scope of this work.

The appearance of the anomalies can be understood analytically with few straightforward simplifications. Let us consider a one-dimensional system along $\hat{\mathbf{x}}$ and $\mathbf{H} = (0, 0, H)$. According to Eq. (4.19) only the TA phonons couple to the magnons leading to the magnon-polaron dispersion

$$\Omega_{1,2k} = \frac{\omega_k + \omega_{1k} \pm \sqrt{(\omega_k - \omega_{1k})^2 + \tilde{\omega}_k^2}}{2}, \tag{4.33}$$

where $\tilde{\omega}_k = (S_\perp k)^{1/2}$ and $S_\perp = (nB_\perp)^2(\gamma\hbar^2/4M_s\bar{\rho}c_\perp)$. The magnon-polaron spin amplitudes $W_{1,2k}$ are

$$W_{1k} = \frac{\omega_k - \omega_{1k} + \sqrt{(\omega_k - \omega_{1k})^2 + \tilde{\omega}_k^2}}{2\sqrt{(\omega_k - \omega_{1k})^2 + \tilde{\omega}_k^2}}, \tag{4.34}$$

and $W_{2k} = 1 - W_{1k}$. Disregarding the small dipolar interactions ($M_s \ll H_\perp$) the uncoupled dispersions touch at $\mu_0 H_\perp = c_\perp^2/4D_{ex}\gamma$. We focus on the contribution of the $k_{\perp}-$ mode (with $k_\perp = c_\perp/2D_{ex}$) to the transport coefficients (4.30) close to the touching field and expand in $\delta H = H - H_\perp$.

As in Fig. 4.2(b), for $k = k_\perp$ and $\delta H \ll H_\perp$, the energies and group velocities of the upper and lower magnon-polarons are approximately the same, i.e., $\Omega_{1k_\perp} \simeq \Omega_{2k_\perp}$ and $\partial_k\Omega_1|_{k=k_\perp} \simeq \partial_k\Omega_2|_{k=k_\perp}$. Eq. (4.34) then reads

$$W_{1k_\perp} = \frac{1}{2}\left[1 + \frac{\tilde{k}\delta H}{\sqrt{1+(\tilde{k}\delta H)^2}}\right], \tag{4.35}$$

with $\tilde{k} = \mu_0\gamma/(4S_\perp k_\perp)^{1/2}$. The scattering times (4.31) can be approximated as

$$\tau_{1,2k_\perp} \sim \frac{\partial_k\Omega_{1,2k}|_{k=k_\perp}}{|v_{\rm ph}|^2}\frac{1}{(1-W_{1,2k_\perp})+\eta W_{1,2k_\perp}}. \tag{4.36}$$

Hence

$$L_{xx}^{nm} \sim \frac{\beta}{L^2|v_{\rm ph}|^2}(\partial_k\Omega_{1k})^3\frac{e^{\beta\hbar\Omega_{1k}}}{(e^{\beta\hbar\Omega_{1k}}-1)^2}(\hbar\Omega_{1k})^n\Big|_{\substack{k=k_\perp,\\ H=H_\perp}} \times y_m(\delta H), \tag{4.37}$$

where

$$y_0(\delta H) = \frac{4\left[1+(\tilde{k}\delta H)^2\right](1+\eta)}{1+\eta\left[2+4(\tilde{k}\delta H)^2+\eta\right]},$$

and

$$y_1(\delta H) = \frac{2\left[1+2(\tilde{k}\delta H)^2+\eta\right]}{1+\eta\left[2+4(\tilde{k}\delta H)^2+\eta\right]}.$$

The indices $n$ and $m$ correspond to those in Eq. (4.30). Both $y_0(\delta H)$ and $y_1(\delta H)$ have a single extremum at $H = H_\perp$, i.e.,

$$y_0^{'}(\delta H)|_{\delta H=0} = y_1^{'}(\delta H)|_{\delta H=0} = 0, \tag{4.38}$$

$$y_0^{''}(\delta H)|_{\delta H=0} \propto (1-\eta)^2, \tag{4.39}$$

$$y_1^{''}(\delta H)|_{\delta H=0} \propto (1-\eta). \tag{4.40}$$

Eqs. (4.38) and (4.39) prove that $y_0$ has a minimum at $H = H_\perp$ for $\eta \neq 1$, while for $\eta = 1$ it is a constant. This explains our numerical results for the heat conductivity $\kappa_{xx}$, which is unstructured for $\eta = 1$ and always display dips for both $\eta < 1$ and $\eta > 1$ (see Fig. 4.7(a)). According to Eqs. (4.38) and (4.40) the function $y_1$ is also stationary at $H = H_\perp$, but it has a minimum only for $\eta < 1$, while an inflection point for $\eta = 1$, and a maximum otherwise. The resulting dependence on $\eta$ of Eq. (4.37) explains the spin

Seebeck coefficient $\zeta_{xx}$, the spin conductivity $\sigma_{xx}$ and magnon heat conductivity $\kappa_{xx}^{(\mathrm{m})}$, in Figs. 4.4(a), 4.6(a) and 4.6(b) respectively. As we have discussed in detail in the reporting of the numerical results, the anomalies can be understood physically in terms of the scattering time of the magnon-polaron. This scattering time is the sum of magnonic and phononic scattering times, so, depending on the value of $\eta$, the spin transport is enhanced ($\eta > 1$) or suppressed ($\eta < 1$) close to the touching point.

### 4.4.2 Spin diffusion length

Integrating the spin-projection of Eq. (4.24) over momentum leads to the spin conservation equation:

$$\dot{n}_s + \boldsymbol{\nabla} \cdot j_s = -g_\mu \mu \,, \tag{4.41}$$

where

$$n_s = \int \frac{d^3\mathbf{k}}{(2\pi)^3} \sum_i f_{i\mathbf{k}}(\mathbf{r}) \,, \tag{4.42}$$

is the total magnon density (in units of $\hbar$), and

$$g_\mu = \beta \int \frac{d^3\mathbf{k}}{(2\pi)^3} \sum_i W_{i\mathbf{k}} \frac{1}{\tau_{i\mathbf{k}}^{\mathrm{nc}}} \frac{e^{\beta\hbar\Omega_{i\mathbf{k}}}}{(e^{\beta\hbar\Omega_{i\mathbf{k}}} - 1)^2} \,, \tag{4.43}$$

is the magnon relaxation rate, and we have introduced the relaxation time $\tau_{i\mathbf{k}}^{\mathrm{nc}}$. Elastic magnon-impurity scattering processes discussed in the previous sections do not contribute to $\tau_{i\mathbf{k}}^{\mathrm{nc}}$. However, we parameterize the spin not-conserving processes as

$$\frac{1}{\tau_{i\mathbf{k}}^{\mathrm{nc}}} = 2\alpha\Omega_{\mathbf{k}i} \,, \tag{4.44}$$

in terms of the dimensionless Gilbert damping constant $\alpha$. In the non-equilibrium steady-state Eq. (4.41) becomes

$$\boldsymbol{\nabla}^2 \mu = \frac{1}{\lambda_n} \mu \,, \tag{4.45}$$

in terms of the magnon diffusion length $\lambda_n \equiv \sqrt{\sigma_{xx}/g_\mu}$ that is plotted in Fig. 4.8. At 10 K and 50 K, the spin diffusion length decreases monotonously with the magnetic field for $\eta = 1$, in agreement with observations at room temperature [93]. For $\eta = 100$ ($\eta = 0.01$) the spin diffusion length displays two peaks (dips) at the critical fields $H_\perp$ and $H_\parallel$, which become more pronounced when lowering the temperature. At $T = 1$ K only the peak (dip) at $H_\perp$ is visible for $\eta = 100$ ($\eta = 0.01$). For $\eta = 1$, the spin diffusion

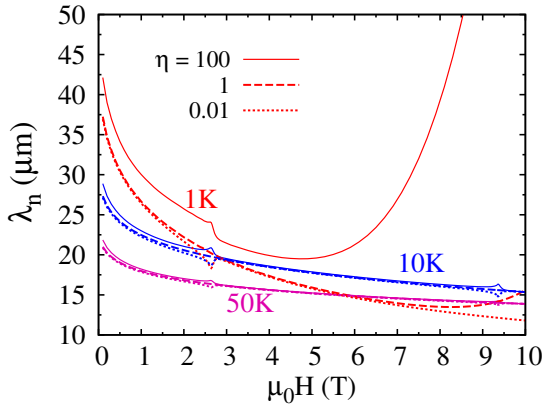


**Figure 4.8:** The magnetic field and temperature dependence of the spin diffusion length $\lambda_n$ for different values of the ratio $\eta$ between magnon and phonon impurity-scattering potentials..

length monotonically decreases with increasing magnetic field. The curve for $\eta = 0.01$ behaves similar except for the dip at $H = H_\perp$. On the other hand, for $\eta = 100$, the spin diffusion length behaves very differently showing strong enhancement at both low and high magnetic fields. This strong increase of the diffusion length (for constant Gilbert damping) happens when

$$\frac{\sigma_{xx}(H_1,\eta)}{\sigma_{xx}(H_2,\eta)} > \frac{g_\mu(H_1)}{g_\mu(H_2)}\,, \tag{4.46}$$

where $H_{1,2}$ are two given values of the applied magnetic field, with $H_1 > H_2$. To understand the dependence of the ratio $\sigma_{xx}(H_1,\eta)/\sigma_{xx}(H_2,\eta)$ on $\eta$ and on the temperature, we recall that the main contribution to the magnon spin conductivity $\sigma_{xx}$ arises from magnon-like branches. At relatively high temperature, the magnon-like branches are sufficiently populated to overcome the phonon contribution to the magnon spin conductivity at all $\eta$. Indeed, Fig. 4.6(a) shows that, at relatively high temperatures, the ratio $\sigma_{xx}(H_1,\eta)/\sigma_{xx}(H_2,\eta)$ hardly depends on $\eta$. On the other hand, when the temperature decreases below the magnon energy, the contribution of the magnon-like branches are quickly frozen out by a magnetic field. The magnitude of $\eta$ then becomes very relevant. On the other hand, while the right-hand side of Eq. (4.46) depends on temperature, it is not affected by $\eta$. For $\eta < 1$, the phonon mobility is smaller than the magnon one and hence the phonons are short circuited by the magnons. For $\eta > 1$, the phonons prevail, leading to a higher ratio $\sigma_{xx}(H_1,\eta)/\sigma_{xx}(H_2,\eta)$ because

the phonon dispersion is not affected by the magnetic field. When $\eta \gg 1$, the condition (4.46) is therefore satisfied. While in this regime the spin current is very small, it is perhaps an interesting limit for studying fluctuation and shot noise in the spin current [71].

### 4.4.3 Comparison with experiments

The spin Seebeck effect was measured in Pt|YIG|GGG structures in the longitudinal configuration, i.e., by applying a temperature difference normal to the interfaces ($x$-direction) and subjecting the sample to a magnetic field $\mathbf{H} \parallel \hat{\mathbf{z}}$ [20]. The thermal bias induces a spin current into the Pt layer that by the inverse Spin Hall effect (ISHE) leads to the detected transverse voltage $V$ over the contact, see Fig. 4.1. The bottom of the GGG substrate and the top of the Pt layer are in contact with heat reservoirs at temperature $T_L$ and $T_H$, respectively. Disregarding phonon (Kapitza) interface resistances, the phonon temperature gradient is $\boldsymbol{\nabla} T = (T_H - T_L)/L$, with $L$ being the thickness of the stack, and average temperature $T = (T_H + T_L)/2$. As discussed, we assume that the magnon and phonon temperatures are the same and disregard the interface mixing conductance. The measured voltage is then directly proportional to the bulk spin Seebeck coefficient.

In the experimental temperature range of $3.5{-}50\,\mathrm{K}$ the thermal magnon, $\Lambda_{\mathrm{mag}}$, and phonon, $\Lambda_{\mathrm{ph},\mu}$, wavelengths are of the order of $1 - 10$ nm. Even if the magnon and phonon thermal mean free paths have been estimated to be of the order of $\sim 100$ $\mu$m at very low temperatures [81], here we assume that the transport in the YIG film of thickness $L \simeq 4\,\mu$m can be treated semiclassically. Note that scattering at the interfaces can make the transport diffusive even when the formal conditions for diffusive transport are not satisfied. The bulk spin Seebeck coefficient is then well-described by Eq. (4.30) and proportional to the observed voltage $V$. These assumptions are encouraged by the good agreement for the observed and calculated peak structures at $H_\perp$ and $H_\parallel$ with a single fitting parameter $\eta = 100$ [20]. We may therefore conclude that the disorder potential scatters the magnons more than the phonons and is therefore likely to be magnetic.

## 4.5 Conclusion and Outlook

We have established a framework which captures the effects of the magnetoelastic interaction on the transport properties of magnetic insulators. In particular, we show that the magnon-phonon coupling gives rise to peak-like

or dip-like structures in the field dependence of the spin and heat transport coefficients, and of the spin diffusion length.

Our numerical evaluation reproduces the peaks in the observed low temperature longitudinal spin Seebeck voltages of YIG|Pt layers as a function of magnetic field. We quantitatively explain the temperature-dependent behavior of these anomalies in terms of hybrid magnon-phonon excitations ("magnon-polarons"). The peaks occur at magnetic fields and wave numbers at which the phonon dispersion curves are tangents to the magnon dispersion, i.e., when magnon and phonon energies as well as group velocities become the same. Under these conditions the effects of the magnetoelastic interaction are maximized. The computed angle dependence shows a robustness of the anomalies with respect to rotations of the magnetization relative to the temperature gradient. The agreement between the theory and the experimental results confirms that elastic magnon(phonon) impurity-scattering is the main relaxation channel that limits the low temperature transport in YIG. Our theory contains one adjustable parameter that is fitted to the large set of experimental data, consistently finding a much better acoustic than magnetic quality of the samples. The spin Seebeck effect is therefore a unique analytical instrument not only of magnetic, but also mechanical material properties. The predicted effects of magnon-polaron effects on magnonic spin and heat conductivity call for further experimental confirmation.

We believe that the presented results open new avenues in spin caloritronics. We focused here on the low energy magnon dispersion of cubic YIG, which is well represented by the magnetostatic exchange waves of a homogeneous ferromagnet [78]. However, the theoretical framework can be easily extended to include anisotropies as well as ferri- or antiferromagnetic order. The magnetoelastic coupling in YIG is relatively small and the conspicuous magnon-polaron effects can be destroyed easily. However, in materials with large magnon-phonon couplings these effects should survive in the presence of larger magnetization broadening as well as higher temperatures.

# 5 Landau-Lifshitz theory of the magnon-drag thermopower

Metallic ferromagnets subjected to a temperature gradient exhibit a magnonic drag of the electric current. We address this problem by solving a stochastic Landau-Lifshitz equation to calculate the magnon-drag thermopower. The long-wavelength magnetic dynamics result in two contributions to the electromotive force acting on electrons: (1) An adiabatic Berry-phase force related to the solid angle subtended by the magnetic precession and (2) a dissipative correction thereof, which is rooted microscopically in the spin-dephasing scattering. The first contribution results in a net force pushing the electrons towards the hot side, while the second contribution drags electrons towards the cold side, i.e., in the direction of the magnonic drift. The ratio between the two forces is proportional to the ratio between the Gilbert damping coefficient $\alpha$ and the coefficient $\beta$ parametrizing the dissipative contribution to the electromotive force.[1]

## 5.1 Introduction

The interest in thermoelectric phenomena in ferromagnetic heterostructures has been recently revived by the discovery of the spin Seebeck effect [29,30]. This effect is now understood to stem from the interplay of the thermally-driven magnonic spin current in the ferromagnet and the (inverse) spin Hall voltage generation in an adjacent normal metal [31]. Lucassen *et al.* [36] subsequently proposed that the thermally-induced magnon flow in a metallic ferromagnet can also produce a detectable (longitudinal) voltage in the bulk itself, due to the spin-transfer mechanism of magnon drag. Specifically, smooth magnetization texture dynamics induce an electromo-

[1] This Chapter is directly based on *Landau-Lifshitz theory of the magnon-drag thermopower*, B. Flebus, R. A. Duine, and Y. Tserkovnyak, EPL **115**, 57004 (2016). For this paper, B. Flebus performed all analytical calculations, while Y. Tserkovnyak conceived the project. B. Flebus drafted the paper, all other authors contributed to the text.

tive force [1,2], whose net average over thermal fluctuations is proportional to the temperature gradient.

In this Chapter, we develop a Landau-Lifshitz theory for this magnon drag, which generalizes Ref. [36] to include a heretofore disregarded Berry-phase contribution. This additional magnon drag can reverse the sign of the thermopower, which can have potential utility for designing scalable thermopiles based on metallic ferromagnets.

## 5.2 Seebeck coefficient

Electrons propagating through a smooth dynamic texture of the directional order parameter $\mathbf{n}(\mathbf{r},t)$ [such that $|\mathbf{n}(\mathbf{r},t)|\equiv 1$, with the self-consistent spin density given by $\mathbf{s}=s\mathbf{n}$] experience the following geometric electromotive force [1,2]

$$F_i=\frac{\hbar}{2}\left(\mathbf{n}\cdot\partial_t\mathbf{n}\times\partial_i\mathbf{n}-\beta\partial_t\mathbf{n}\cdot\partial_i\mathbf{n}\right), \tag{5.1}$$

for spins up along $\mathbf{n}$ and $-F_i$ for spins down. The resulting electric current density is given by

$$j_i=\frac{\sigma_\uparrow-\sigma_\downarrow}{e}\langle F_i\rangle=\frac{\hbar P\sigma}{2e}\langle\mathbf{n}\cdot\partial_t\mathbf{n}\times\partial_i\mathbf{n}-\beta\partial_t\mathbf{n}\cdot\partial_i\mathbf{n}\rangle, \tag{5.2}$$

where $\sigma=\sigma_\uparrow+\sigma_\downarrow$ is the total electrical conductivity, $P=(\sigma_\uparrow-\sigma_\downarrow)/\sigma$ is the conducting spin polarization, and $e$ is the carrier charge (negative for electrons). The averaging $\langle\ldots\rangle$ in Eq. (5.2) is understood to be taken over the steady-state stochastic fluctuations of the magnetic orientation. The latter obeys the stochastic Landau-Lifshitz-Gilbert equation [94]

$$s(1+\alpha\mathbf{n}\times)\partial_t\mathbf{n}+\mathbf{n}\times(H\mathbf{z}+\mathbf{h})+\sum_i\partial_i\mathbf{j}_i=0, \tag{5.3}$$

where $\alpha$ is the dimensionless Gilbert parameter [7], $H$ parametrizes a magnetic field (and/or axial anisotropy) along the $z$ axis, and $\mathbf{j}_i=-A\mathbf{n}\times\partial_i\mathbf{n}$ is the magnetic spin-current density, which is proportional to the exchange stiffness $A$. For $H>0$, the equilibrium orientation is $\mathbf{n}\to-\mathbf{z}$, which we will suppose in the following.

The Langevin field stemming from the (local) Gilbert damping is described by the correlator [95]

$$\langle h_i(\mathbf{r},\omega)h_j^*(\mathbf{r}',\omega')\rangle=\frac{2\pi\alpha s\hbar\omega\delta_{ij}\delta(\mathbf{r}-\mathbf{r}')\delta(\omega-\omega')}{\tanh\frac{\hbar\omega}{2k_BT(\mathbf{r})}}, \tag{5.4}$$

upon Fourier transforming in time: $\mathbf{h}(\omega) = \int dt e^{i\omega t}\mathbf{h}(t)$. At temperatures much less than the Curie temperature, $T_c$, it suffices to linearize the magnetic dynamics with respect to small- angle fluctuations. To that end, we switch to the complex variable, $n \equiv n_x - in_y$, parametrizing the transverse spin dynamics. Orienting a uniform thermal gradient along the $x$ axis, $T(x) = T + x\partial_x T$, we Fourier transform the Langevin field (5.4) also in real space, with respect to the $y$ and $z$ axes. Linearizing Eq. (5.3) for small-angle dynamics results in the Helmholtz equation:

$$A(\partial_x^2 - \kappa^2)n(x, \mathbf{q}, \omega) = h(x, \mathbf{q}, \omega), \tag{5.5}$$

where $\kappa^2 \equiv q^2 + [H - (1 + i\alpha)s\omega]/A$, $h \equiv h_x - ih_y$, and $\mathbf{q}$ is the two-dimensional wave vector in the $yz$ plane.

Solving Eq. (5.5) using the Green's function method, we substitute the resulting $n$ into the expression for the charge current density (5.2), which can be appropriately rewritten in the following form (for the nonzero $x$ component):

$$j_x = \frac{\hbar P\sigma}{2e}\int \frac{d^2\mathbf{q}d\omega}{(2\pi)^3}\omega\,\mathrm{Re}\frac{(1+i\beta)\langle n(x,\mathbf{q},\omega)\partial_x n^*(x,\mathbf{q}',\omega')\rangle}{(2\pi)^3\delta(\mathbf{q}-\mathbf{q}')\delta(\omega-\omega')}\,. \tag{5.6}$$

Tedious but straightforward manipulations, using the correlator (5.4), finally give the following thermoelectric current density:

$$j_x = \frac{\alpha s P\sigma\partial_x T}{4eA^2k_BT^2}\int \frac{d^2\mathbf{q}d\omega}{(2\pi)^3}\frac{(\hbar\omega)^3}{\sinh^2\frac{\hbar\omega}{2k_BT}}\mathrm{Re}\left[(1+i\beta)I\right], \tag{5.7}$$

where $I(\kappa) \equiv \kappa/|\kappa|^2(\mathrm{Re}\,\kappa)^2$, having made the convention that $\mathrm{Re}\,\kappa > 0$.

To recast expression (5.7) in terms of magnon modes, we incorporate the integration over $q_x$ by noticing that, in the limit of low damping, $\alpha \to 0$,

$$I = \frac{2}{\pi}\int dq_x \frac{1 + iq_x^2/\alpha\tilde{\omega}}{(\tilde{\omega} - q_x^2 - q^2 - \xi^{-2})^2 + (\alpha\tilde{\omega})^2}\,. \tag{5.8}$$

Here, we have introduced the magnetic exchange length $\xi \equiv \sqrt{A/H}$ and defined $\tilde{\omega} \equiv s\omega/A$. After approximating the Lorentzian in Eq. (5.8) with the delta function when $\alpha \ll 1$, Eq. (5.7) can finally be expressed in terms of a dimensionless integral

$$J(a) \equiv \int_{a/\sqrt{2}}^{\infty} dx \frac{x^5\sqrt{2x^2 - a^2}}{\sinh^2 x^2}, \tag{5.9}$$

as

$$\mathbf{j} = \left(1 - \frac{\beta}{3\alpha}\right) J\left(\frac{\lambda}{\xi}\right)\frac{k_B P\sigma}{\pi^2 e}\left(\frac{T}{T_c}\right)^{3/2}\boldsymbol{\nabla}T\,. \tag{5.10}$$

Here, $T$ is the ambient temperature, $k_B T_c \equiv A(\hbar/s)^{1/3}$ estimates the Curie temperature, and $\lambda \equiv \sqrt{\hbar A/sk_B T}$ is the thermal de Broglie wavelength in the absence of an applied field. We note that $\alpha, \beta \ll 1$ while $\alpha \sim \beta$, in typical transition-metal ferromagnets [2].

For temperatures much larger than the magnon gap (typically of the order of 1 K in metallic ferromagnets), $\lambda \ll \xi$ and we can approximate $J(\lambda/\xi) \approx J(0) \sim 1$. This limit effectively corresponds to the gapless magnon dispersion of $\epsilon_{\mathbf{q}} \equiv \hbar\omega_{\mathbf{q}} \approx \hbar A q^2/s$. Within the Boltzmann phenomenology, the magnonic heat current induced by a uniform thermal gradient is given by $\mathbf{j}_Q = -\boldsymbol{\nabla} T \int [d^3\mathbf{q}/(2\pi)^3](\partial_{q_x}\omega_{\mathbf{q}})^2 \tau(\omega_{\mathbf{q}})\epsilon_{\mathbf{q}}\partial_T f_{\mathrm{B}}$, where $\tau^{-1}(\omega_{\mathbf{q}}) = 2\alpha\omega_{\mathbf{q}}$ is the Gilbert-damping decay rate of magnons (to remain within the consistent LLG phenomenology) and $f_{\mathrm{B}} = [\exp(\epsilon_{\mathbf{q}}/\mathrm{k_B T}) - 1]^{-1}$ is the Bose-Einstein distribution function. By noticing that

$$\epsilon_{\mathbf{q}}\partial_T f_{\mathrm{B}} = k_B \left[\frac{\hbar\omega_{\mathbf{q}}/2k_B T}{\sinh(\hbar\omega_{\mathbf{q}}/2k_B T)}\right]^2 , \tag{5.11}$$

it is easy to recast the second, $\propto \beta$ contribution to Eq. (5.10) in the form

$$\mathbf{j}^{(\beta)} = \beta \frac{\hbar P\sigma}{2eA}\mathbf{j}_Q \, , \tag{5.12}$$

which reproduces the main result of Ref. [36].

The magnon-drag thermopower (Seebeck coefficient),

$$S = -\left.\frac{\partial_x V}{\partial_x T}\right|_{j_x=0} , \tag{5.13}$$

corresponds to the voltage gradient $\partial_x V$ induced under the open-circuit condition. We thus get from Eq. (5.10):

$$S = \left(\frac{\beta}{3\alpha} - 1\right) J\frac{k_B P}{\pi^2 e}\left(\frac{T}{T_c}\right)^{3/2} = (\beta - 3\alpha)\,\frac{\hbar P\kappa_m}{2eA} \, , \tag{5.14}$$

where $\kappa_m = (2/3\pi^2)Jk_B A(T/T_c)^{3/2}/\alpha\hbar$ is the magnonic contribution to the heat conductivity. Such magnon-drag thermopower has recently been observed in Fe and Co, with scaling $\propto T^{3/2}$ over a broad temperature range and opposite sign in the two metals [37]. Note that the sign depends on $\beta/\alpha$ and the effective carrier charge $e$.

## 5.3 Discussion and conclusions

Equations (5.10) and (5.14) constitute the main results of this Chapter. In the absence of Gilbert damping, $\alpha \to 0$, the magnon-drag thermopower

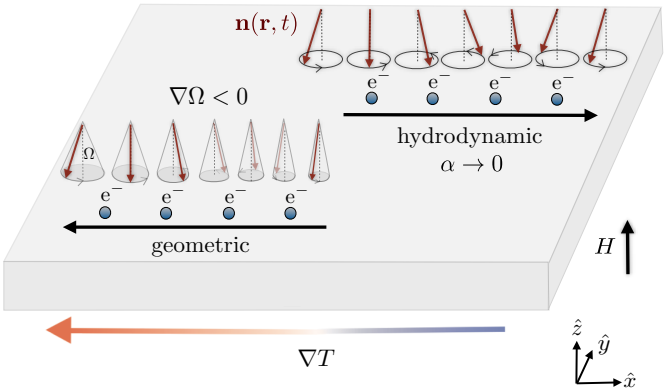


**Figure 5.1:** Schematics for the two contributions to the electron-magnon drag. In the absence of decay (i.e., $\alpha \to 0$), magnons drifting from the hot (left) side to the cold (right) side drag the charge carriers viscously in the same direction, inducing a thermopower $\propto \beta$. The (geometric) Berry-phase drag governed by the magnon decay is proportional to $\alpha$ and acts in the opposite direction. It is illustrated for a spin wave that is thermally emitted from the left. As the spin wave propagates to the right, the solid angle $\Omega$ subtended by the spin precession shrinks, inducing a force oriented to the left for spins parallel to $\mathbf{n}$.

$S$ is proportional to the heat conductivity. This contribution was studied in Ref. [36] and is understood as a viscous hydrodynamic drag. In simple model calculations [2], $\beta P > 0$ and this hydrodynamic thermopower thus has the sign of the effective carrier charge $e$. When $P > 0$, so that the majority band is polarized along the spin order parameter $\mathbf{n}$, the $\propto \alpha$ contribution to the thermopower is opposite to the $\propto \beta$ contribution. (Note that $\alpha$ is always $> 0$, in order to yield the positive dissipation.)

The underlying geometric meaning of this result is sketched in Fig. 5.1. Namely, the spin waves that are generated at the hot end and are propagating towards the cold end are associated with a decreasing solid angle, $\partial_x \Omega < 0$. The first term in Eq. (5.1), which is rooted in the geometric Berry connection [97–100], is proportional to the gradient of this solid angle times the precession frequency, $\propto \omega \partial_i \Omega$, resulting in a net force towards the hot side acting on the spins collinear with $\mathbf{n}$.

Note that we have neglected the Onsager-reciprocal backaction of the spin-polarized electron drift on the magnetic dynamics. This is justified as including the corresponding spin-transfer torque in the LLG equation would yield higher-order effects that are beyond our treatment. The backaction by the spin-transfer torque would be absent when the longitudinal spin current, $\mathbf{j}_i = \sigma(PE_i + F_i/e)\mathbf{n}$, vanishes, where $E_i$ is the electric field

and $F_i$ is the spin-motive force (5.1). Understanding Eq. (5.10) as pertaining to the limit of the vanishing spin current $\mathbf{j}_i$ rather than electric current $j_i = \sigma(E_i + PF_i/e)\mathbf{n}$ would, however, result in higher-order (in $T/T_c$) corrections to the Seebeck coefficient (5.13). These are beyond the level of our approximations.

The diffusive contribution to the Seebeck effect, $\propto T/E_F$, where $E_F$ is a characteristic Fermi energy, which has been omitted from our analysis, is expected to dominate only at very low temperatures [37]. The conventional phonon-drag effects have likewise been disregarded. A systematic study of the relative importance of the magnon and phonon drags is called upon in magnetic metals and semiconductors.

# Outlook

This Thesis has dealt with two overarching themes: the interplay between coherent and incoherent spin dynamics, with a particular focus on planar magnets, where the coherent dynamics is superfluid in nature, and the mutual interaction between magnons, electrons and phonons. While our research has lead to progress within both directions, it has yielded, at the same time, new open questions.

The first concerns the interactions between coherent and incoherent spin dynamics, and precisely more the magnitude of the coupling constants appearing in our theory. While an analytical estimate has already been given, only fitting our theoretical predictions to experimental data can indisputably assess the order of magnitude of the coupling constants and thus the relevance of the coupled dynamics. This could be achieved by utilizing well-established techniques capable of generating coherent dynamics such as microwave pumping, without invoking spin superfluid dynamics, whose detection and manipulation is still largely unexplored.

Concerning the latter, the presented transport framework provides an adequate basis to address the concomitant experimental progress. As in this work we focused solely on spin transport phenomena, we still need to address the coupled spin and heat dynamics and assess how spin superfluidity influences heat propagation.

In most of materials, however, there are further anisotropies within the $xy$ plane, e.g., an easy-axis anisotropy along the $\hat{x}$ or $\hat{y}$ direction. These anisotropies break the helical spin winding, pertaining to the spin superfluid, down into particle-like topological solitons. In the case of an easy-axis anisotropy, for example, in a magnetic wire, chiral domain walls take over as elementary building blocks of a general planar spin texture (see Fig. 5.2). While these anisotropies might appear detrimental to spin superfluidity as they lift the $U(1)$ symmetry, a more robust hydrodynamics than the superfluid one seems to emerge from them. This hydrodynamics is rooted in the conserved topological charge, which supersedes the $z$-component of the spin angular momentum. In the case of the magnetic textures depicted

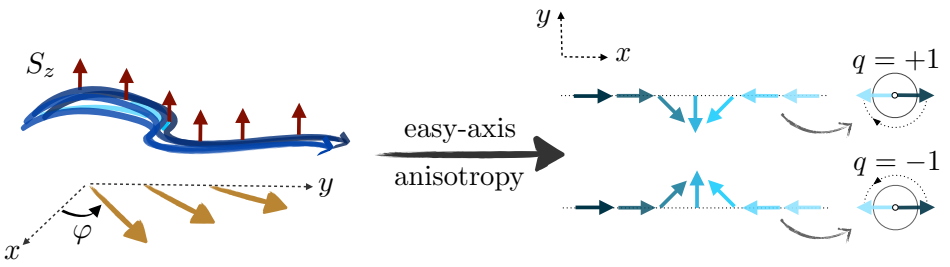


**Figure 5.2:** In a planar ferromagnet, the winding of the phase $\varphi$ carries the flow of the $z$-component $S_z$ of the spin angular momentum. Subjected to an easy-axis anisotropy along the $x$ axis, the spin winding in the $xy$ plane breaks down into a train of domain walls. Defining the topological charge of a domain wall in terms of its chirality, we assign $q = +1$ to the clockwise-wound domain walls and $q = -1$ to the anticlockwise-wound ones. The conservation of the net winding of the phase in the $xy$ plane ensures the conservation of the net topological charge, which is carried by single domain walls.

in Fig. 5.2, the topological charge is a measure of the chirality of the domain wall, i.e., we assign $q = +1$ to the clockwise-wound domain walls and $q = -1$ to the anticlockwise- wound ones. The topological charge density is carried by individual domain walls and its transport mimics many manifestations of spin superfluidity [67].

In this sense, part of the work carried out in this Thesis can be regarded as a foundation for investigating broader superfluids dynamics, which go beyond the $U(1)$ superfluidity, and still all rely on the idea of superseding the exponential decaying magnon hydrodynamics with a purely geometric spin dynamics. The concepts illustrated by the above example are general and in future work they could be extended to any topological invariant that can be distributed over particle-like topological defects in magnetic system. For example, a two-dimensional physical realization is provided by a magnetic film carrying an ensemble of vortices or skyrmions, with the net skyrmion number playing the role of a topological invariant [103].

Moving to the research conducted on the effects on magnon-phonon coupling on thermally-driven spin transport, our results are in excellent agreement with the experimental observations, which is a good indicator of the validity of our approach. Therefore, our further predictions on the other spin and heat transport coefficients, will hopefully encourage future experimental investigations. Of interest would be also to extend our theory to capture the transport properties of magnon-polarons arising in magnetic systems with different crystalline symmetries, and in antiferromagnetic ma-

terials. The unambiguous observation of signatures of coupling mechanisms between thermal magnons and collective excitation suggests that the interaction between the superfluid dynamics and phonons could lead as well to a number of unexplored phenomena and still needs to be addressed.

Turning to our last Chapter, the discovery of a novel magnon drag contribution to the thermopower, whose sign is opposite to the one of the previously known contribution, carries important consequences. As recent experiments demonstrated, the magnon drag contribution can dominate the thermopower over a broad range of temperatures. The ratio $\alpha/\beta$ between the different magnon-drag contributions depends on microscopic details of the system under consideration, and can possibly be controlled by doping the material [96]. As the possibility of engineering ferromagnetic metals with opposite thermopowers suggests intriguing perspective for a new generation of devices, we hope that our results will stimulate experimental efforts in this direction. We want to remark that in our work only the mutual electron-magnon interaction has been taken into account, as the inclusion of phononic degrees of freedom leads to a considerably more convoluted and involved dynamics. Nonetheless, in the future the mutual phonon, magnon and electron interactions should be addressed systematically.

# Summary

Efficient storage and transmission of information has been and remains among the most desired technological objectives. These needs have fueled tremendous basic research on electron transport in condensed matter. While the traditional devices based on semiconductors and metals rely solely on electric charge flows, cutting-edge research has been shifting towards novel transport phenomena involving spin degrees of freedom in magnetic materials. Specifically, a vigorous interest in spin transport phenomena activated by heat fluxes has risen recently, as the possibility of converting energy abandoned as waste heat back to electric power carries promising potential for more efficient and sustainable devices.

In this Thesis, we have investigated the magnetic dynamics in both insulating and metallic magnetic systems, with an eye on deepening the understanding of well-established thermally-activated spin transport phenomena, and on exploring alternative ways of transmitting information via spin dynamics. Chapter 1 is intended to give the reader an overview of the state-of-the-art, and also introduces the experimental techniques to which we refer in the following chapters. Moreover, it acquaints the reader with the concept of magnon, i.e., the quantized version of the spin-wave oscillations in the magnetization, as a carrier of spin.

In the first part of this Thesis, we depart from the paradigm of diffusive particle-like magnon transport by focusing on coherent spin dynamics. Specifically, we turn our attention to systems in which the coherent spin dynamics is constrained by anisotropies to undergo planar precession. In such cases, we can benefit from the notion of spin superfluidity as the collective dynamics mimics the one of neutral superfluids. The geometric spin superfluid dynamics is fundamentally distinct from the incoherent magnetic dynamics, which is activated only at finite temperature and suffers from Ohmic-like dissipation. It differs as well from the coherent spin motion induced by RF or microwave fields, as the spontaneous character of a spin superfluid allows it to carry currents, which suffer of very little dissipation, without any external driving source. In Chapter 2, we investigate the finite

temperature dynamics of a spin superfluid in a planar magnet. Namely, we derive a two-fluid theory describing the interplay between a spin superfluid and thermal magnons. We discuss as well how thermoelectric measurements can be deployed to probe spin superfluidity. In Chapter 3, we build a general phenomenology describing the coupling between coherent and incoherent spin dynamics in magnetic insulators. Our results pave the way for converting waste heat into coherent spin dynamics in a controlled fashion. While our derivation focuses on magnetic insulators with $U(1)$ symmetry, it can be easily extended to other systems. As an example, we address a planar ferromagnet, whose coherent dynamics is superfluid in nature, coupled to a magnet hosting a domain-wall. We show how the interconversion between thermal magnons and spin superfluid can be used to control the motion of a domain-wall in low dissipation regimes.

The overarching theme of the second part of this Thesis is the interplay between the magnetization dynamics and other degrees of freedom, such as electrons and collective lattice excitations. Motivated by recent spin transport experiments, in Chapter 4 we derive a transport theory for magnon-polarons, i.e., the quasi-particles arising from the coupling between magnetic and elastic excitations. Our results show that the hybridization between magnons and phonons is responsible for the appearance of anomalous features in the magnetic-field dependence of the transport coefficients, in agreement with the experimental observations. Besides, we unveil how these features can be interpreted to assess the relative magnetic and acoustic quality of a sample. Our further predictions of anomalies in spin and heat transport coefficients will hopefully encourage additional experimental investigation. In Chapter 5, we turn our focus to the charge transport induced by a thermal bias in a ferromagnetic metal. We investigate how the resulting magnetization dynamics influences the electrons' motion, resulting in two magnon-drag contributions to the thermopower, one of viscous nature, the other rooted in the geometry of the damped magnetic precession. The magnon drag contributions have opposite sign and their relative magnitude can possibly be controlled by manufacturing processes, opening new prospects for thermoelectric devices based on metals.

# Samenvatting

Het efficiënt opslaan en verzenden van informatie is een erg belangrijke technologische behoefte. Deze drijfveer heeft uiteindelijk geleid tot een stroom aan fundamenteel onderzoek naar elektronentransport binnen de gecondenseerde materie. De meeste traditionele apparaten zijn immers gebaseerd op halfgeleiders of metalen, en deze zijn daarom sterk afhankelijk van de manier waarop elektrische lading door deze materialen stroomt. In het hedendaagse onderzoek verschuift de aandacht echter langzaam naar nieuwe transportmechanismen waarbij de spinvrijheidsgraden in magnetische materialen een belangrijke rol spelen. In het bijzonder is er recentelijk veel interesse naar spintransportverschijnselen die geactiveerd worden door middel van warmtefluxen. Op deze manier kan afvalwarmte indirect worden omgezet naar elektriciteit en dit kan weer leiden tot de ontwikkeling van duurzame apparaten.

In dit proefschrift hebben we de magnetisatiedynamica in isolerende en metallische, magnetische systemen onderzocht met een speciale nadruk op het begrijpen van de welbekende thermisch geactiveerde spintransportverschijnselen. Tevens hebben we alternatieve manieren onderzocht om informatie te verzenden door middel van spindynamica.

Hoofdstuk 1 geeft de lezer een samenvatting van het hedendaagse onderzoek, en bovendien worden de experimentele technieken beschreven waar we in latere hoofdstukken naar zullen verwijzen. Ook leggen we het concept magnon uit (gekwantiseerde trillingen van spingolven in de magnetisatie) en we zetten uiteen hoe dit gebruikt kan worden om spin over te dragen.

In het eerste gedeelte van dit proefschrift leiden we een theorie af dat gebruikmaakt van coherente spindynamica, en dit gaat verder dan het paradigma van diffusieve magnonentransport waarbij de magnonen als deeltjes behandeld worden. In het bijzonder brengen we systemen onder de aandacht waarbij de coherente spindynamica beperkt wordt door anisotropieën, wat ertoe leidt dat alleen precessie van de magnetisatie in een tweedimensionaal vlak mogelijk is. In deze gevallen kunnen we gebruikmaken van de notie spinsuperfluïditeit, aangezien de collectieve dy-

namica hetzelfde is als die van neutrale superfluïde vloeistoffen. De geometrische spinsuperfluïditeitsdynamica is fundamenteel anders dan de incoherente magnetisatiedynamica. Laatstgenoemde kan immers alleen geactiveerd worden bij eindige temperaturen met daarbij het optreden van de onwenselijke Ohmse dissipatie. Ook verschilt het van de coherente beweging van spins die door radiofrequente straling of door microgolven ontstaat. De spontane vorming van een superfluïde spinvloeistof leidt namelijk tot het ontstaan van dissipatievrije stromen zonder dat er een externe bron nodig.

In hoofdstuk 2 onderzoeken we de spindynamica van een superfluïde spinvloeistof bij een eindige temperatuur, waarbij de magnetisatie beperkt is in een tweedimensionaal vlak. We leiden een twee-fluïda theorie af die de wisselwerking beschrijft tussen een superfluïde spinvloeistof en thermische magnonen. We beschrijven tevens hoe thermo-elektrische metingen gebruikt kunnen worden om spinsuperfluïditeit vast te stellen.

In hoofdstuk 3 beschrijven we fenomenologisch de koppeling tussen coherente en incoherente spindynamica in magnetische isolatoren. Onze resultaten laten zien dat het mogelijk is om op een gecontroleerde manier afvalwarmte om te zetten naar een coherente spindynamica. Onze theoretische afleiding richt zich op magnetische isolatoren met $U(1)$ symmetrie, maar dit kan makkelijk worden uitgebreid naar andere systemen. Als een voorbeeld nemen we een ferromagneet waarbij de magnetisatie slechts in een tweedimensionaal vlak kan bewegen. De coherente dynamica van de ferromagneet kan worden beschreven als een superfluïde vloeistof gekoppeld aan een magneet met domeinmuren. We laten zien dat de omzetting van thermische magnonen naar een superfluïde spinvloeistof gebruikt kan worden om de beweging van domeinmuren te manipuleren in regimes met weinig dissipatie.

Het tweede gedeelte van dit proefschrift gaat over de wisselwerking van de magnetisatiedynamica met andere vrijheidsgraden, zoals elektronen of collectieve roosterexcitaties. In hoofdstuk 4 leiden we een transporttheorie af voor zogenaamde magnon-polaronen, die een belangrijke rol zal spelen voor het begrijpen van recente spintransportexperimenten. Deze quasideeltjes ontstaan door de koppeling tussen magnetische en elastische excitaties. Onze resultaten laten zien dat de hybridisatie tussen magnonen en fononen resulteert in een atypische afhankelijkheid van transportcoefficiënten als functie van het magnetische veld, wat weer overeenstemt met experimentele waarnemingen. Bovendien hebben we laten zien hoe we deze kenmerken kunnen begrijpen met informatie over de relatieve magnetische en akoestische kwaliteit van het experimentele monster. Onze voorspellingen

betreft het atypische gedrag van spin- en warmtetransportcoefficiënten zal hopelijk leiden tot nieuwe experimenten.

In hoofdstuk 5 richten we ons op het ladingstransport dat geïnduceerd wordt door een thermische bias in een ferromagnetisch metaal. We onderzoeken hoe de resulterende magnetisatiedynamica de elektronenbeweging beïnvloedt, en hoe dit uiteindelijk leidt tot twee wrijvingsbijdragen van de magnonen aan het thermovermogen: hiervan is één van viskeuze aard, terwijl de andere bijdrage geometrisch van aard is met betrekking tot de gedempte magnetische precessie. Deze magnonwrijvingsbijdragen hebben een tegengesteld teken en hun relatieve grootte kan worden gemanipuleerd in het productieproces. De laatstgenoemde kan uiteindelijk weer leiden tot nieuwe mogelijkheden om thermo-elektrische apparaten te maken die gebaseerd zijn op metalen.

# Curriculum Vitae

I was born on September 18th, 1989 in Cividale del Friuli, a town in the north-east of Italy. I attended the Liceo Classico Stellini in Udine, from which I obtained my high school diploma *cum laude* in 2007. In the fall of the same year, I enrolled in the Bachelor program in Physics at the University of Trieste. I graduated *cum laude* in the summer of 2010 with an experimental thesis on nanostructures of carbon nanotubes and DNA for protein detection. In the fall of 2010, I enrolled in a master program in Physics and Applications at UPMC Institute in Paris. I pursued my master thesis research in Netherlands at the Kavli Institute of Nanoscience under the supervision of Cees Dekker, and I have received my degree in 2012. The following year, I was awarded a degree in Physics from the École Polytechnique Fédérale de Lausanne. My master thesis research, focused on Majorana fermions in superconductor-Luttinger liquid junctions, was conducted at UVA under the supervision of Jean-Sébastien Caux. In April 2013 I started my PhD research in Utrecht in under the supervision of Prof. Rembert Duine. The results of this research are the main subjects of this thesis.

# Acknowledgments

First of all I would like to thank my supervisor Rembert for the guidance he gave me and all the discussions we had during these years. For your patience with my impatience, for trusting me in being able to finalize my work even when I did not trust it myself, for downplaying my unjustified moments of panic with references to the innate hysteria of Italian women, for reminding me every week that, despite every possible bad thing, at least my expiration date was not there yet, and overall for your incredibly warm and fun personality which made these years a great experience. Secondly, I would like to thank my collaborator Yaroslav for giving me the incredible opportunity of working with him. Not only you taught me in such short time so many things about physics and being a physicist, but during this last year you managed to make me probably one of the most knowledgeable Italians on Soviet history and the maleficence of Russia. I promise you, always slava Ukraini!

I would like to thank also Scott, Ka, Pramey, Gerrit and all the experimental group of Saitoh in Japan for the nice collaborations we had. I would like to thank all my colleagues and former colleagues for nice atmosphere that there has always been at the department, especially Arie-Willem and Jeffrey. The first two years we spent together in the department were great, I have been missing you a lot. And Scott and Camilo, lunch breaks became way more fun since you arrived! A special note to Karoline, you have been such a wonderful colleague. I hope we will stay friends no matter where life will bring us.

An enormous thanks to all my friends here in Utrecht, I can not even imagine what life would have been without you. For those who have been here all the time, those who already departed, those who came later, thanks to all of you for making me feel so much at home and making this town one of the places in which I have been the happiest. Thank you Ale for all our chats, for being always able to count on you and for you being a wonderful person and friend. Thank you Angela for the amazingly good energy you brought in my life, for all fun we had hanging around in the

middle of the nights and the festivals and all the serious talks and all the desperate cigarette breaks from work that we had in the between. Thank you Dora for taking a chance with me as a flatmate long time ago, and for not having given up even after I set the microwave on fire and filled the house with smoke only a week later. Thank you even more for keeping being my friend after, you have such a happy and strong personality that you have been an inspiration to me. You, Ana, are the first real friend I met in Utrecht almost four years ago and having met you has been a true blessing. You are one of the sweetest people I have ever met, and finding you again in Los Angeles was great. Thank you Bastiaan for all our discussions, all your teasing and your fabulous dancing and our sometimes infinite paranoia analysis sessions. You have been one of my greatest friend here in Utrecht.

Thank you Diana for the great lunches we had together, for the afternoons spent in your old house, to Eduardo for all the conversations and inside jokes, to Wing for the funniest dances and amazing dumplings (both dances and dumplings chicken-based), to Gwen for being almost too fun to be true, and to Nacho for all the beers and great chats, and to you all for being always so welcoming. You are truly amazing people, I am so happy I have met you! Thank you Camilla F. for never boring me for a second, you are one of the most exciting people I have ever met. Meeting you in Utrecht and feeling always welcome in Venice is unbeatable. Thank you Lauri, you are such a sweet, nice and fun person. You have been a great friend and I wish that everything you hope for will become true. Thank you Carlo and Anna R. for both making my day when we meet and especially when you said 'uovo' with your accent, it is as adorable as both you. Thank you Camilla D. for the evenings we spent together, you are one of the people with which I have had the most interesting conversations here and one of the most charming I know. Thank you Stefano and Davide for our many sessions of talking and drinking that started with the promise of 'only a single beer' and ending up in way too many. I always headed home feeling happy all those times, and no, it was not just because of the beers. Thank you Marko and Diana for our conversations, and for making me notice I close my eyes everytime I drink and for that amazing dinner designed around my (imaginary) allergies. Thank you Anna V., Tania and Sandro for all the fun we had especially the first years, all the dinners and meetups. It was great (and still is!) to have you around. Thanks also to Melissa, Vaia, Federica, Shima, Clement, Jonas, Jabiz and Gisela for the time we spent together, and a special thank to my former and present roomates to cooperate with all my messiness and forgetfulness. I would like to

thank also every great person and friend I met elsewhere, you all together contributed to the richness of all these years. A special mention goes to Jacopo, Oktavia, Roland and Micheal. I would like to thank my family, especially my brother and my sister-in-law, for still loving me even if I am almost never home and for being such good people that it makes me feel really proud and lucky to know I am part of your family.

The biggest thank of all is to Fabiana, my mom. It is difficult to thank you for something specific, because I would have to thank you for every single step I took and I am going to take. You have been and you are my biggest inspiration. So, where to start? Thanks you for raising me up all by yourself without ever complaining, thanks for being able to make the best jokes about the worst things that happened, thank you for never giving up, thank you for your vivid imagination and your stories, thank you for showing me how someone can be intellectually honest, independent, strong, caring, so generous, incredibly lively and humorous at the same time. Thank you for always repeating me how important a job should be, especially to a woman, in all the moments in which I felt lost and unmotivated in mine, it has been a precious lesson to recall. Thank you for always being there for me, at any time and anywhere, I do not know you do that!

# Bibliography


[1] R. A. Duine, Phys. Rev. B **77**, 014409 (2008).

[2] Y. Tserkovnyak and M. Mecklenburg, Phys. Rev. B **77**, 134407 (2008).

[3] S. O. Demokritov, V. E. Demidov, O. Dzyapko, G. A. Melkov, A. A. Serga, B. Hillebrands and A. N. Slavin, Nature **443**, 430-433 (2006).

[4] E. B. Sonin, Sov. Phys. JETP **47**, 1091 (1978); Adv. Phys. **59**, 181 (2010).

[5] Yu. M. Bunkov and G. E. Volovik, J. Phys.: Condens. Matter **22**, 164210 (2009).

[6] L. D. Landau and E. M. Lifshitz, Phys. Z. Sowj. **8**, 153 (1935).

[7] T. L. Gilbert, IEEE Trans. Magn. **40**,3443 (2004)

[8] L. Landau, J. Phys. (USSR) **5**, 51 (1941); L. Landau, J. Phys. (USSR) **11**, 205 (1947).

[9] T. Holstein and H. Primakoff, Phys. Rev. **58**, 1098 - 1113 (1940).

[10] A. Griffin, T. Nikuni, and E. Zaremba, *Bose-condensed Gases at Finite Temperatures*, Cambridge University Press, Cambridge (2009).

[11] H. Stoof, J. Low Temp. Phys. **114**, 11-108 (1999).

[12] S. A. Bender, R. A. Duine, A. Brataas, and Y. Tserkovnyak, Phys. Rev. B **90**, 094409 (2014).

[13] L. Berger, Phys. Rev. B **54**, 9353-9358 (1996).

[14] J. C. Slonczewski, J. Magn. Magn. Mater. **159**, L1–L7 (1995).

[15] S. E. Barnes and S. Maekawa, Phys. Rev. Lett. **98**, 246601 (2007).

[16] L. Onsager, Phys. Rev. **37**, 405 (1931); **38**, 2265 (1931).

[17] S. A. Bender, R. A. Duine, and Y. Tserkovnyak, Phys. Rev. Lett., **108**, 246601 (2012).

[18] Y. Tserkovnyak, A. Brataas, and G. E. W. Bauer, Phys. Rev. Lett. **88**, 117601, 2002.

[19] Y. Tserkovnyak, A. Brataas, and G. E. W. Bauer, Phys. Rev. B **66**, 224403, 2002.

[20] T. Kikkawa, K. Shen, B. Flebus, R. A. Duine, K. Uchida, Z. Qiu, G. E. W. Bauer and E. Saitoh, Phys. Rev. Lett. **117**, 207203 (2016).

[21] E. Abrahams and C. Kittel, Phys. Rev. 88, 1200 (1952); Rev. Mod. Phys. **25**, 233 (1953).

[22] C. Kittel, Phys. Rev. **110**, 836 (1958).

[23] T. Kobayashi, R. C. Barker, J. L. Bleustein, and A. Yelon, Phys. Rev. B **7**, 3273 (1973).

[24] M. I. Kaganov and V. M. Tsukernik, Sov. Phys. JETP **9**, 5 151 (1959).

[25] M.I. Dyakonov and V.I. Perel, Phys. Lett. A **35**, 459 (1971).

[26] J. E. Hirsch, Phys. Rev. Lett. **83**, 1834-1837 (1999).

[27] S. Maekawa, Nature Materials **8**, 777 (2009).

[28] Y. Kajiwara, K. Harii, S. Takahashi, J. Ohe, K. Uchida, M. Mizuguchi, H. Umezawa, H. Kawai, K. Ando, K. Takanashi, S. Maekawa, and E. Saitoh, Nature **464**, 262-266 (2010).

[29] K. Uchida, S. Takahashi, K. Harii, J. Ieda, W. Koshibae, K. Ando, S. Maekawa, and E. Saitoh, Nature **455**, 778-781 (2008).

[30] K. Uchida, H. Adachi, T. Ota, H. Nakayama, S. Maekawa, and E. Saitoh, Appl. Phys. Lett. **97**, 172505 (2010).

[31] J. Xiao, G. E. W. Bauer, K. Uchida, E. Saitoh, and S. Maekawa, Phys. Rev. B **81**, 214418 (2010).

[32] H. Adachi, J. ichiro Ohe, S. Takahashi, and S. Maekawa, Phys. Rev. B **83**, 094410 (2011).

[33] E. J. Guo, J. Cramer, A. Kehlberger, C. A. Ferguson, D. A. MacLaren, G. Jakob, and M. Kläui, Phys. Rev. X **6**, 031012 (2016).

[34] G. E. W. Bauer, E. Saitoh and B. J. van Wees, Nature Materials **11**, 391-399 (2012).

[35] L. J. Cornelissen, J. Liu, R. A. Duine, J. Ben Youssef, and B. J. van Wees, Nature Physics **11**, 10221026 (2015).

[36] M. E. Lucassen, C. H. Wong, R. A. Duine, and Y. Tserkovnyak, Appl. Phys. Lett. **99**, 262506 (2011).

[37] S. J. Watzman, R. A. Duine, Y. Tserkovnyak, H. Jin, A. Prakash, Y. Zheng, and J. P. Heremans, Phys. Rev. B **94**, 144407 (2016).

[38] P. Kapitza, Nature **141**, 74 (1938).

[39] L. Tisza, Nature, **141**, 913 (1938).

[40] L. D. Landau, Phys. Rev. **60**, 356 (1941).

[41] V. L. Ginzburg, Zh. Eksp. Teor. Fiz. **14**, 134 (1944).

[42] T. Fukuzawa, E. E. Mendez, and J. M. Hong, Phys. Rev. Lett. **64**, 3066 (1990).

[43] J. P. Eisenstein and A. H. MacDonald, Nature **432**, 691 (2004).

[44] Y. Yamamoto, Nature **405**, 629 (2000).

[45] J. Kasprzak, M. Richard, S. Kundermann, A. Baas, P. Jeambrun, J. M. J. Keeling, F. M. Marchetti, M. H. Szymanska, R. Andre, J. L. Staehli, V. Savona, P. B. Littlewood, B. Deveaud, and Le Si Dang, Nature **443**, 409 (2006).

[46] A. Oosawa, M. Ishii and H. Tanaka, J. Phys. Condens. Matter. **11**, 265 (1999).

[47] T. Nikuni, M. Oshikawa, A. Oosawa, and H. Tanaka, Phys. Rev. Lett. **84**, 5868 (2000).

[48] T. Giamarchi, C. Rüegg, C. and Tchernyshyvov, Nature Phys. **4**, 198 (2008), and references therein.

[49] H. T. C. Stoof, *J. Low Temp. Phys.*, **114**, 11 (1999).

[50] L. D. Landau and E. M. Lifshitz, *Statistical Physics*, Part 2, 3rd ed., Course of Theoretical Physics, Vol. 9 (Pergamon, Oxford, 1980); T. L. Gilbert, IEEE Trans. Magn. **40**, 3443 (2004).

[51] S. A. Bender and Y. Tserkovnyak, Phys. Rev. B **93**, 064418 (2016).

[52] B. I. Halperin and P. C. Hohenberg, Phys. Rev. **188**, 898 (1969).

[53] S. Takei, B. I. Halperin, A. Yacoby, and Y. Tserkovnyak, Phys. Rev. B **90**, 094408 (2014).

[54] Y. Tserkovnyak, S.A. Bender, R.A. Duine, and B. Flebus, Phys. Rev. B **93**, 100402 (2016).

[55] A. Brataas, Y. Tserkovnyak, G. E. W. Bauer, and P. J. Kelly, in *Spin Currents*, edited by S. Maekawa, S. O. Valenzuela, E. Saitoh, and T. Kimura (Oxford University Press, Oxford, 2012) pp. 87-135, arXiv:1108.0385.

[56] Y. Tserkovnyak, A. Brataas, G. E. W. Bauer, and B. I. Halperin, Rev. Mod. Phys. **77**, 1375 (2005).

[57] S. Takei, A. Yacoby, B. I. Halperin, and Y. Tserkovnyak, Phys. Rev. Lett. **116**, 216801 (2016).

[58] B. Flebus, S. A. Bender, Y. Tserkovnyak, and R. A. Duine, Phys. Rev. Lett. **116**, 117201 (2016).

[59] P. Upadhyaya, S. K. Kim, and Y. Tserkovnyak, "Magnetic domain wall floating on a spin superfluid", ArXiv:1608.00683.

[60] L. J. Cornelissen, K. J. H. Peters, G. E. W. Bauer, R. A. Duine, and B. J. van Wees, Phys. Rev. B **94**, 014412 (2016).

[61] R. R. Birss, *Symmetry and Magnetism* (North-Holland, Amsterdam, 1966).

[62] S. Takei and Y. Tserkovnyak, Phys. Rev. Lett. **112**, 227201 (2014).

[63] A. A. Thiele, Phys. Rev. Lett. **30**, 230 (1973).

[64] O. A. Tretiakov, D. Clarke, G. W. Chern, Y. B. Bazaliy, and O. Tchernyshpyov, Phys. Rev. Lett. **100**, 127204 (2008).

[65] A. A. Kovalev and Y. Tserkovnyak, Europhys. Lett. **97**, 67002 (2012).

[66] S. K. Kim and Y. Tserkovnyak, Phys. Rev. B **92**, 020410(R) (2015).

[67] S. K. Kim, S. Takei, and Y. Tserkovnyak, Phys. Rev. B **92**, 220409(R) (2015).

[68] A. Rückriegel, P. Kopietz, D. A. Bozhko, A. A. Serga, and B. Hillebrands, Phys. Rev. B **89**, 184413 (2014).

[69] M. Weiler, H. Huebl, F. S. Goerg, F. D. Czeschka, R. Gross, and S. T. B. Goennenwein Phys. Rev. Lett. **108**, 176601 (2012).

[70] K. Uchida, H. Adachi, T. An, H. Nakayama, M. Toda, B. Hillebrands, S. Maekawa and E. Saitoh, J. Appl. Phys. **111**, 053903 (2012).

[71] A. Kamra, H. Keshtgar, P. Yan, and G. E. W. Bauer Phys. Rev. B **91**, 104409 (2015).

[72] V. Cherepanov, I. Kolokolov, and V. L'vov, Phys. Rept. **229**, 81 (1993).

[73] I. S. Tupitsyn, P. C. E. Stamp, and A. L. Burin, Phys. Rev. Lett. **100**, 257202 (2008).

[74] F. Keffer, *Spin Waves* (Springer, Verlag, 1966), Vol. XVIIIP, handbuch der Physik.

[75] E. Schlömann, J. Appl. Phys. **31**, 1647 (1960).

[76] E. M. Lifshitz and L. P. Pitaevskii, *Statistical Physics* (Elsevier, Singapore, 2007).

[77] R. Damon and J. Eshbach, J. Phys. Chem. Solids **19**, 308 (1961).

[78] J. Barker and G.E. W. Bauer, Phys. Rev. Lett. **117**, 217201 (2016).

[79] C. Kittel, *Quantum Theory of Solids* (John Willey and Sons, New York, 1963).

[80] J. Colpa, Physica A: Statistical Mechanics and its Applications **93**, 327 (1978).

[81] S. R. Boona and J. P. Heremans, Phys. Rev. B **90**, 064421 (2014).

[82] T. Kikkawa, K. Uchida, S. Daimon, Z. Qiu, Y. Shiomi, and E. Saitoh, Phys. Rev. B **92**, 064413 (2015).

[83] P. A. M. Dirac, Proc. R. Soc. Lond. A **114**, 243- 265 (1927).

[84] M. A. Gilleo and S. Geller, Phys. Rev. **110**, 73 (1958).

[85] A. B. Harris, Phys. Rev. **132**, 2398 (1963).

[86] S. A. Manuilov, S. I. Khartsev, and A. M. Grishin, J. Appl. Phys. **106**, 123917 (2009).

[87] C. M. Srivastava and R. Aiyar, J. Phys. C **20**, 1119 (1987).

[88] W. Strauss, in *Physical Acoustics, Principles and Methods*, edited by W. Mandson (Academic Press, New York, 1967), Vol. 4, pt.B, Applications to Quantum and Solid State Physics.

[89] A. G. Gurevich and G. A. Melkov, *Magnetization Oscillations and Waves* (CRC Press, Boca Raton, 1996).

[90] F. G. Eggers and W. Strauss, J. Appl. Phys. **34**, 1180 (1963).

[91] P. Hansen, Phys. Rev. B **8**, 246 (1973).

[92] H. Jin, S. R. Boona, Z. Yang, R. C. Myers, and J. P. Heremans, Phys. Rev. B **92**, 054436 (2015).

[93] L. J. Cornelissen, and B. J. van Wees Phys. Rev. B **93**, 020403(R) (2016).

[94] S. Hoffman, K. Sato, and Y. Tserkovnyak, Phys. Rev. B **88**, 064408 (2013).

[95] W. F. Brown, Phys. Rev. **130**, 1677 (1963).

[96] Y. Tserkovnyak, A. Brataas, and G. E. W. Bauer, J. Magn. Magn. Mater. **320**, 1282 (2008).

[97] M. V. Berry, Proc. R. Soc. London A **392**, 45 (1984).

[98] G. E. Volovik, J. Phys. C: Sol. State Phys. **20**, L83 (1987).

[99] S. E. Barnes and S. Maekawa, Phys. Rev. Lett. **98**, 246601 (2007).

[100] Y. Tserkovnyak and C. H. Wong, Phys. Rev. B **79**, 014402 (2009).

[101] C. Burrowes, B. Heinrich, B. Kardasz, E. A. Montoya, E. Girt, Y. Sun, Y.-Y. Song, and M. Wu, Appl. Phys. Lett. **100**, 092403 (2012).

[102] S. A. Bender and Y. Tserkovnyak, Phys. Rev. B **91**, 140402 (2015).

[103] H. Ochoa, S. K. Kim, and Y. Tserkovnyak, Phys. Rev. B **94**, 024431 (2016).